
Master Thesis

submitted within the UNIGIS Master's program
"Geographical Information Science & Systems – (UNIGIS MSc)"
to the Department of Geoinformatics - Z_GIS,
Paris-Lodron University of Salzburg

# Exploring Flood Impacts on Riparian Zones Using Geospatial Analysis and Remote Sensing

## A Case Study of the August 2023 Flood Event in Slovenia

by

Urška Kušar, B.A.
Student number: 106955

Supervisor:
Dr. Ivan Tomljenović

In partial fulfilment of the requirements for
the Degree of
"Master of Science", abbreviated "MSc"

Reteče, May 2024

## ACKNOWLEDGMENT

I am grateful to the Paris Lodron University of Salzburg for offering the comprehensive Geographic Information Science and Systems Master of Science program. The knowledge and skills I have acquired during these studies are truly priceless. I extend my heartfelt appreciation to Dr. Ivan Tomljenović for his invaluable guidance throughout my academic journey.

I am deeply thankful to my family for their love, encouragement, support, and patience.

Reteče, May 4, 2024, Urška Kušar

## SCIENCE PLEDGE

I hereby declare that the thesis is entirely the result of my work. I have cited all sources I have used in my thesis; I have always indicated their origin. This thesis was not previously presented to another examination board and has not been published.

Reteče, May 4, 2024, Urška Kušar

## ABSTRACT

This Master Thesis investigates the impacts of floods on riparian zones through a comprehensive analysis of flood-affected areas in Slovenia during the August 2023 flood event. Utilizing freely available remote sensing data from Copernicus' Sentinel-1 and Sentinel-2 missions, the study delineates flood-affected areas and examines the spatial relationship between floods and land cover/land use patterns in riparian zones.

The first part of the study focuses on delineating flood-affected areas using Sentinel-1 SAR and Sentinel-2 optical data processed with Google Earth Engine. Two approaches, single image and change detection, are employed to identify flooded areas, revealing the significance of vegetation changes, particularly detected through the Normalized Difference Vegetation Index (NDVI), in observing flood impacts.

In the second part, the study analyses the impacts of floods on riparian zones, characterized by their vulnerability to flooding due to unique soil, hydrology, and biotic conditions. Landscape pattern analysis and assessment of riparian forest buffers' role in flood mitigation are conducted to understand flood effects on different land cover/land use types.

Key findings indicate that flood impacts disproportionately affect agricultural and grassland areas over urban and forested regions, with sub-alpine basins experiencing more severe impacts despite covering smaller areas of riparian zones. Riparian forest buffers show potential for flood mitigation, but their influence on flood outcomes varies across different study units.

The study underscores the importance of tailored flood management strategies in different riparian zone environments to mitigate adverse impacts and enhance ecosystem resilience. The approach demonstrates the effectiveness of utilizing remote sensing data for comprehensive flood impact assessment, providing valuable insights for flood management and land use planning in riparian zones.

# CONTENT

## LIST OF FIGURES

## LIST OF TABLES

# 1. INTRODUCTION

## 1.1. Introduction

Climate change poses significant challenges to ecosystems worldwide, disrupting their structure, function, and biodiversity (Mooney et al., 2009). Vulnerability and resilience of natural and human systems are at the centre of interest of countless scientific studies, aiming to add to the understanding of mechanisms behind the destruction and suggesting possible adaptation measures (Fiedler et al., 2021; Pörtner et al., 2022; Rodríguez-González et al., 2022). Riparian zones, transition areas between water and land, are anticipated to play a pivotal role in determining both, the vulnerability and ability to adapt (Capon et al., 2013). Riparian zones are exposed and very sensitive to many of the expected climatic shifts, such as changes in temperatures and the water cycle, and, at the same time, one of the globally most degraded, fragmented, and lost ecosystems (Capon et al., 2013; Tockner and Stanford, 2002; Weissteiner et al., 2016). On the other hand, their natural ecosystems have evolved under constantly changing environmental conditions (water level fluctuations, shifting sediments, etc.) which contributes to high heterogeneity and adaptability (Capon et al., 2013).

The global human population is expected to experience climate change primarily through alterations in the water cycle (Douville et al., 2021). Changes have already begun, resulting, among other effects, in more frequent and severe weather events, including heavy precipitation events leading to floods (Feyen et al., 2020; Hirabayashi et al., 2013). Mitigating floods cannot be done efficiently without considering riparian zones and their capacity to absorb and retain water, reduce erosion, and filter pollution (Salazar et al., 2012; Tóth, 2019). The capacity of a riparian zone to provide this kind of ecosystem service is its condition, largely influenced by existing vegetation, demonstrated also as (un)suitable land cover/ land use areas (Salazar et al., 2012). Prominently important features for water management, not only flood mitigation, are buffer zones, linear green features or forest buffer zones (Fribourg-Blanc et al., n.d.; Graziano et al., 2022) in proximity to rivers and other water bodies. Stripes of relatively undisturbed vegetated areas can provide several functions related to water quality and flow moderation. Riparian trees are adept at absorbing surplus nutrients and can enhance infiltration rates. By slowing down water flow, riparian buffers mitigate water and sediment runoff into surface waters (Apan et al., 2002; Fribourg-Blanc et al., n.d.; Graziano et al., 2022). River bank vegetation and forest and semi-natural areas in riparian zones are propagated as green infrastructure elements in many policy/ management guidelines for mitigating floods (Piedelobo et al., 2019; Taramelli et al., 2019)

Riparian areas are extended in a more or less limited buffer zone along all rivers and watercourses and thus embrace extensive areas (Weissteiner et al., 2016). To understand the state of an individual site along a watercourse, it is necessary to understand the state, pressure, and responses of the entire watercourse - upstream and downstream. Therefore, in the study of riparian zones, the expansion of

remote sensing techniques, the availability of products from satellite systems as well as the possibility to process large amounts of data in cloud systems are important advances (Weissteiner et al., 2016). The products and services of the European Union's Copernicus Programme aim to provide information to help public authorities and other actors improve European citizens' quality of life by utilizing vast amounts of global data from satellites and other measurement systems (Thépaut et al., 2018) The information services provided are free and openly accessible to users (Thépaut et al., 2018).

Geospatial data and images from the Copernicus Emergency Management Service (CEMS) have been used as support to the management of a major flood event that affected Slovenia in early August 2023. This study aims to utilize this and other Copernicus products to assess the impact that the flood event had in the riparian zone of the Slovenian sub-alpine and sub-pannonian water basins, focusing on the riparian zone's land cover/ land use.

## 1.2. Literature Review

### 1.2.1. Impact of floods on riparian zones

Riparian zones are interfaces between terrestrial and aquatic systems, areas along land and freshwater ecosystems, characterized by unique soil, hydrology and biotic conditions (Naiman et al., 2010; Weissteiner et al., 2016). The riparian zone comprises the stretch of the stream channel between its low and high water marks, as well as the adjacent terrestrial area extending from the high water mark towards the uplands, including active floodplains and adjacent terraces (Naiman and Bilby, 2001).

Riparian zones are strongly influenced by stream water and particularly susceptible to the flooding events. Effects of floods in riparian zones include erosion of soil and uprooting of vegetation, deposition of sediments, affecting soil structure and nutrient content, displacing of the habitats of wildlife species dependent on riparian zones e.g. loss of nesting sites (Gregory et al., 1991). Floods can cause erosion around human infrastructure in riparian areas, leading to the loss or damage of buildings, roads, and bridges. Agricultural areas in riparian zones may experience damage to crops, soil fertility changes, and disruption to farming practices. Severe flood events can alter natural flow patterns, affecting the hydrology and overall landscape (Apan et al., 2002; Graziano et al., 2022; Olokeogun et al., 2020).

Understanding the relationship between land use and flood impacts in riparian zones is essential for effective flood risk management, ecosystem conservation, and land use planning (Graziano et al., 2022; Weissteiner et al., 2016).

#### 1.2.1.1. Land use in riparian zones

Riparian zones exhibit unique land use characteristics due to their proximity to water bodies and their ecological significance. They feature diverse vegetation types, including trees, shrubs, grasses, and wetland plants adapted to fluctuating water levels and periodic flooding. Riparian vegetation provides

habitat for wildlife, stabilizes streambanks, and contributes to water quality improvement (Lozano de Sosa et al., 2017). Riparian zones often encompass floodplains, periodically inundated areas adjacent to rivers and streams. Floodplains support unique vegetation communities adapted to flooding and provide important ecological functions, such as floodwater storage, groundwater recharge, and sediment deposition (Tockner and Stanford, 2002).

The main pressures causing increased vulnerability of riparian zones are land use changes and hydrogeomorphological modifications of rivers and streams (Rodríguez-González et al., 2022; Tockner and Stanford, 2002). Structural modifications such as channelization and dam construction can alter the flow regime and sediment transport dynamics in riparian zones, affecting floodplain inundation patterns and ecosystem connectivity (Hohensinner et al., 2018). Channelized streams and impounded rivers may experience increased flood velocities, reduced floodplain inundation, and altered sediment deposition, impacting riparian habitats and floodplain ecosystems (van Oorschot et al., 2018).

Changes in land use, such as urbanization, deforestation, and agricultural intensification, can alter the hydrological dynamics of riparian zones (Olokeogun et al., 2020). Encroachment into floodplain areas through development increases exposure to flood hazards, exacerbating flood risks. This encroachment reduces natural flood storage capacity, limits floodplain connectivity, and impairs the ability of riparian areas to absorb floodwaters (van Oorschot et al., 2018). Urbanization and infrastructure development in riparian zones lead to habitat loss, fragmentation, and degradation, affecting water quality and ecosystem services (Gregory et al., 1991; Piedelobo et al., 2019). Impervious surfaces associated with urbanization intensify surface runoff, leading to accelerated stormwater runoff and higher flood peaks (Jiménez-Jiménez et al., 2020; Miller et al., 2014). Consequently, urban areas developed on former riparian zones experience heightened flood risk, necessitating extensive mitigation efforts (Liu et al., 2014; Salazar et al., 2012).

Implementing flood-resilient land use practices in riparian zones is essential to minimize the adverse effects of floods and enhance the overall resilience of these ecosystems (Graziano et al., 2022; Weissteiner et al., 2016).

#### 1.2.1.2. Vegetated green buffers

To increase resilience, the promotion of green infrastructure is suggested, such as vegetated buffer strips and riparian corridors, to absorb and attenuate floodwaters, the maintenance of natural vegetation in riparian zones to stabilize soils and reduce erosion during floods, and preserving or enhancing floodplains (Tockner and Stanford, 2002; Tóth, 2019). Riparian vegetation plays a crucial role in regulating flood impacts by stabilizing streambanks, reducing erosion, and attenuating floodwaters. Deforestation or removal of riparian vegetation can weaken streambank stability, increase sedimentation, and reduce floodplain connectivity, exacerbating flood risks and channel instability (Naiman et al., 2010; Rodríguez-González et al., 2022).

Riparian zones may contain vegetated buffer strips along water bodies, consisting of native vegetation or restored riparian plant communities. These green buffer strips along water bodies help mitigate flood impacts by intercepting surface runoff, filtering pollutants, and reducing erosion (Naiman et al., 2010; Piedelobo et al., 2019; Taramelli et al., 2019). Well-managed riparian buffers can enhance floodwater retention, promote groundwater recharge, and provide natural floodplain storage, buffering communities from flood hazards. Buffer strips help filter sediment and pollutants, reduce erosion, and protect water quality by intercepting runoff from adjacent lands. Riparian vegetation provides food, shelter, nesting sites, and breeding habitat for wildlife, contributing to biodiversity conservation and ecological resilience (Gregory et al., 1991; Hohensinner et al., 2018; Naiman et al., 2010).

#### 1.2.1.3. Land cover/ land use analysis

To analyse the impacts of floods on riparian zones several approaches are available, including change detection analysis and spatial analysis using landscape metrics.

The change detection approach focuses on the analysis of changes in land use/land cover over time using temporal snapshots. Change detection techniques such as image differencing or pre-post-classification comparison help identify areas of change, such as land use change due to urban expansion, deforestation, agricultural encroachment, or disaster-impacted areas – e.g. burnt-up or flooded. (Chughtai et al., 2021).

Spatial analysis is used to quantify and characterize land use patterns, fragmentation, connectivity, and spatial relationships between different land use types. Spatial analysis techniques, such as overlay analysis, buffering, and proximity analysis, help assess the spatial distribution and arrangement of land use features as well as the relationship of changes regarding landscape characteristics (Agoha et al., 2024; Da Silva et al., 2015). Descriptive statistics and visualization of results on graphs and maps are used to enhance understanding of existing relationships.

For riparian zones, landscape pattern analysis can be used to characterize them by quantifying their spatial extent, configuration, and connectivity. This information is valuable for assessing the ecological functions of riparian areas, such as habitat connectivity, nutrient cycling, and biodiversity conservation as well as their health and resilience (Burdon et al., 2020). Resilience to floods-related erosion in relation to vegetation along stream banks, gullies, and riparian areas, especially in deeply incised channels in landscapes dominated by agriculture was presented in the studies e.g. (Zaimes et al., 2019) and (Zaimes and Iakovoglou, 2020).

Landscape metrics quantify various aspects of landscape structure and configuration, providing numerical measures of spatial heterogeneity, connectivity, and fragmentation. Commonly used landscape metrics include patch size, shape, diversity, edge density, connectivity indices, and landscape shape indices (Ma et al., 2019; O'Neill et al., 1988). By comparing landscape metrics researchers can

evaluate different riparian landscape patterns and assess the impacts of floods on different land use types.

### 1.2.2. Floods and mapping of flooded area

Floods occur when water overflows its natural or artificial banks onto normally dry land, such as a river inundating its floodplain (Schmidt-Thomé et al., 2005). Floods can be caused by excessive precipitation (long-lasting, heavy rain or snow) or damage to structures (dams) (Munich RE, 2000). The impacts of floods on the human and natural environment are manifold – sometimes beneficial (fertilization, soil moisture) (Gardiner, 1994), but mostly disruptive, due to a lack of resilience and preparedness (Gautam and Van Der Hoek, 2003). When the impact of natural or semi-natural events adversely affects human activities, it is identified as damage and considered a natural disaster (Smith, 2006).

River flooding stands out as one of the most frequent and devastating natural disasters in Europe (Feyen et al., 2020). Substantial efforts have been made to better understand, model, and assess flood losses (Bakkensen and Blair, 2020). Damages caused by floods are tangible and intangible, direct and indirect. Tangible damages include the destruction of buildings and infrastructure, erosion of agricultural soil, destruction of harvest, damage to livestock, costs of evacuation, rescue measures, and clean-up, as well as interruption of business and public services (Merz et al., 2010). Intangible damages are loss of lives, injuries, loss of memorabilia, psychological distress, damage to cultural heritage, negative effects on ecosystems, trauma, and loss of trust in authorities (Bakkensen and Blair, 2020; Merz et al., 2010). Some damages are direct, occurring through physical contact of floodwater with humans, property, or any other objects. Indirect damages are induced by the flood event but occur outside the flooded area or after the inundation and nevertheless contribute to the overall impact (Gautam and Van Der Hoek, 2003).

Flood damage assessments are necessary to assess vulnerability and resilience, map flood risk, inform flood mitigation decisions, manage disaster relief and assistance decisions, conduct insurance appraisals, etc. (Bakkensen and Blair, 2020; Merz et al., 2010). The essential factor in flood damage assessment is high-quality data. They can be found across various sources; advancements in spatial data and remote sensing have enabled important advancements (Adeel et al., 2020; Bakkensen and Blair, 2020).

While flood-related damages can be direct and indirect, tangible and intangible, a key indicator of direct tangible damages and an important data set for a flood-related analysis is the extent of the area inundated with flood water - flooded area (Atreya and Ferreira, 2015; Merz et al., 2010). There is a vast research on the mapping of flooded areas utilizing different approaches and techniques (Mudashiru et al., 2021), 2021). Remote sensing, including satellite products, provides a means to obtain fast and crucial knowledge about significant spatial and temporal changes in land use and water resources (Brivio et al., 2002; Cerdà et al., 2021; Rahman et al., 2021; Rango and Salomonson, 1974).

#### 1.2.2.1. Water area vs. flood impact

There are generally two approaches to the detection of flooded areas: direct identification of the water area during the flood event and the detection of changes caused by flood (Atefi and Miura, 2022).

The majority of studies aim to directly identify inundated areas using Synthetic Aperture Radar (SAR) products from ERS1-2, ENVISAT, RADARSAT 1 and 2, Sentinel-1 and TerraSAR-X or from optical instruments on satellite systems like MODIS, Landsat, and Sentinel-2 (Cerbelaud et al., 2021; Mudashiru et al., 2021). These are satellite remote sensing systems with earth observation programs characterized by relatively high spatial resolution and revisit time frequency (Tarpanelli et al., 2022).

Intensified weather extremes have increased interest in the effects that different precipitation patterns can have on the development of different types of floods, such as flash floods (Laudan et al., 2020) and pluvial floods (Atefi and Miura, 2022; Merz et al., 2010). In recent years a growing number of authors suggested that not all areas impacted by floods are adequately detected with approaches applied to detect present inundation (Cerbelaud et al., 2021; Diakakis et al., 2020; Kobiyama and Goerl, 2007; Laudan et al., 2020). Depending on rainfall magnitude, rate and duration, and watershed characteristics (topography, lithography, pedology, land cover) flood events vary in hydrological impacts and time scale. Flooding can have different hydrological consequences, such as increased water levels in rivers and streams, inundation of low-lying areas, and damage to infrastructure. Flooding events can persist over different time scales, ranging from hours to weeks. Flash floods are usually short-lived, while riverine floods can last for extended periods (Bell and Om Kar, 1969; Cerdà et al., 2021). When a flood event is associated with heavy rainfall and steep slopes significant amount of water overflows for a short period, which cannot be captured with satellite sensors as open water areas(Atefi and Miura, 2022). Although in a short period of time, water overflow can cause significant damage, partially due to its association with other elements, such as debris flows, mud deposits, landslides, and soil erosion (Cerbelaud et al., 2023; Laudan et al., 2020, 2017).

#### 1.2.2.2. Flooded area detection using SAR (Sentinel 1)

Active microwaves of Synthetic Aperture Radar (SAR) sensors penetrate clouds and provide images regardless of day and night or weather conditions (Tarpanelli et al., 2022) . SAR imagery can detect the presence of water bodies by exploiting the differences in backscatter between water and surrounding land. Water typically appears as dark regions in SAR images due to its low backscatter properties (Meyer, 2019). However, challenges arise in areas with emergent vegetation and wind-induced waves, leading to increased backscatter and confusion between inundated areas and dry land surfaces. (Bangira et al., 2021). The interaction between SAR signals and vegetation involves volume scattering from plant structures and canopy, as well as double-bounce scattering from horizontal and vertical surfaces. The amount of vegetation within a pixel significantly affects the SAR signal, making flood detection in vegetated areas more complex compared to open water features (Bangira et al., 2021).

Specific settings and characteristics of different SAR systems or products define how a SAR system operates and what are the properties of the resulting SAR images. Key SAR parameters and their impact on derived products are listed in Table 1.

*Table 1: SAR Parameters and their implications on derived images*

| | |
|---|---|
| **Frequency** | SAR systems operate at microwave frequencies, typically ranging from L-band (1-2 GHz) to X-band (8-12 GHz), C-band (4-8 GHz), and higher frequencies such as Ku-band and Ka-band. The choice of frequency affects the resolution, penetration capability, and sensitivity to surface properties e.g. t longer wavelength signals penetrate deeper into vegetation canopies and soils. |
| **Polarization** | SAR signals can be transmitted and received in different polarization states, such as HH (horizontal-horizontal), VV (vertical-vertical), HV (horizontal-vertical), and VH (vertical-horizontal). Polarization affects the sensitivity of SAR imagery to surface roughness, orientation, and scattering mechanisms. e.g. VV polarization is sensitive to the backscatter from targets with vertical structure, such as forests, buildings, and some types of agricultural crops. VH polarization is sensitive to the backscatter from targets with horizontal structure, such as bare soil, water bodies, and certain types of terrain features. Both are influenced by surface roughness and moisture conditions. |
| **Swath Width** | The swath width of SAR imagery refers to the horizontal extent covered by a single radar pulse. Wide swath SAR systems capture larger areas in a single pass but typically have coarser spatial resolution, while narrow swath systems offer higher resolution but cover smaller areas. |
| **Incidence Angle** | The angle at which the radar signal interacts with the Earth's surface, known as the incidence angle, affects the backscatter intensity and image characteristics. Different incidence angles result in varying levels of sensitivity to terrain slope, surface roughness, and vegetation structure. |
| **Radiometric Resolution** | SAR imagery is characterized by its radiometric resolution, which determines the number of quantization levels or bits used to represent the intensity of radar backscatter. Higher radiometric resolution allows for better discrimination of subtle variations in surface properties. |
| **Noise Level** | SAR imagery may contain noise caused by various sources, such as electronic interference, atmospheric effects, and speckle noise inherent to radar imaging. Noise levels affect image quality and the accuracy of quantitative analysis. |
| **Spatial Resolution** | SAR imagery has spatial resolutions ranging from meters to tens of meters, depending on the imaging mode and system specifications. Higher spatial resolution allows for detailed mapping of surface features, while lower resolution provides broader coverage. |
| **Temporal Resolution** | SAR systems can acquire imagery repeatedly over time to monitor changes in the Earth's surface, such as urban growth, agricultural activities, and natural disasters. Temporal resolution refers to the frequency of image acquisition, which can range from days to months depending on the satellite revisit time. |

*Source: summarized from (Meyer, 2019; Tarpanelli et al., 2022; Tsyganskaya et al., 2018)*

Raw SAR data require pre-processing steps such as radiometric calibration, orthorectification, speckle filtering, and geometric correction to ensure data quality and comparability (W. Huang et al., 2018; Kuntla, 2021; Meyer, 2019; Tavus et al., 2022; Vollrath et al., 2020).

The most common approaches to detect flooded areas from SAR images are backscatter thresholding, texture analysis, change detection analysis, and time-series analysis (Marzi and Gamba, 2021; Tavus et al., 2022).

SAR backscatter values can be used to establish a threshold for detecting flooded areas. Water in SAR images reflects most of the signal away from instruments so pixels with backscatter values lower than the established threshold can be classified as open water. On the other hand, areas with flooded vegetation can experience volume scattering or double-bounce effect, which is presented as higher backscatter values and optimal thresholding varies significantly depending on the land cover characteristics (Bangira et al., 2021). Land cover characteristics, particularly vegetation cover also influences presentation of soil moisture in SAR - soil moisture generally leads to higher backscatter intensity, especially in areas with relatively smooth surfaces and little to no vegetation cover (Zhang et al., 2018).

SAR imagery provide information about the texture or roughness of the surface. Flooded areas often exhibit different textures compared to dry land, which can be used as an additional indicator for flood detection. (Tsyganskaya et al., 2018).

The change detection approach utilizes SAR images acquired before and after a flood event: areas that were dry in the pre-flood image but appear inundated (open water, increased soil moisture or flooded vegetation) in the post-flood image indicate the extent of the flooded area (Cerbelaud et al., 2021). For regularly or seasonally reoccurring floods time series analysis is often applied, where SAR data collected over time can be used to monitor changes in flood extent and dynamics (Bangira et al., 2021).

Interferometric SAR (InSAR) techniques can be applied to SAR data to measure changes in surface elevation caused by flooding. By comparing interferograms generated from pre-flood and post-flood SAR images, it's possible to estimate changes in water level and identify flooded areas (Refice et al., 2014).

#### 1.2.2.3. Flooded area detection with spectral imagery

Detecting water areas using optical satellites involves analysing the spectral characteristics of water bodies in satellite imagery. Water bodies have specific spectral signatures in the visible and near-infrared portions of the electromagnetic spectrum. In the visible spectrum, water absorbs most of the shorter wavelengths (blue and green) and reflects longer wavelengths (red and near-infrared) to varying degrees. Near-infrared radiation is strongly reflected by water, making it a useful band for water detection (McFeeters, 1996).

To obtain water areas form optical imagery several approaches are used – single band, multi band spectral indices, multiband machine learning segmentation/ clustering etc.(Lombana and Martínez-Graña, 2022; TV and K N, 2019)

Multi-spectral remotely sensed imagery is comprised of various bands, forming a composite image for interpretation and analysis. This type of imagery allows for the transformation of individual bands within the composite, highlighting specific features and patterns for better visibility. Transforming image bands is a widespread technique, commonly employed to produce novel images by combining two or more bands, facilitating information extraction by enhancing the representation of ground objects, such as vegetation or water (Huang et al., 2021). This often involves composing spectral indices, which are mathematical combinations of spectral bands designed to highlight specific features or characteristics in satellite imagery.

To delineate water extent several spectral indices were derived, most commonly used are the Normalized Difference Water Index - NDWI (McFeeters, 1996), Normalized Difference Moisture Index (Gao, 1996; Strashok et al., 2022), and Normalized Difference Vegetation Index (Kriegler et al, 1969).

#### 1.2.2.3.1. Normalized Difference Water Index (NDWI)

The Normalized Difference Water Index (NDWI) is a commonly used spectral index for water detection in optical imagery. As water bodies strongly absorb light in visible to infrared electromagnetic spectrum, NDWI uses green and near-infrared bands to highlight the appearance of water features while reducing the impact of soil and terrestrial vegetation features (McFeeters, 1996). It is sensitive to built-up land and can result in over-estimation of water bodies ("JNCC Sentinel-2 indices Analysis Ready Data (ARD)," n.d.)

Water bodies typically have high NDWI values, distinguishing them from other land cover types. Index values greater than 0,5 usually correspond to water bodies. Vegetation usually corresponds to much smaller values and built-up areas to values between zero and 0,2 (Sinergise, n.d.).

#### 1.2.2.3.2. Normalized Difference Moisture Index (NDMI)

The Normalized Difference Moisture Index (Gao, 1996; Strashok et al., 2022) is a normalized difference index, that uses near-infrared (NIR) and the short-wave infrared (SWIR) to highlight water content in vegetation. It was proposed by Gao (1996), who named it NDWI. SWIR captures both vegetation water content and structure changes, while NIR reflects leaf structure and dry matter (Ceccato et al., 2001). Combining NIR with SWIR removes variations from leaf structure and dry matter, enhancing the accuracy in retrieving the vegetation water content. SWIR reflectance is inversely related to leaf water content (Tucker, 1979).

NDMI values range between -1 and 1. Most often it is used to measure water stress in vegetation. Water stress would be signalled by the negative values approaching -1, with values below 0,8 indicating bare soil, while the values above 0,4 indicate high canopy cover with no water stress, and +1 may indicate waterlogging (EOS Data Analytics, 2022).

#### 1.2.2.3.3. Normalized Difference Vegetation Index (NDVI)

Normalized Difference Vegetation Index (Kriegler et al., 1969) is an index that normalizes green leaf scattering in near-infrared (NIR) wavelengths with chlorophyll absorption in red wavelengths. It is widely used as an index for quantifying the health, density, and vigour of vegetation.

NDVI values close to +1 typically represent healthy, dense vegetation with high chlorophyll content and abundant green biomass. Values around zero indicate bare soil, rock, or water bodies. Negative values are rare in natural environments but can occur in urban areas, snow-covered regions, or areas with dense shadows and open water. (Stembatch, n.d.)

#### 1.2.2.3.4. Soil-adjusted vegetation index (SAVI)

The Soil-adjusted vegetation index (Huete, 1988) is a modification of the Normalized Difference Vegetation Index (NDVI) designed to reduce the influence of soil colour, soil moisture and saturation effects from high density vegetation.

SAVI is calculated using the near-infrared band, the red band, and a constant (L) ranging from 0 to 1 that adjusts the soil brightness effect. Typical values for L range from 0.5 to 1, with higher values used in areas with brighter soils.

SAVI values range from -1 to +1, similar to NDVI. Positive SAVI values indicate vegetation presence, with higher values corresponding to denser vegetation cover. (Staembatch, n.d.)

#### 1.2.2.3.5. Bare Soil Index (BI)

The Bare Soil Index (Rikimaru et al., 2002) is a normalized index that combines blue, red, NIR and SWIR spectral bands to capture bare soil variations. The SWIR and the red spectral bands are used to quantify the soil mineral composition, while the blue and the NIR spectral bands are used to enhance the presence of vegetation. BI has primarily been used in forest research to differentiate between bare soil and other land cover types (Rikimaru et al., 2002).

The Bare Soil Index values range between −1 and 1, where a higher value indicates a higher change on bare soil (Sinergise, n.d.)

#### 1.2.2.3.6. Automated Water Extraction Index – shadows (AWEIsh)

Automated Water Extraction Index (Feyisa et al., 2014) is spectral index that maximize the accuracy of classification of water pixels and non-water pixels by band differencing, band addition and applying c*oefficients to enhance contrast between water pixels and other dark surfaces that might otherwise get classified as water* (TV and K N, 2019). The version of the index AWEInsh will further improve the accuracy by removing the shadow pixels as well and is best suited if the scene is obscured by shadow (Feyisa et al., 2014).

The index is designed to use 0 as a threshold value – with water pixels above zero and non-water pixels to be below zero (TV and K N, 2019).

#### 1.2.2.3.7. Parameters and processing

Satellite optical imagery, captured by sensors that detect sunlight reflected or emitted from the Earth's surface in different wavelengths, contains various parameters that characterize its properties and capabilities. Parameters to be considered when using satellite optical images to detect flooded areas are selection of spectral bands, spatial radiometric and temporal resolution, swath width, geometric accuracy and application of atmospheric correction.

Pre-processing steps necessary before analysis of data depend on the product and include spatial filtering, clipping to area of interest, atmospheric correction and masking. Masking out can includes non-water features like clouds and shadows (Tarpanelli et al., 2022)

After applying spectral indices, threshold is often applied to extract areas of interest – e.g. water areas or flood impacted areas (Atefi and Miura, 2022; Lombana and Martínez-Graña, 2022; TV and K N, 2019).

Change detection and multi temporal analysis utilize images acquired before and after the studied event. to detect changes and their patterns. In studies for floods these can be the changes from (dry) land to water inundated areas (Hansana et al., 2023; Landuyt et al., 2020; Lombana and Martínez-Graña, 2022) or detection of indirect marks of flood impact, such as changes to vegetation, soil moisture and bare soil exposure (Atefi and Miura, 2022; Cerbelaud et al., 2021; F. Huang et al., 2018).

Post processing steps are used to improve spatial coherence and remove noise. These include spatial filtering of small isolated areas or merging adjacent pixels into larger areas (Atefi and Miura, 2022)

### 1.2.2.4. Thresholding

Thresholding is often used with spectral indices or SAR backscatter imagery: a threshold value is applied to classify pixels as water or non-water. Pixels with values above/below the threshold are classified as water, while those below are classified as non-water.

Most straightforward method is fixed, empirically based method, where visual interpretation of frequency histograms, prior knowledge of the data or trial and error techniques are used to set the threshold optimal for selected study (Lombana and Martínez-Graña, 2022).

Among methods of automatic histogram-based algorithms the Otsu's Method is most widely used (Lombana and Martínez-Graña, 2022). Otsu's method automatically calculates an optimal threshold by maximizing the between-class variance in the image histogram. It demonstrates efficacy for bimodal histograms when the classes of interest are well-separated (Otsu, 1975).

Adaptive thresholding techniques adjust the threshold value dynamically based on local image characteristics. This can be particularly beneficial in where the background is heterogeneous (Tzeng et al., 2009).

### 1.2.3. Accuracy Assessments

Accuracy assessments help validate the quality of remote sensing products, such as land cover maps, vegetation indices, or water body delineations, by comparing them to ground truth data collected through field surveys, high-resolution imagery, or other reliable sources. (Ye et al., 2018). They aim to provide insights into the strengths and limitations of remote sensing techniques, sensor capabilities, and image processing algorithms, aiding in the interpretation and use of products derived from satellite imagery. As accuracy assessment is an integral part of remote sensing image classification it is important to report information about validation design.(Ye et al., 2018). Selection of the basic approach (per pixel or per-polygon), sample design, reference dataset, and type of accuracy analysis are elements of validation design.

Per-pixel approach involves comparing each pixel's classified label to a reference dataset (usually ground truth data) to determine its correctness. Per-polygon approaches aim to evaluate the correctness of entire spatial objects, such as land cover polygons, rather than individual pixels (Stehman and Wickham, 2011). Per-polygon approaches are considered to be more suitable for object-based analysis (Stehman and Wickham, 2011; Ye et al., 2018). Per-pixel approaches are more methodologically developed and used more often, particularly in pixel-based classification approaches. The per-pixel accuracy assessment is easy to design and interpret but is very sensitive to positional errors (Congalton, 1991).

Accuracy assessments typically involve comparing the results of a study with real-world features. Ground-truth data can be collected in the form of field measurements, GPS points, or high-resolution imagery, representing the true conditions on the ground (Ye et al., 2018). The sample design includes the choice and distribution of samples that critically determine the representativeness of validation. (Ye et al., 2018). Researchers often use probabilistic sampling distribution such as simple random, systematic random (e.g. grid), or stratified random sampling (Ye et al., 2018). In some cases, the alternative dataset is used as a reference dataset (Congalton, 1991; Foody, 2008).

Besides unbiased distribution, sample size impacts how meaningful and statistically powerful is the accuracy assessment. (Ye et al., 2018). The optimal sample size can be determined with the multinomial distribution analysis (Congalton, 1991). A minimum sample size of 50 per map category is often suggested as a rule of thumb (Congalton and Green, 2019; Ye et al., 2018). Nevertheless, Ye (2018) reported that a substantial share of examined studies used less than 50 samples per mapped category, as the particular goal of the application must be considered.

The most common metric to report results of accuracy assessment is overall accuracy (OA) (Ye et al., 2018). It represents the proportion of correctly classified pixels or objects (such as polygons) to the total number of pixels or objects in the dataset. In a pixel-based classification scenario, OA measures the percentage of pixels that are correctly classified across all classes (Congalton and Green, 2019). Anderson et al. (1976) suggested 85% overall accuracy as the level, that is the desirable threshold between acceptable and unacceptable results, and this threshold is often adopted in various applications (Ye et al., 2018). However different objectives in mapping and classification, different landscapes, and different input remote sensing data require very different levels of accuracy (Anderson, 1976; Ye et al., 2018).

For a deeper understanding of the validity of results, other metrics can be calculated, such as the confusion matrix. The confusion matrix is a cross-tabulation of the mapped class versus the reference data. It provides a basis to describe overall accuracy and characterize specific errors (Foody, 2002). True positives (TP), true negatives (TN), false positives (FP), and false negatives (FN) are basic elements of confusion metrics, from which other metrics are calculated. Producer's accuracy (PA) (also called Recall) quantifies the probability that a pixel or object belonging to a specific class in the reference dataset (ground truth) is correctly classified as that class by relating TP to the sum of TP and FN. User's accuracy (UA) (also called Precision) quantifies the probability that a pixel or object classified as a specific class is indeed that class according to the reference dataset (ground truth) by dividing the number of TP by the sum of TP and FP (Congalton and Green, 2019). Kappa coefficient, F measure, and other metrics are used for specific purposes in validation. (Ye et al., 2018)

In summary, accuracy assessments play a crucial role in evaluating the reliability and utility of remote sensing data for various applications, providing confidence in the interpretation and use of satellite imagery for scientific research, resource management, and decision-making purposes.

#### 1.2.4. Data availability

Availability of free open access data plays a crucial role in flood detection and flood management for several reasons including rapid access, cost-effectiveness, global coverage, transparency and accountability (Atefi and Miura, 2022).

Free open-access data ensures that essential information is available to a wide range of users, including researchers, policymakers, emergency responders, humanitarian organizations and the general public. This accessibility allows for widespread use and dissemination of data, enabling more effective flood detection efforts. Free access to data eliminates financial barriers for users, particularly in resource-constrained regions or organizations. Rapid access to satellite imagery and other data is essential for timely flood detection and response. Free open access data platforms often provide near-real-time or regularly updated datasets, allowing users to monitor flood events as they unfold and to respond

promptly to emerging situations (Atefi and Miura, 2022). This promotes transparency and accountability as multiple users can access and verify the data used, enhancing confidence in the results.

In addition, free open access data platforms often offer global coverage, providing data for regions around the world. This global reach is essential for monitoring floods in diverse geographic areas, including remote or hard-to-reach regions where traditional ground-based monitoring may be limited (Atefi and Miura, 2022; Hansana et al., 2023).

There is a growing amount of data from satellite remote sensing products which demand huge processing power capacity in order to utilize their potential. Powerful cloud-based platforms for accessing, analyzing, and visualizing Earth observation data, such as Google Earth Engine or Sentinel Hub are often used by researchers, scientists, developers, and NGOs for monitoring environmental changes, studying land cover dynamics and addressing various other global challenges, including floods (Agoha et al., 2024; Atefi and Miura, 2022; Hansana et al., 2023; Wu, 2020).

### 1.3. Study Area/ Event

Severe weather events in the summer of 2023 caused devastating flooding and flash-flooding damages in Slovenia. From August 3rd to 6th, a vast part of Slovenia experienced a prolonged period of rainfall, marked by frequent storms, heavy downpours, and showers. During the night of August 3rd to 4th, unusually intense rainfall occurred in the catchment areas encompassing the alpine and sub-alpine parts of the country. Within a span of 6 to 12 hours, these regions received an unprecedented amount of rainfall, ranging from 150 to 200 mm. This deluge led to a significant surge in numerous torrents, smaller streams, and rivers. This resulted in extensive and destructive flooding, affecting numerous residential and commercial areas. Landslides were also triggered, and bridges and roads were washed away, as rivers carried massive volumes of floodwater (Agencija Republike Slovenije za okolje, 2023).

Heavy rains persisted on August 4th and 5th, albeit with slightly lower intensity, extending across the entire country. In the central part of Slovenia rivers with their karst tributaries experienced flooding in regions prone to periodic flooding, while the flooded floodplain areas along the Drava and Mura remained inundated up until August 9th. The maximum flow rates experienced in the catchment areas of the alpine rivers were estimated to be of the order of 100 years or more. An exceptional aspect of this event was that the three largest Slovenian rivers – Sava, Drava, and Mura – all experienced flooding simultaneously (Agencija Republike Slovenije za okolje, 2023). The disaster, considered the largest in the nation's history, had far-reaching and devastating consequences for approximately two-thirds of the country's territory (European Flood Awareness System (EFAS), 2023).

*Table 2: The time frame of the studied event*

| | Begin | End | Duration of high water levels |
|---|---|---|---|
| **Flash Flood** | 4.8.2023 | 5.8.2023 (subalpine region) | 15 min – 6 hours |
| **Riverine flood** | 5.8.2023 | 9.8.2023 (karst and sub-pannonian region) | 5 days |

*Source: summarized from (Agencija Republike Slovenije za okolje, 2023)*

*Table 3: The study area – spatial units: effected water basins, riparian zones and watercourses, characterised by surface area, watercourse length and land cover/land use composition*

| Study units | Description | Surface Area; Watercourse Length | Elevation | Land Cover/ Land Use (%) |
|---|---|---|---|---|
| **Water basins (WBASIN)** | Water basins effected by the event | 7.730,68 km$^2$ | Min:128 m asl<br>Max: 2864 m asl | Water & wetlands: 1,1%<br>Forest & semi natural: 65,1%<br>Grassland: 17,3%<br>Agricultural: 10,2%<br>Urban: 6,4% |
| **Riparian Zone (RZ)** | Areas of delineated potential riparian zone in the water basins effected by the event | 438,09 km$^2$ | Min:128m asl<br>Max:781m asl | Water & wetlands: 14,4%<br>Forest & semi natural: 22,8%<br>Grassland: 17,3%<br>Agricultural: 28,6%<br>Urban: 16,9% |
| **Watercourses** | Total length of rivers and streams in the studied:<br>- Water basins<br>- Riparian Zones | <br>20.315 km<br>1.924 km | | |

*Source: contains modified data from (Agencija Republike Slovenije za okolje, 2023; Direkcija RS za vode, 2024)*

| a) | b) | c) |
|---|---|---|
| **Precipitation on August 4 2023** | **Precipitation August 4-9 2023 – cumulative** | **River water level status 4 August** |

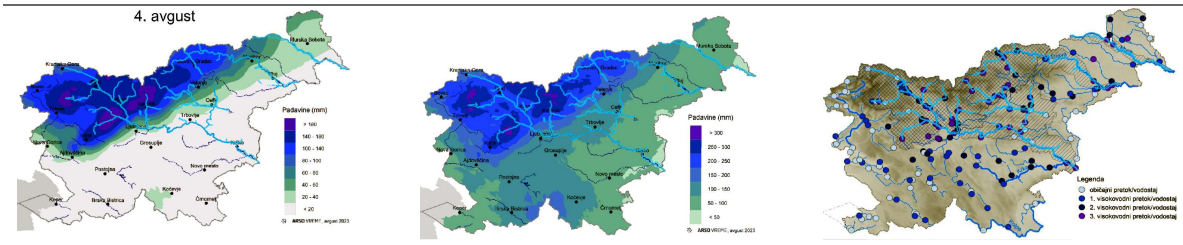


*Figure 1: Maps of (a) cumulative precipitation on August 4 2023 (b) precipitation on days from 4 to 9 August 2023 and (c) river water level status on August 4 2023*

*Source: (Agencija Republike Slovenije za okolje, 2023)*

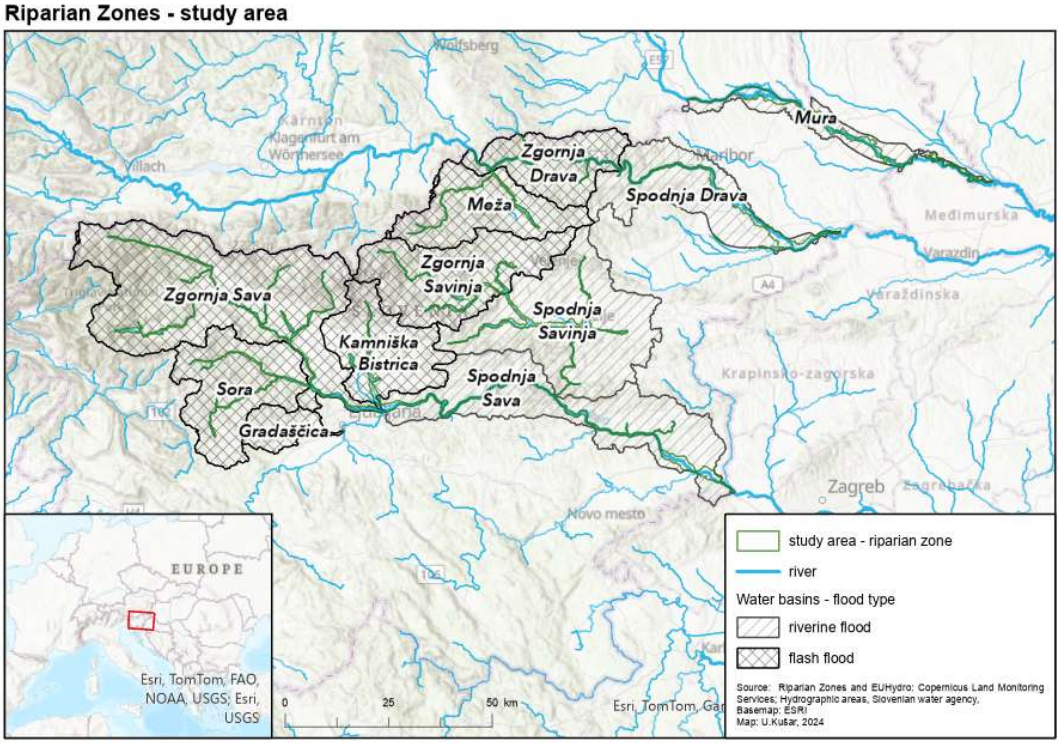


*Figure 2: Map of effected water basins and delineated riparian zones - study area*

### 1.3.1. Subdivision – water basins

The study aims to analyse the impacts of flood events on riparian zones, considering variations in flood occurrence types. The study area is partitioned into ten water basins, each allocated based on the type of flood occurrence. The primary criterion for allocation is the geographical location concerning the precipitation amount during the flood event. Water basins that received over 150 mm of rainfall are categorized as flash flood areas (Figure 1 b). These areas include the upper and middle Sava river basins, the Sora, Gradaščica, and Kamniška Bistrica water basins, the upper part of the Savinja water basin, the Meža water basin (including the tributary of the Mislinja river), and the upper part of the Drava river basin in Slovenia.

These basins are characterized by their geographical extent, encompassing high-lying alpine areas, and exhibit a typical snow-rainfall hydrological regime. The rivers and their tributaries often form steep and narrow gorges in the catchment areas, which transition into terraced valleys downstream. The river plains are anthropogenically modified and regulated, with partial urbanization. Particularly in the lower areas, rivers and riparian zones have undergone significant modification and regulation to mitigate channel alteration, manage floods, facilitate agricultural activities, and accommodate human settlements and energy infrastructure.

The study includes water basins downstream of the regions experiencing intense rainfall. This encompassed the lower reaches of the Sava, Savinja, and Drava rivers, as well as the Mura River

catchment area, allowing for comparisons between floods exhibiting characteristics more akin to typical riverine floods. In contrast to flash floods, these floods typically manifest with slower rates of water rise and fall, lower flow velocities, prolonged inundation durations, and comparatively larger flooded extents, albeit with shallower depths (Bell and Om Kar, 1969; Diakakis et al., 2020).

The riparian zones of these river basins are distinguished by the presence of extensive (former) floodplains, albeit in large part modified by human activities. These modifications include channel regulation, dam construction for hydropower generation, and the implementation of various flood control measures. Some river areas, such as those along the Mura River, also feature extensive floodplains characterized by riparian forest and semi-natural vegetation.

### 1.4. Aim and objectives

This study aims to use geospatial analysis and freely accessible remote sensing products to explore how floods impact riparian zones depending on flood type and land cover/ land use, using the August 2023 flood event in Slovenia as a case study.

The goal is to answer the following questions:

- Can flood-affected areas in sub-alpine regions during flash flood events be accurately identified using open-source satellite remote sensing products from Copernicus earth observation programs Sentinel-1 and Sentinel-2? Which indices are effective, and which ones cannot be recommended for this purpose?
- Are disparities in land cover/land use within riparian zones manifested in the observable effects of flooding? Is there a difference in water basins affected by different types of flood (flash flood/ riverine flood)? Can an effect of flood protection by riparian green buffer be identified?

To answer these questions specific objectives are set:

1. To delineate flood-affected areas within study area's riparian zones (potential riparian zones as delineated by Copernicus Land Monitoring Service) by exploring and applying optical imagery spectral indices (specifically NDVI, NDWI, AWEInsh, BI, SAVI, NDMI) derived from Sentinel-2 products, and Sentinel-1 SAR products (VH, VV polarisation) to pre- and post- study event situation, using pixel-based change detection approach.
2. To compile and classify ground-truth samples (points), utilizing various auxiliary data, including post-event orthophotos, Rapid Mapping Products, and damage claims for humanitarian organizations (flooded buildings).
3. To conduct a point-based accuracy assessment (confusion matrix with calculated producers', users', and overall accuracy) to validate the performance and compare the suitability of various indices from objective 1, by land cover/ land use class and flood type (flash flood/ riverine flood).

4. To use a geospatial approach for delineation of flooded areas based on the findings from objective 1 and 3.
5. To identify differences in flooded area within riparian zones of affected water basins, in various land cover/ land use categories (e.g. urban, forested/semi-natural, agricultural, grassland), taking into account the different types of flood event (riverine flood, flash flood). Spatial analysis addresses:
    - flooding extent across areas of different land use types, in comparison to the predictions derived from flood risk maps;
    - riparian zone landscape pattern, with focus on riverbanks land cover/ land use and connectivity of forested riparian buffer;
    - relationship between flooded buildings and existence of forested green buffer.

### 1.5. Limitations of the research

The study aims to explore basic resources to achieve objectives. In most of the steps only (simple) straightforward approaches for pre-processing, processing and post-processing remote sensing products are used. More complex and advanced methods are available, and were applied with various successes (Lombana and Martínez-Graña, 2022; TV and K N, 2019).

The study is based on freely available open-source data, focusing on products from Copernicus programme. Use of other data sources e.g. with higher spatial or temporal resolution could produce more detailed and more accurate results.

The study of the riparian zones does not aim to be a thorough geographical study of the area/impacts; its observation is limited only to a few elements.

### 1.6. Structure of thesis

Chapter one focuses on introduction of topic, including literature review, study area and event, presents aim and explains limitations of the research.

In chapter two research approach and conceptual framework are presented. Methods, data sources and tools are presented for both parts of the research: firstly, the detection of flooded areas with remote sensing products and secondly, applying the results to assess the impact of floods on riparian zone.

Chapter three presents the results of applied procedures and provides basic analysis. Deeper analysis and synthesis on the results is discussed in chapter four, including possible implications of the findings, assessment of strength and weaknesses of applied approach and suggestions for further work. Summary of the study and final remarks are presented in concluding, fifth chapter. Thesis includes list of tables, figures and references.

# 2. METHODS AND MATERIALS

## 2.1. Research Approach

After the selection of a topic for the study, a thorough literature review was conducted to gather existing knowledge, theories, and relevant findings. The literature review includes the topics: flood types, flood impacts, riparian zones, spatial analysis of land cover/ land use, riparian vegetation buffer, flood detection with satellite-based spectral indices and SAR products, and verification-accuracy assessments of derived products.

Based on the aim of the study and findings from the literature review a research approach was selected. It includes:

- Supervised pixel-based approach with thresholding for detection of open water areas and change detection approach with identification of relative differences in spectral indices (Sentinal-2), dual polarisation (Sentinel 1) for detection of flood-impacted areas;
- Accuracy assessment: point-based accuracy assessment approach with the calculation of confusion matrix and relevant metrics (total accuracy, producer accuracy, user accuracy) to verify the relevance of the resulted flooded area;
- Geospatial analysis with multiple techniques (overlay, landscape pattern analysis, proximity analysis, descriptive statistics) to identify spatial relationships and patterns of flood-impacted riparian zones.
- Use of a cloud-based platform to process remote sensing products.
- Use of GIS tools to perform geospatial analyses.

## 2.2. Study Conceptual Framework

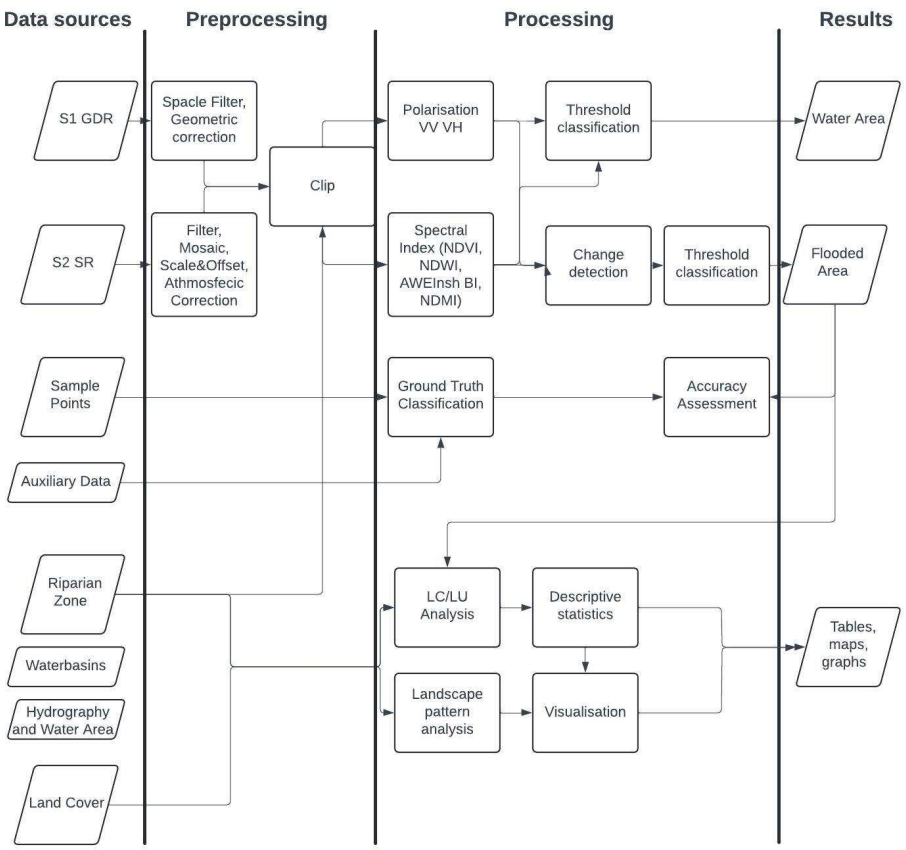


*Figure 3: Methodology flowchart*

## 2.3. Methods, tools and data

### 2.3.1. Geospatial data

#### 2.3.1.1. Sentinel-1 SAR (S1)

Sentinel-1 data offers several advantages for flood damage assessment, including its all-weather capability, high spatial resolution, frequent revisit times, and free and open access policy. These characteristics make it a valuable tool for monitoring and assessing flood events on a large scale and in near real-time.

Sentinel-1(S1) is a satellite mission developed by ESA as part of the Copernicus program for Earth observation. The S1 constellation consisted of two satellites, Sentinel-1A and Sentinel-1B, launched in 2014 and 2016, respectively, but the spacecraft of Sentinel 1B experienced an anomaly related to the instrument electronics power supply and is unable to deliver radar data since 23rd December 2021. The launch of Sentinel-1C is planned at the beginning of 2024 (Sentiwiki, 2024).

S1 is in a near-polar, sun-synchronous orbit with a 12-day repeat cycle and 175 orbits per cycle for a single satellite (Sentiwiki, 2024). It carries a C-band SAR instrument that provides all-weather, day-and-night imaging capabilities. S1 can collect several different images from the same series of pulses by using its antenna to receive specific polarisations simultaneously and is a phase-preserving dual polarisation SAR system. It can transmit a signal in either horizontal (H) or vertical (V) polarisation, and then receive in both H and V polarisations (Sentiwiki, 2024).

S1 data is collected with several different instrument configurations, resolutions, band combinations during both ascending and descending orbits (Google Developers, 2024). It requires several pre-processing steps. (Google Developers, 2024).

For this study S1 data collection were acquired from Google Earth Engine platform. The collection available includes the S1 Ground Range Detected (GRD) scenes, processed to generate a calibrated, ortho-corrected product. Each scene was pre-processed with European Space Agency's Sentinel-1 Toolbox (Sentinel Online, 2024) in following steps: applying orbit file, remove thermal noise, removing GRD border noise, radiometric calibration to $\sigma 0$ an range-doppler terrain correction (Google Developers, 2024). The output are the geocoded backscatter bands calibrated to the normalized radar cross section $\sigma 0$ in dB scale as well as a band containing the nominal incidence angle $\theta i$ (Vollrath et al., 2020). In the S1 collection each scene has one of 3 resolutions (10, 25 or 40 meters), 4 band combinations (corresponding to scene polarization) and 3 instrument modes.

The characteristics of the study area – relatively vast extent and diverse, steep terrain - require production of the mosaic dataset from several images and additional pre-processing. Filtering and further processing were done with geemap (Wu, 2020), a Python package for interactive mapping with Google Earth Engine (GEE), which is a cloud computing platform with a multi-petabyte catalogue of satellite imagery and geospatial datasets (Gorelick et al., 2017; Wu, 2020).

Parameters for filtering down to homogenous datasets included a selection of instrument mode, time frames, and orbit pass direction (ascending or descending).

The Interferometric Wide (IW) swath mode was selected as a suitable instrument mode. IW is the main acquisition mode over land and acquires data with a 250 km swath at 5 m by 20 m spatial resolution (single look) (Sentinel Online, 2023).

Time periods for pre-event, during event, and post-event were framed with the objective of obtaining images available for a) relevant event, b) with matching orbit pass directions, and c) full coverage of the study area with minimum time distance within the single mosaic. Figure 4 presents selected parameters.

To avoid radiometric distortions over rugged terrain, that originate from the side-looking SAR imaging geometry, which can be strong enough to exceed differences in the signal due to variations in land cover

(Small, 2011), the angular-based radiometric slope correction routine proposed by (Vollrath et al., 2020) was applied.

Next necessary step is to reduce speckle noise. Speckle manifests as a textured "salt and pepper" pattern in an image, resulting from the random constructive and destructive interference of multiple scattering returns within each resolution cell. (Jaybhay and Shastri, 2015). The speckle effect was reduced by applying smoothing with a 3x3 median filter to each of the mosaic datasets.

Mosaic datasets were produced for each period and each polarization, and clipped to the study area – with riparian zone (RZ) vector layer. The default projection was set to ETRS89 / LAEA Europe (EPSG 3035).

| **Pre event** | **Event (During event)** | **Post event** |
|---|---|---|
| **Orbit pass direction:** | | |
| ascending | ascending | ascending |
| **Time frame** | | |
| 24.-31.7.2023 | 5.8.2023 | 12.-17.8.2023 |
| **Images** | | |
| 20230724T165056_20230724T165121_049568_05F5D7_97E5<br>20230729T165906_20230729T165931_049641_05F820_CA6A<br>20230731T164253_20230731T164318_049670_05F906_287E | 20230805T165057_20230805T165122_049743_05FB3C_AB7B | 20230812T164253_20230812T164318_049845_05FEAD_261A<br>20230817T165057_20230817T165122_049918_060121_5E3A |
| **Bands – polarisation** | | |
| VV, VH | VV, VH | VV, VH |
| 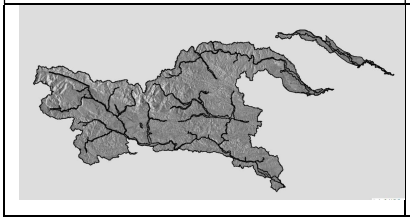 | 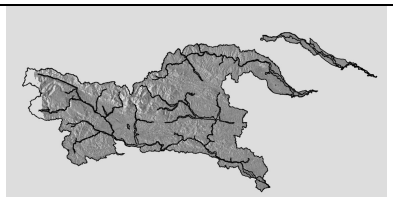 | 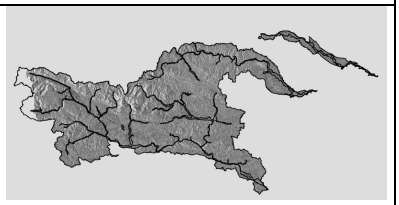 |

*Figure 4: COPERNICUS/S1_GRD image selection for pre-event, event and post event time frames, matching orbit pass (ascending) and selected polarisation bands.*

*Source: Contains modified Copernicus Sentinel data [2024] processed by Google Earth Engine*

#### 2.3.1.2. Sentinel-2 (S2)

Like Sentinel-1, a Sentinel-2 (S2) is a satellite constellation developed by the European Space Agency (ESA) as part of the Copernicus program. It consists of twin satellites, Sentinel-2A and Sentinel-2B, launched in 2015 and 2017, respectively (Sentiwiki, 2023).

Sentinel-2 satellites carry a multispectral instrument. They produce spectral bands, ranging from visible to shortwave infrared. Its high spatial resolution (10 meters to 60 meters) and frequent revisit times

(every 5 days) make it well-suited for applications requiring detailed and up-to-date information about the land surface (Sentiwiki, 2023).

| Pre event | Event | Post event |
|---|---|---|
| Period: | | |
| 14.-16.7.2023 | 4.-5.8.2023 | 13.8.2023 |
| 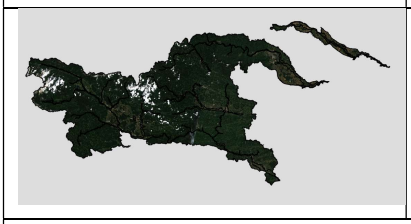 | 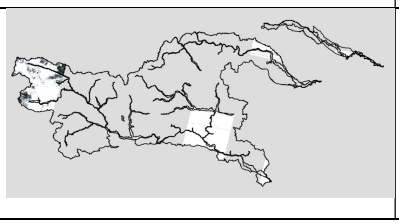 | 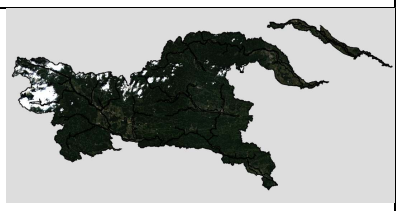 |
| Cloudless image available for the study area (riparian zone) –share of total area | | |
| 99,3% | 0% | 96,1% |
| Images | | |
| 20230714T095559_20230714T100440_T33TUM<br>20230714T095559_20230714T100440_T33TVL<br>20230714T095559_20230714T100440_T33TVM<br>20230714T095559_20230714T100440_T33TWL<br>20230714T095559_20230714T100440_T33TWM<br>20230714T095559_20230714T100440_T33TXM<br>20230716T095031_20230716T095032_T33TWL<br>20230716T095031_20230716T095032_T33TWM<br>20230716T095031_20230716T095032_T33TXM | 20230805T095031_20230805T095033_T33TVL<br>20230805T095031_20230805T095033_T33TWL<br>20230805T095031_20230805T095033_T33TWM<br>20230805T095031_20230805T095033_T33TXM | 20230813T095559_20230813T100712_T33TUM<br>20230813T095559_20230813T100712_T33TVL<br>20230813T095559_20230813T100712_T33TVM<br>20230813T095559_20230813T100712_T33TWL<br>20230813T095559_20230813T100712_T33TWM<br>20230813T095559_20230813T100712_T33TXM |

*Figure 5: COPERNICUS/ S2_SR_HARMONIZED image selection for pre-event, event and post event time frames, minimal cloud cover (if available) and share of cloudless study area (riparian zone).*

*Source: Contains modified Copernicus Sentinel data [2024] processed by Google Earth Engine*

For this study, S2 data collection was acquired from Google Earth Engine platform. The collection available includes Harmonized Sentinel-2 MSI: MultiSpectral Instrument, Level-2A dataset ((Google Developers, 2023) provided originally by ESA, with application of atmospheric correction processor Sen2Cor to ensure correction of satellite images for atmospheric effects (Main-Knorn et al., 2017). The collection contains 16 spectral bands representing SR scaled by 10000, several L2-specific bands including three QA bands, where one (QA60) is a bitmask band with cloud mask information (Google Developers, 2023).

Filtering and additional pre-processing are done by processing with geemap (Wu, 2020), a Python package for interactive mapping with Google Earth Engine (GEE).

The characteristics of the study area, event, and limitation of optical imagery, relatively vast extent and cloudy conditions accompanying flood events, require the production of the mosaic dataset from several images and additional pre-processing.

Time periods for pre-event, during event, and post-event were framed with the objective to obtain images available for a) relevant event, b) minimal cloud cover, and c) full coverage of the study area with minimum time distance within the single mosaic. Figure 5 presents selected parameters.

Mask with of the study area with cloudless condition in pre event and post event images was produced using s2cloudless algorithm and COPERNICUS/S2_CLOUD_PROBABILITY dataset available on GEE (Batič, 2018; Google Developers, n.d.; Sanchez et al., 2020).

Mosaic datasets were produced for each period, based on the quality layer (QA60) for minimum cloud probability clipped to the study area using riparian zone (RZ) vector layer. Additionally, the cloudless mask was applied to enable pre-post change detection.

Eemont Python package (Montero, 2021) was used to apply suitable scale and offset as well as to calculate spectral indices (Montero et al., 2023). The default projection was set to ETRS89 / LAEA Europe (EPSG 3035).

#### 2.3.1.1. Riparian Zones (RZ)

Delineation of Riparian Zones (RZ) is one of the Riparian Zones products, whose production was coordinated by the European Environment Agency in the frame of the EU Copernicus program (EEA geospatial data catalogue, 2015). The delineation of Riparian Zones is produced as a variable buffer zone of selected rivers (Strahler levels 2-9 derived from EU-Hydro) across Europe and is based on a complex spatial modelling approach, making use of the Riparian Zones' LC/LU classification, large-scale earth observation data and a range of additional geo-data sources, as well as derived spatially explicit indicators (Weissteiner et al., 2016). Inputs are regionally parameterized and weighted according to relative importance in a fuzzy modelling approach (Weissteiner et al., 2016).

In this study, a vector layer Potential Riparian Zones was used primarily as a layer delineating area of interest. Potential Riparian Zones mapped areas with a natural, physio-geographic disposition to host riparian zones. RZ are modelled based on the input features river network, terrain topography, soil properties, flood zones, modelled topographic wetness, and the land cover/land use (LCLU) class "Water" (Weissteiner et al., 2016).

The dataset is available ETRS89 / LAEA Europe (EPSG 3035) projection.

The dataset in shape format was acquired from European Environment Agency's Datahub: https://www.eea.europa.eu/en/datahub/datahubitem-view/85448806-1cd8-4fdf-95f5-fe13e1371943?activeAccordion=1083709

#### 2.3.1.1. Hydrographic Areas (WBASINS)

The hydrographic areas dataset (WBASINS) is a spatial collection in the Water Cadastre, an official national data source managed by the Slovenian Water Agency (INSPIRE SI, 2023a; Kušar and Vrenko, n.d.). Data collection includes hierarchically organized hydrographic areas, delineated by watershed boundaries, organized and coded in 4 levels based on the Slovenian hydrographic network: At the highest level, Slovenia is divided into six main hydrographic regions: Sava River basin; Kolpa River basin; Drava River basin; Mura River basin; Coastal basin; Soča River basin. At the next level, there are 31 of water basins, and at the third level, there are 155. At the lowest, fourth level, there are a total of 583 hydrographic areas/ water basins.

The dataset was acquired from eVode Portal: http://www.evode.gov.si/index.php?id=84

The dataset was projected to ETRS89 / LAEA Europe (EPSG 3035) projection.

#### 2.3.1.2. Hydrography and Water Lands (VZ)

Hydrography and Water Lands Dataset (EHVZ) is part of the spatial data collection in the Water Cadastre, an official national data source managed by the Slovenian Water Agency (INSPIRE SI, 2023a; Kušar and Vrenko, 2017). The land on which continental water is permanently or occasionally present, forming special hydrological, geomorphological, and biological conditions that determine the aquatic and riparian ecosystem, is referred to as water land of continental waters (WL).

Water land of running waters includes the main bed of running waters, including the riverbank, up to a significant geomorphological change. Water land of standing waters includes the bottom of standing waters, including the shore, up to the highest recorded water level. Abandoned riverbeds and gravel bars periodically flooded by water, marshes, and land flooded by water due to spatial intervention are also considered water land (INSPIRE SI, 2023a; Kušar and Vrenko, 2017).

Areas of continental waters are presented by hydrography layers – liner for watercourses axis and narrow linaer objects (HIDRO-LIN), whereas watercourses which are wider than 2 m meters are presented also by polygons (HIDRO-POLY) capturing the area inundated for most part of the year, representing areas of permanent water bodies.

The datasets WL, HIDRO-LIN and HIDRO-POLY were acquired from eVode Portal: http://www.evode.gov.si/index.php?id=84.

The datasets were projected to ETRS89 / LAEA Europe (EPSG 3035) projection.

#### 2.3.1.3. Land Use Database (RABA)

The Land Use Database (RABA) is a unified official dataset of the actual use of agricultural and forest land. A basic mapping unit is a polygon of actual use, which is the consolidated area of land of the same type. It is primarily intended to determine the state of land use as a condition for the implementation of measures of the common agricultural policy of the European Union (INSPIRE SI, 2023b).

The data for actual land use records are primarily sourced from orthophotos (aerial photographs), supplemented by additional information gathered from field visits conducted by the Ministry of Agriculture and other control authorities, as well as input from customers. Daily maintenance of the data occurs at two levels: capture and verification (INSPIRE SI, 2023b). The reported spatial resolution of RABA dataset is 1:5000.

Data are acquired from the Ministry's web page: https://rkg.gov.si/vstop/.

The dataset was projected to ETRS89 / LAEA Europe (EPSG 3035) projection.

#### 2.3.1.4. Integrated map of flood risk (IKPN)

The integrated map of flood risk (IKPN) is part of the spatial data collection in the Water Cadastre, an official national data source managed by the Slovenian Water Agency (Kušar and Vrenko, 2017). Areas of flood hazard are primarily determined based on flood warning maps, preferably for areas where there may be significant risk. The determination of these areas is carried out using modelling and analysis methods based on hydrological, geological, geomorphological, and geodetic data, as well as land use and land cover data.

Spatial objects represent the extent of areas prone to flooding at the Q500 Q100 and Q10 flow rates. Hydrological-hydraulic studies have defined hydraulic processing areas and areas of validity (OVR) of hydraulic model results. The primary purpose of the data layer is to provide a detailed representation of flood conditions in a specific area and to provide a professional basis for classifying flood-prone areas into flood hazard classes. The data is also intended for planning flood risk reduction measures, spatial planning and spatial interventions, informing and raising public awareness, planning protection and rescue measures, and fulfilling international obligations (INSPIRE SI, 2023c)

For this study vector layer of areas prone to flooding at the Q100 flow rate was used, along with the area of validity (AOV) of the results.

The dataset was acquired from: eVode Portal: http://www.evode.gov.si/index.php?id=84

The dataset was projected to ETRS89 / LAEA Europe (EPSG 3035) projection.

#### 2.3.1.5. Buildings (BA)

Locations of buildings data are included in the Realestate cadastre managed by Slovenian Mapping and Survaying Authority. The realestate cadastre is the fundamental record of the Republic of Slovenia's data on the location, shape, physical and other characteristics of plots, buildings and parts of buildings, which shows the actual state of real estate.

The dataset was acquired from: eProstor Portal: https://www.e-prostor.gov.si/podrocja/parcele-in-stavbe/kataster-nepremicnin/?acitem=1707-1708

The dataset was projected to ETRS89 / LAEA Europe (EPSG 3035) projection.

#### 2.3.1.6. Other - auxiliary data

Auxiliary geospatial datasets were used as reference layers for the classification of "ground truth" sample points in verification process, as well as a reference layer for interpretation of the results. Auxiliary datasets are listed in Table 4.

*Table 4: Auxiliary geospatial datasets*

| Geospatial Dataset | Theme | provider | Processing |
|---|---|---|---|
| **Poplavljena_obmocja_avgust_2023_CIR**<br>**Poplavljena_obmocja_avgust_2023_RGB** | post event areal ortho-photos | Slovenian Water Agency | Mosaic, projection |
| **EMSR680 - Flood in Slovenia, Rapid Mapping Product** | Flooded areas, impacted infrastructure for selected areas in Slovenia – maps and , various products | Copernicus Emergency Management Service | |
| **Flooded homes** | Locations of flooded houses– damage claims | Red Cross Slovenia | Addresses' geocoding |
| **Water infrastructure repair operations** | Locations of operations | Slovenian Water Agency | projection |
| **Hydrography** | Hydrography network (rivers, streams, objects) | Slovenian Water Agency | projection |

### 2.3.2. Water and flooded areas detection in remote sensing

Pre-processed S1 and S2 mosaics were used a) to detect flooded/ open water areas and b) to detect changes caused by floods as an indicator of flood-impacted - flooded areas.

#### 2.3.2.1. Water area detection in S1 (SAR)

Open water areas were delineated with the application of selected thresholds to both polarisation bands – VV and VH. Previous studies (e.g. Bangira et al., 2021; Zhang et al., 2018) suggest that both are suitable for flood mapping.

SAR data are particularly suited for binarisation of images to water/non-water areas. In this study threshold value was set with the use of Otsu's algorithm (Table 6). Pre-event and during-event S1 mosaics were used to detect areas with open water. Detection of flooded vegetation, which could be expressed with high backscatter values of double-bounced signals, was tested (not shown), but was not successful, presumably because of excessive confusion with urban and other areas with high backscatter characteristics.

Calculated values for thresholds using Otsu's algorithm have not changed significantly between the three S1 mosaics (pre-event, during-event) mosaics, indicating high comparability, especially with VV polarisation (Table 6).

*Table 5: S1 mosaic's bands – polarisations and medium in the focus of detection*

| **Polarisation** | | **Medium** |
|---|---|---|
| **VH** | Vertical transmit – horizontal receive | open water |
| **VV** | Vertical transmit – vertical receive | open water |

*Table 6: S1 data selected threshold and applied thresholding approach*

| | **Threshold – Otsu** | | | **Applied Threshold approach** |
|---|---|---|---|---|
| | Pre-event | During-event | Post-event | |
| **VH** | ≤-17.4 | ≤-17.7 | ≤-17.4 | Otsu |
| **VV** | ≤-11.7 | ≤-11.7 | ≤-11.7 | Otsu |

#### 2.3.2.2. Flooded area detection in S1 (SAR)

The applied approach for detecting flood-impacted areas was the change detection procedure suggested by UN-SPIDER for "Flood Mapping and Damage Assessment Using Sentinel-1 SAR Data in Google Earth Engine" (UN-SPIDER, 2023), with some adaptation in data pre-processing (terrain correction, spackle filter).

One of the most important advantages of SAR products over optical imaging is their availability in cloudy conditions, which are normally present during a flood event (Tarpanelli et al., 2022). To exploit this advantage, the change detection was applied to pre-event / during-event S1 mosaics. Post-event mosaic is available for the later period but was deemed as less useful, particularly considering that open water is no longer present (Agencija Republike Slovenije za okolje, 2023) and soil moisture is less expressed compared to the situation during or immediately after the flood event.

Suggested change detection is based on a simple, straightforward change detection approach: dividing the during-event mosaic by the pre-event S1 mosaic to generate a raster layer illustrating change intensity per pixel. Bright pixels represent high change, while dark pixels indicate minimal change. (UN-SPIDER, 2023).

In next step binary pixel- based classification to flooded/ unflooded pixels is conducted. A threshold of 1.15 was applied, assigning 1 to values above 1.15 and 0 to values below. The threshold value of 1.15 was selected by on trial and error (expert assessment) and is lower as the value 1,25 proposed as the baseline in UN-SPIDER approach. Detection of flooded vegetation, which is expressed with an increase of backscatter values caused by increase of double-bounced signals, was conducted by applying 0,7 threshold for binary classification – values below threshold were assigned class *flooded vegetation*. A threshold was selected on trial and error basis. Change detection was conducted for both polarisation bands (VV and VH).

#### 2.3.2.3. Water area detection in S2 (Spectral indices)

Open water areas were delineated with the application of fixed, empirical based thresholding to spectral indices bands, produced in the pre-processing. Spectral indices were selected (Table 7) from a long list of available indices (Montero et al., 2023) based on their use frequency, diversity of media in focus, and diversity of spectral bands that are used for their calculations. The objective of selection was the exploration of diverse spectral band combinations for this specific flood event, characterized by different flood types (flash flood/ riverine flood).

*Table 7: Applied spectral indices overview.*

| | Name | Formula | Sentinel 2 Bands | Medium | Reference |
|---|---|---|---|---|---|
| **BI** | **Bare Soil Index** | **((SWIR1 + RED) - (NIR + BLUE))/ ((SWIR1 + RED) + (NIR + BLUE))** | **B2, B4, B8, B11** | **bare soil** | **Rikimaru et al., 2002** |
| **NDMI** | **Normalized Difference Moisture Index** | **(NIR-SWIR1)/ (NIR+SWIR1)** | **B8, B11** | **moisture in vegetation** | **Wilson, E. H., & Sader, S. A., 2002** |
| **NDVI** | **Normalized Difference Vegetation Index** | **(NIR-RED) / (NIR+RED)** | **B4, B8** | **vegetation** | **Rouse, 1974** |
| **SAVI** | **Soil-Adjusted Vegetation Index** | **(1.0+0,5)×(NIR-R) / (NIR+RED+0,5)** | **B4, B8** | **vegetation** | **Heute, 1988** |
| **AWEInsh** | **Automated Water Extraction Index with Shadows Elimination** | **„0×(GREEN - SWIR1) – 0,2×(NIR+ 2.,75×SWIR2)** | **B2, B3, B8, B11 , B12** | **water** | **Feyisa, G. L., Meilby, H., Fensholt, R., & Proud, S. R. (2014)** |
| **NDWI** | **Normalized Difference Water Index** | **(GREEN-NIR)/(GREEN+NIR)** | **B3, B8** | **water** | **McFeeters, 1995** |

Binarisation of S2 mosaic to water/ non water areas using thresholds was done with different approaches. For indices that are focused on water media (NDWI, AWEInsh) and present bi-modal histogram for study area, automatic Otsu's approach was used. For other indices Otsu's threshold values were calculated, but only as an indication for histogram based trial and error approach.

*Table 8: Spectral indices – classification thresholds – water area*

| | Threshold – Otsu | Threshold - applied | Applied Threshold approach |
|---|---|---|---|
| **BI** | ≥ 0,06 | ≥ 0,2 | Histogram/ expert |
| **NDMI** | ≤ -0,01 | ≤ -0,12 | Histogram/ expert |
| **NDVI** | ≤ -0,13 | ≤ -0,13 | Otsu |
| **SAVI** | ≤ -0,06 | ≤ -0,15 | Histogram/ expert |
| **AWEInsh** | ≥ 0,09 | ≥ 0,2 | Histogram/ expert |
| **NDWI** | ≥ 0,12 | ≥ 0,12 | Otsu |

#### 2.3.2.4. Flooded area detection in S2 (Spectral Indices)

The change detection approach for flood-impacted area is based on the observation that very few flood events/ flooded areas can be observed with satellite remote sensing images during the event, due to the

timing of images and cloud cover (Atefi and Miura, 2022; Tarpanelli et al., 2022; Tavus et al., 2022). This is particularly true for flash flood events (Atefi and Miura, 2022; Cerdà et al., 2021), which are common in European sub-alpine areas. Changes are calculated using simple pixel-by-pixel difference between pre-event and post-event values of spectral indices.

Binary pixel- based classification was used to differentiate flooded and unflooded pixels. For each index difference image, a threshold is applied, assigning 1 to flooded and 0 to unflooded class pixels. Thresholds were index specific, calculated with the help of Otsu's algorithm, but in most cases corrected with visual inspection of histograms and trial and error. Table 9 provides thresholds

*Table 9: Thresholds for classification of spectral indices' difference image to flooded and unflooded class.*

| | **Threshold – Otsu** | **Threshold - applied** | **Applied Threshold approach** |
|---|---|---|---|
| **BI** | ≥0,03 | ≥0,20 | Histogram/ expert |
| **NDMI** | ≤0,01 | ≤-0,12 | Histogram/ expert |
| **NDVI** | ≤ -0,13 | ≤-0,13 | Otsu |
| **SAVI** | ≥ -0,03 | ≥-0,15 | Histogram/ expert |
| **AWEInsh** | ≥ 0,09 | ≥-0,20 | Histogram/ expert |
| **NDWI** | ≥ 0,12 | ≥ 0,12 | Otsu |

*Figure 6: Areal ortophotos (left) before event (right) after (left) the event on August 7 2023.*

*Flood event impacts that can be detected with changed spectral characteristics in visual spectrum include overflown water areas, erosion of riverbanks, deposition of material on agriculture, forest and urban areas, uprooting of vegetation, damages of infrastructure and buildings.*

*Source: Contains modified Slovenian Water Agency's data (2024), processed by The Water Atlas, Slovenian Water Agency.*

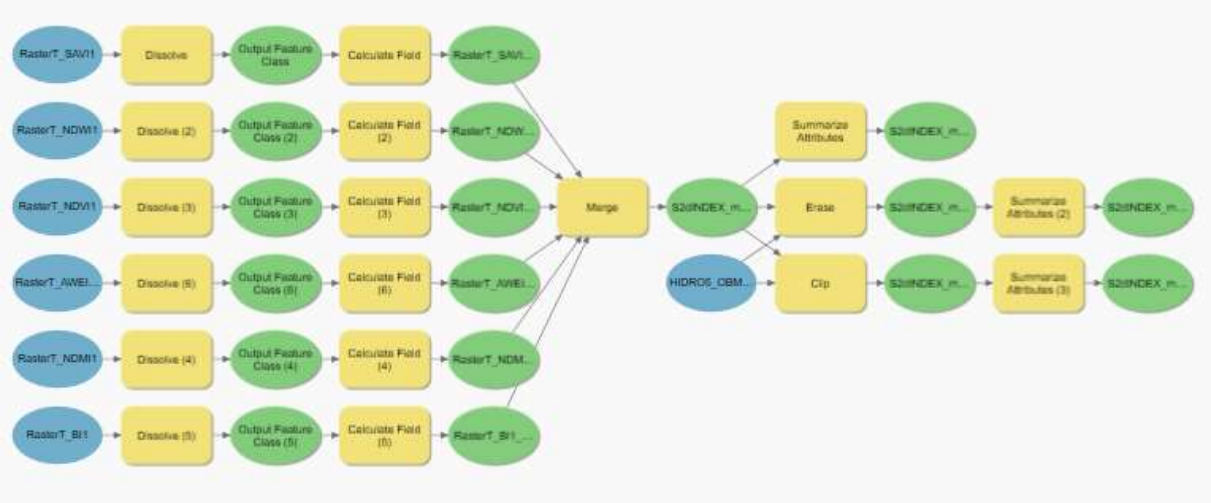


*Figure 7: Model of S2dINDEX calculation and summary statistics*

*Source: modified from ArcGIS PRO, 2024*

### 2.3.3. Ground Truth Samples

Ground Truth Samples (GT Points) for accuracy assessment analysis were created as points in a stratified random sample in River Zone (RZ) using ArcGIS Pro tool. The stratification was based on land use categories in the Land use database (RABA) and flood type categories from WBASINS layer.

GT Points were classified as flooded/ unflooded with point-by-point assessment based on:

- visual interpretation from Post event orthophotos (RGB, CIR)
- EMSR680 - Flood in Slovenia, Rapid Mapping Products (Copernicus)
- geolocated damage claims (humanitarian organizations)
- locations of reported water infrastructure repair works
- georeferenced photos from social media.

None of the above sources was available for the entire extent of the study area, with better coverage of the sub-alpine water basins (more damaged) and less in south-eastern water basins with less severe flood impacts to urban areas and infrastructure.

### 2.3.4. Accuracy assessment

Overall accuracy (OA), producers' (PA) and users' accuracy (UA) were used to assess the flooded areas results of change detection. A cross-tabulation of the flooded class areas in the products versus the flooded/unflooded classification of ground truth sample points was presented in the confusion matrix, produced with the Compute Confusion Matrix tool in Arc GIS Pro.

Points with true positives (TP), true negatives (TN), false positives (FP), and false negatives (FN) were counted and presented with the metrics for two flood type categories (flash flood/ riverine flood) and four land cover/ land use categories (forest, grassland, agricultural and urban areas).

### 2.3.5. Flood area delineation

Final flooded area delineation was produced on the basis of results of previous steps and post-processing.

Based on accuracy assessment results the products with suitable overall quality were selected for further processing. Post-processing included overlay analysis with layers resulting from processing data with other indices. Unions of flooded area layers (results analysis from previous steps) were created and tested for accuracy. To enhance spatial coherence and remove noise spatial filtering of small isolated areas (1 pixel) and merging adjacent pixels into larger areas were applied.

Dataset was converted from raster to vector for further applications. The result is a vector layer with polygons representing riparian zone areas that were flooded in the August 2023 flood event in Slovenia in with minimum mapping unit of 10x10m in ETRS89 / LAEA Europe (EPSG 3035) projection.

### 2.3.6. Riparian zone land use/land cover and flood

#### 2.3.6.1. Flooded area and land use/ land cover

Spatial analysis techniques, such as overlay analysis, buffering, and proximity analysis, is used in this study to assess the spatial relationships and patterns in flood impacted riparian zone.

Overlays of flooded areas layer included:

- flood type layer (WBASINS) to evaluate a rate of impact in relation to different flood types.
- land cover/ land use layer (RABA) to evaluate a rate of impact in relation to land cover/ land use type.
- flood risk map (IKPN) layer to evaluate the rate of impact to previously registered flood risk areas.

Descriptive statistics on water basin level and visualization using maps and graphs were used to facilitate the interpretation of results.

To gain further understanding of the water basins' characteristics regarding spatial patterns of land use, landscape pattern indices were calculated using ZonalMatrics, a Python package for zonal landscape structure analysis prepared to be used as a toolbox in ArcGIS (Adamczyk and Tiede, 2017).

Landscape pattern indices are quantitative measures used to characterize various aspects of spatial arrangement, configuration, and heterogeneity within landscapes. These indices provide information for

understanding landscape structure, dynamics, and ecological processes. Table 10 provides the list of used landscape pattern indices.

*Table 10: Landscape pattern indices description*

| Index | Description |
|---|---|
| **Patch Density (PD)** | Patch density measures the number of landscape patches per unit area. It indicates the degree of fragmentation or patchiness of different land use within a riparian zone of the water basin. |
| **Patch Size (PS)** | Patch size represents the average area of individual patches within the landscape (water basins). It provides insights into the distribution of patch sizes and the dominance of particular land use types. |
| **Edge Density (ED)** | Edge density quantifies the amount of edge or boundary between different land cover types within the landscape (water basins). It indicates the degree of landscape fragmentation and habitat diversity. |

#### 2.3.6.2. Riparian vegetation buffer

In mid – to lower altitudes of temperate zones, such as Slovenian sub-alpine and sub-pannonian region, forested vegetation is predominant natural vegetation of riparian zones. Techniques of spatial analysis and landscape pattern analysis were used to evaluate the presence and extent of riparian forest buffers in riparian zones of water basins as well as the level of flood-related impacts to them.

Riparian forest buffers (RFB) were delineated with spatial overlay ("select by location" tool in Arc GIS PRO) of patches with land use class "forest and semi-natural vegetation" in land use dataset (RABA) with water land areas dataset (VZ). Descriptive statistics (sum, share, average) were presented as well as visualization with maps and graphs.

To evaluate the characteristics of the riparian forest buffers of the water basins Spatial pattern metrics, including basic area metrics and connectedness metrics, were calculated with the use of ZonalMetrics - a Python toolbox for zonal landscape structure analysis (Adamczyk and Tiede, 2017).

Basic Zone Metrics was calculated for patches – land use polygons of forest and semi-natural vegetation class. Indicators of Connectedness Metrics were modified to present the connectivity of forest and water class. Metrics are calculated for patches of forest buffer i.e. forest patches that are connected to water land use class.

*Table 11: Landscape Pattern Indices - Zonal Metrics applied for Riparian Forest Buffer characterization*

| Index | Description |
|---|---|
| | **Basic Zonal Metrics** |
| **Class Area (CA)** | **Area of the patches of the corresponding class (forest) within the statistical zone (water basin).** |
| **Number of patches per class (NPC)** | **Number of patches for a class (forest) within the statistical zone (water basin).** |
| **Zone area (ZA)** | **Area of the statistical zone in which landscape metrics are calculated (water basin).** |
| **Percentage of zone (PZONE)** | **Percentage of the area of the class (forest) per statistical zone** |
| | **Connectedness Metrics** |
| **Number of Patches (CI-NP)** | **Number of distinct connected patches of forest in forest buffer** |
| **Connected area (CI-PA)** | **Area of parts of patches within the range of connection and its percentage per water basin** |
| **Share of connected area (CI-PP)** | **Percentage of connected patch area (forest buffer) to water basin** |

#### 2.3.6.3. Urban areas and buildings

To evaluate the impact of floods in riparian zones to urban areas and buildings with a focus on the presence of riparian forest buffers spatial pattern analysis and spatial proximity analysis were used.

##### 2.3.6.3.1. Urban – water contrast

Contrast Metrics from spatial pattern metrics were used to characterize water basins regarding the spatial position of urban areas next to water areas. High level of this contrasting relationship is assumed to represent the lack of riparian forest buffer – and less protection from them in case of flood related overflow and bank erosion events.

*Table 12: Spatial Pattern Indices – Contrast Metrics applied to characterize exposure of urban areas*

| Index | Description |
|---|---|
| | **Contrast Metrics** |
| **Edge Length(EL):** | length of a selected focus class sharing a boundary with corresponding contrast classes (calculated per class). |
| **Contrast Class Edge (CCE):** | percentage of edge length of the focus class shared with contrast classes |

##### 2.3.6.3.2. Flooded buildings

Spatial analysis with overlay and proximity analysis were performed to evaluate the impact of floods to the buildings regarding their location in relation to riparian forest buffers.

Buildings from BA layer were classified as flooded or unflooded with the overlay of the flooded area layer (FA).

For each building, the shortest distance to the nearest riparian forest buffer polygon (RFB) and distance to the nearest water area polygon (VZ) were calculated. Descriptive statistics as well as visualizations were presented for each water basin.

# 3. RESULTS

## 3.1. Introduction

On 4 August 2023, an extreme precipitation event occurred in Slovenia. Over a period of 6-12 hours, some areas of the Sava, Savinja and Drava river basins received up to 200 mm of precipitation. (Agencija Republike Slovenije za okolje, 2023). The rainfall caused spills in the form of river, surface and underground flooding and, with high velocities and increased erosive power, large movements of material. The areas of overflowing rivers and streams and areas altered by the action of water and erode and transported material were observed by the study using Sentinel-1 and Sentinel-2 satellite imagery.

Chapter 3.2 presents the results and accuracy assessment of flooded area delineation, chapter 3.3 results of spatial analysis of flood impacts in the riparian zone.

## 3.2. Results – Flooded area delineation

### 3.2.1. Sentinel-1 - SAR results

During the extreme precipitation event on August 5, 2023, open water covered approximately 25% of riparian zones in water basins affected by floods. This amounted to 11.096 out of 43.809 hectares of the studied area. Inundated areas were detected by applying thresholds set by Otsu's algorithm -11,4 dB for S1 during-event mosaic with VV polarisation. Same threshold applied to pre-event mosaic amounted approximately 4.243 ha fewer water areas, and similar for post-event mosaic, captured 9 days later (Table 13). Overlay with permanent water bodies layer (HIDRO-POLY) reveals that only smaller proportion of water areas (1.074 ha) were detected on surface of river and lakes and that 9.518 ha of detected open water areas could be considered flooded by method of single-image S1 thresholding approach. Same approach with VH polarisation (-17.4 dB threshold) is presenting even more interesting results, indicating that water areas more than a week after the event extended to 9.494 ha, which is more than areas during the event (8.812 ha), with 7.739 ha of this outside the polygon of permanent waters.

*Table 13: Water area/ flooded area - results of single image water detection approach and change detection approach based on Sentinel-1 SAR VV and VH polarisation.*

| | **Single image approach** | | | | | |
|---|---|---|---|---|---|---|
| | Water surface area (ha) | | | | | |
| | Pre-event | During-event | Post event | Water area Difference (During-event – Pre-event) | **Water area during event on permanent water bodies** | **Water area during event outside permanent water bodies** |
| **VV** | 6.853 | 11.096 | 6.945 | 4.243 | **1.074** | **9.518** |
| **VH** | 8.747 | 8.812 | 9.494 | 65 | **1.579** | **7.739** |

| | **Change detection approach** | | | | |
|---|---|---|---|---|---|
| | Areas (ha) – difference detected during flood/ pre flood | | | | |
| | Open water areas | Flooded vegetation | Flooded - total | Difference detected on permanent water areas | **Flooded outside permanent water areas** |
| **VV** | 3.650 | 8.039 | 11.689 | 887 | **10.802** |
| **VH** | 1.705 | 1.662 | 3.367 | 157 | **3.210** |

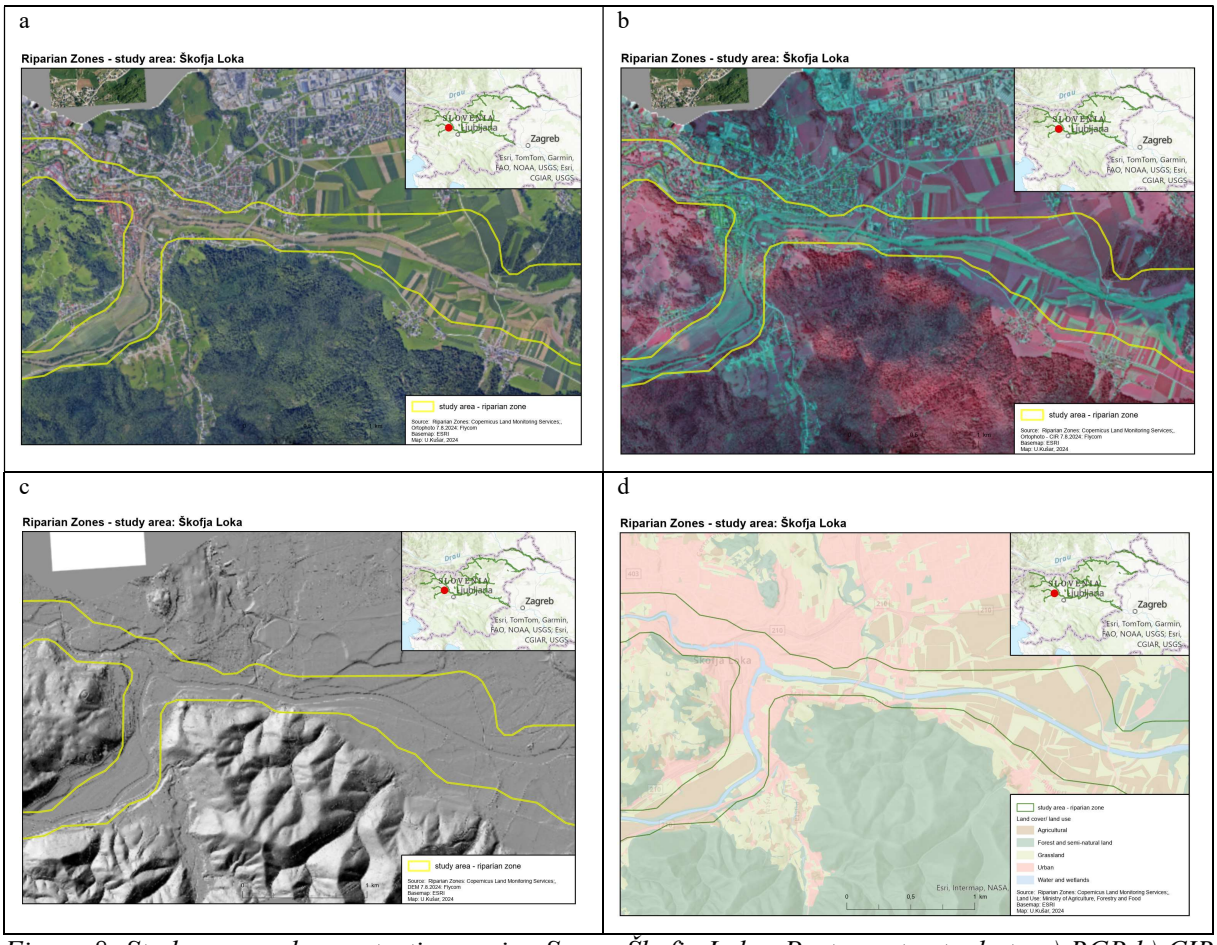


*Figure 8: Study area – demonstration region Sora - Škofja Loka; Post event ortophoto a) RGB b) CIR c) DEM d) Land use/ land cover*

a b

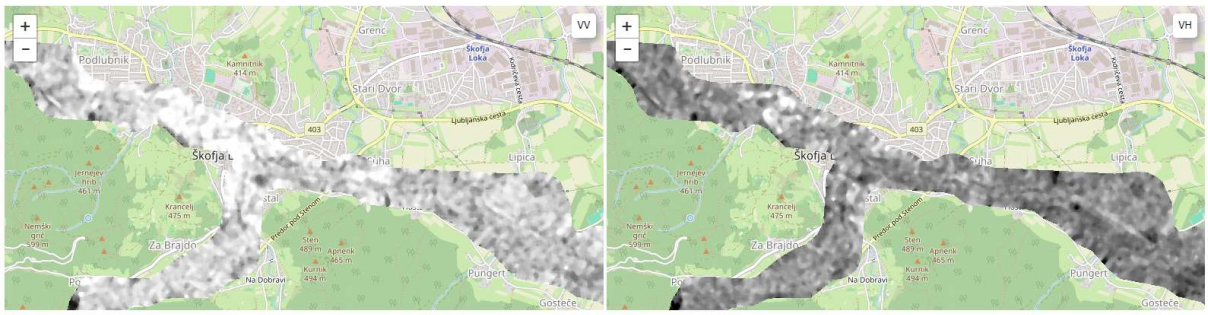


*Figure 9: Study area – demonstration region Škofja Loka: Pre-event S1 SAR a) VV b) VH*

*Source: Contains modified Copernicus Sentinel data [2024] processed by Google Earth Engine*

a b

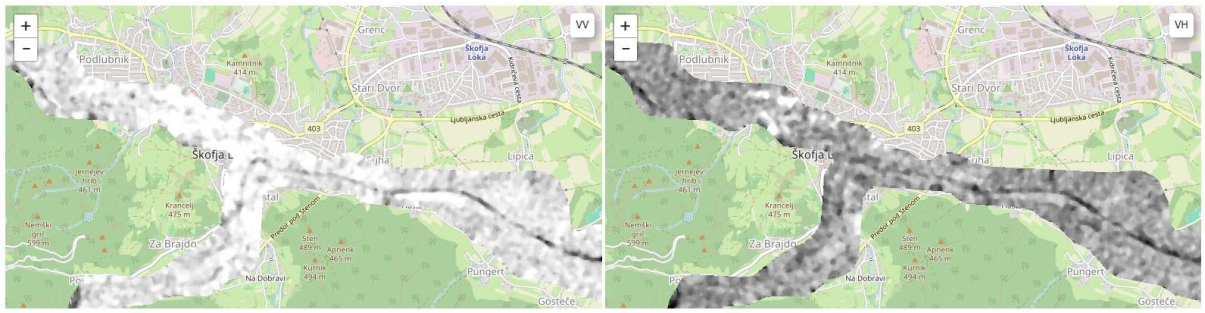


*Figure 10: Study area – demonstration region Škofja Loka: During-event S1 SAR a) VV b) VH*

*Source: Contains modified Copernicus Sentinel data [2024] processed by Google Earth Engine*

a b

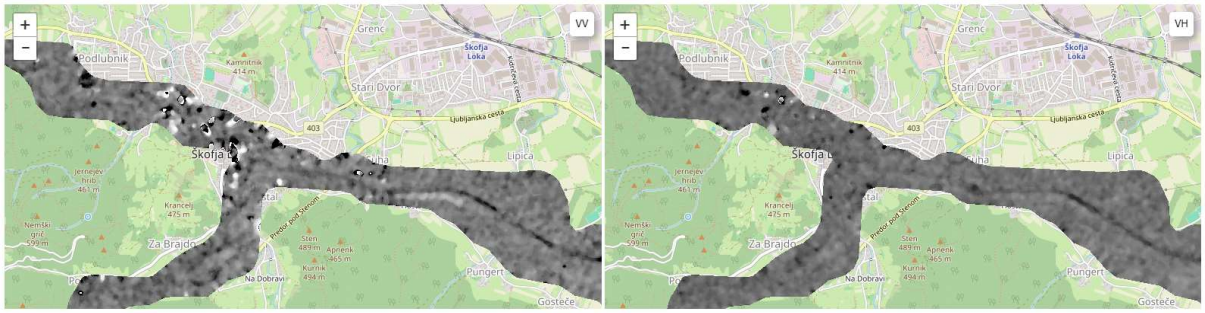


*Figure 11: Study area – demonstration region Škofja Loka: During-pre event difference in S1 SAR a) VV b) VH*

*Source: Contains modified Copernicus Sentinel data [2024] processed by Google Earth Engine*

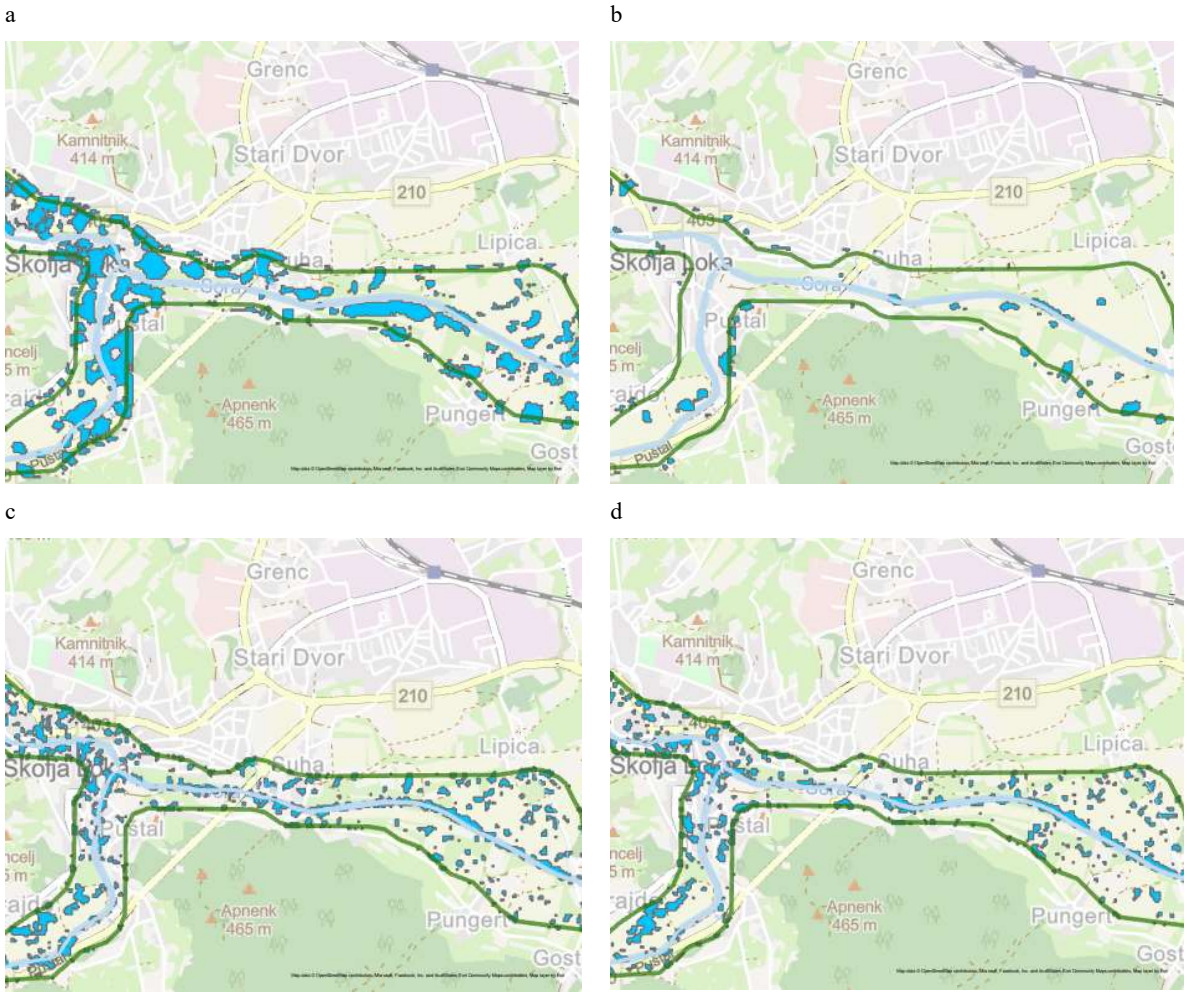


*Figure 12: Study area – demonstration region Škofja Loka: Flooded area as detected by S1 SAR and thersholding a) VV –during event b) VH –during event c) VV – change detection d) VH - – change detection*

*Source: Contains modified Copernicus Sentinel data [2024] processed by Google Earth Engine*

a b

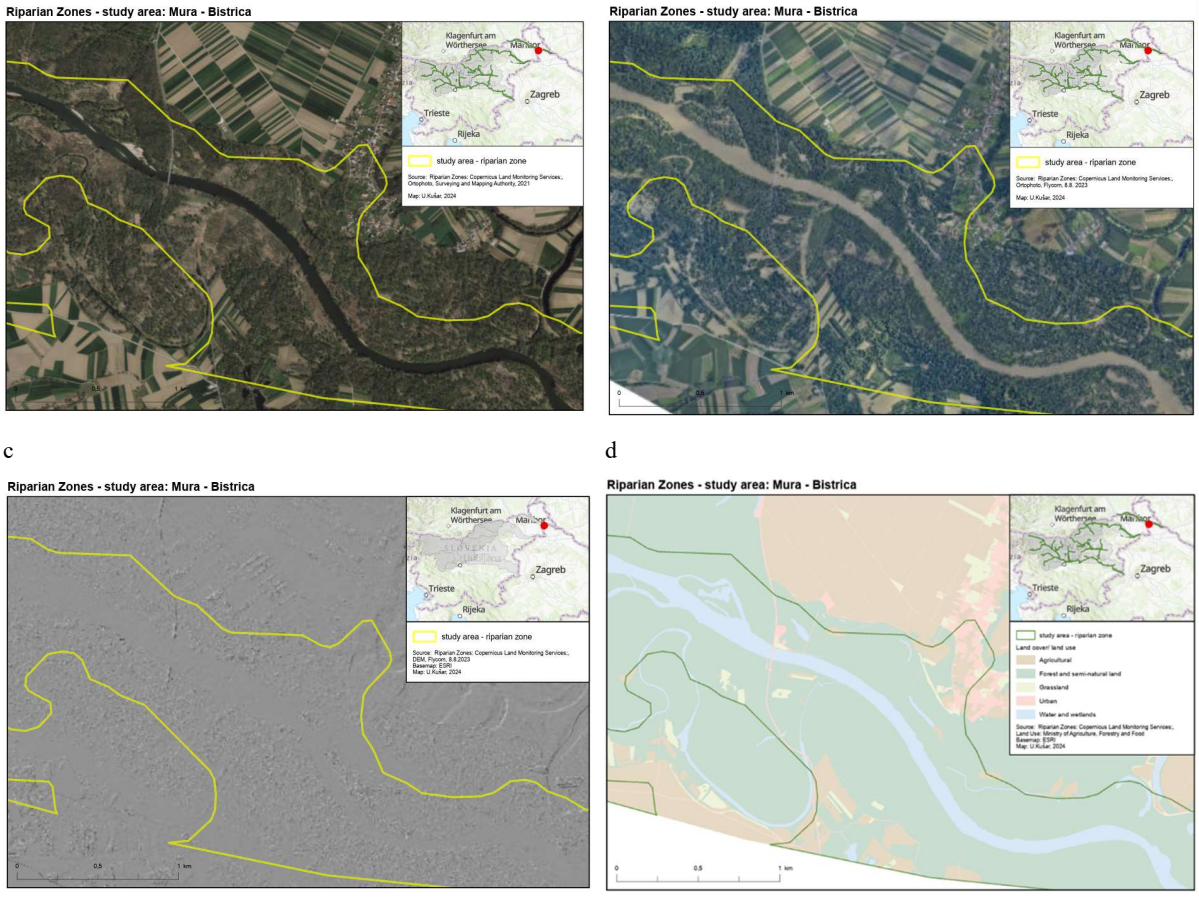


*Figure 13: Study area – demonstration region Mura - Dolenja Bistrica; a) pre-event ortophoto (RGB) b) pre-event ortophoto (RGB) c) DEM d) Land use/ land cover*

a b


*Figure 14: Study area – demonstration region Mura - Dolenja Bistrica: Pre-event S1 SAR a) VV b) VH*

*Source: Contains modified Copernicus Sentinel data [2024] processed by Google Earth Engine*

a b

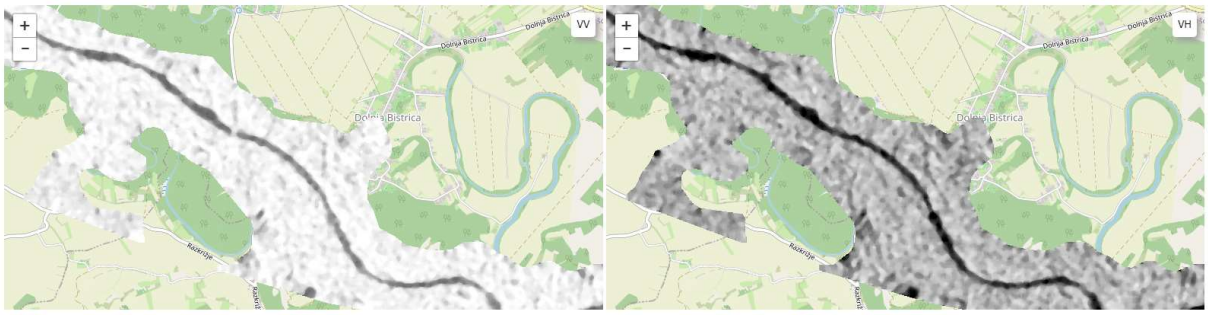


*Figure 15: Study area – demonstration region Mura - Dolenja Bistrica: Post (during) event S1 SAR a) VV b) VH*

*Source: Contains modified Copernicus Sentinel data [2024] processed by Google Earth Engine*

a b


*Figure 16: Study area – demonstration region Mura - Dolenja Bistrica: Post-pre event difference in S1 SAR a) VV b) VH*

*Source: Contains modified Copernicus Sentinel data [2024] processed by Google Earth Engine*

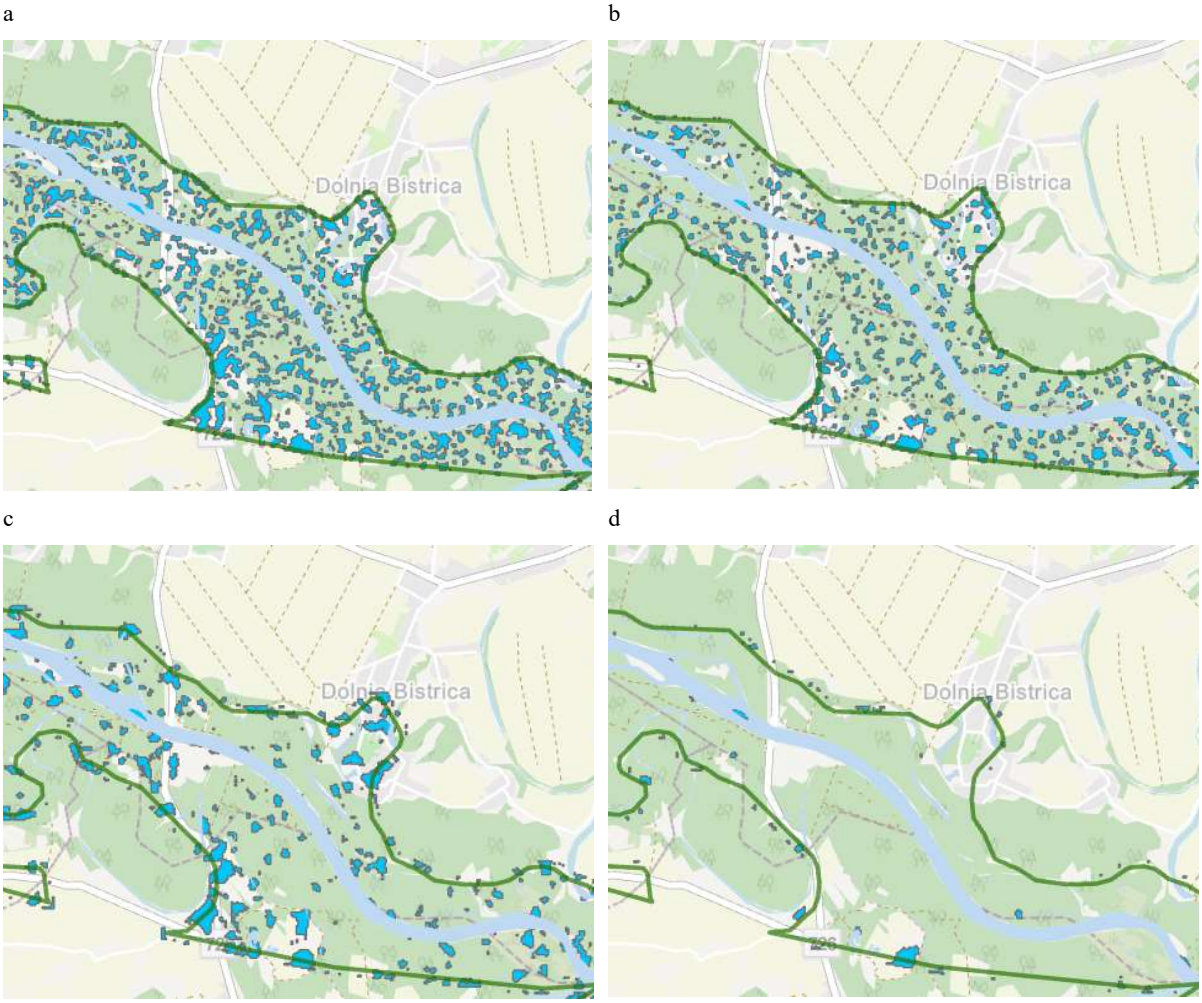


*Figure 17: Study area – demonstration region Mura – Dolenja Bistrica: Flooded area as detected by S1 SAR and thersholding a) VV –during event b) VH – during event c) VV – change detection d) VH – change detection*

*Source: Contains modified Copernicus Sentinel data [2024] processed by Google Earth Engine*

Visual comparison of maps of demonstration areas of Sora – Škofja Loka in sub-alpine region and Mura – Dolenja Bistrica in sub-pannonian region reveal that permanent water areas are much better detected in S1 images in the case of wider rivers (Mura, Sora downstream) in both VV and VH polarisations. As most of the rivers and streams in the studied riparian zones are less than 10 m wide the detection of permanent water areas is limited single S1 images. Increased surface roughness of water during the precipitation and flash floods could further increase backscatter values and even decreased areas detected as water by the means of thresholding.

With change detection approach 10.802 ha were detected and flooded areas with VV polarisation and 3.120 with VH polarisation. Change detection was examined as the difference between pre-event and during-event situation on per-pixel basis, the area that exhibits significant decreased backscatter,

indicating increased water presence, was 1.705 ha detected with VH polarisation and 3.650 detected with VV polarisation. Visual comparison of during and pre-event imagery revealed significant areas of increased backscatter, which could not be explained by other changes then inundated areas of vegetation. 8.039 ha of areas with significantly increased backscatter were detected as flooded vegetation with VV polarisation and 1.662 ha with VH polarisation. As expected, only minor proportions of these changes were detected on permanent water areas.

### 3.2.2.Sentinel-2 – spectral indices results

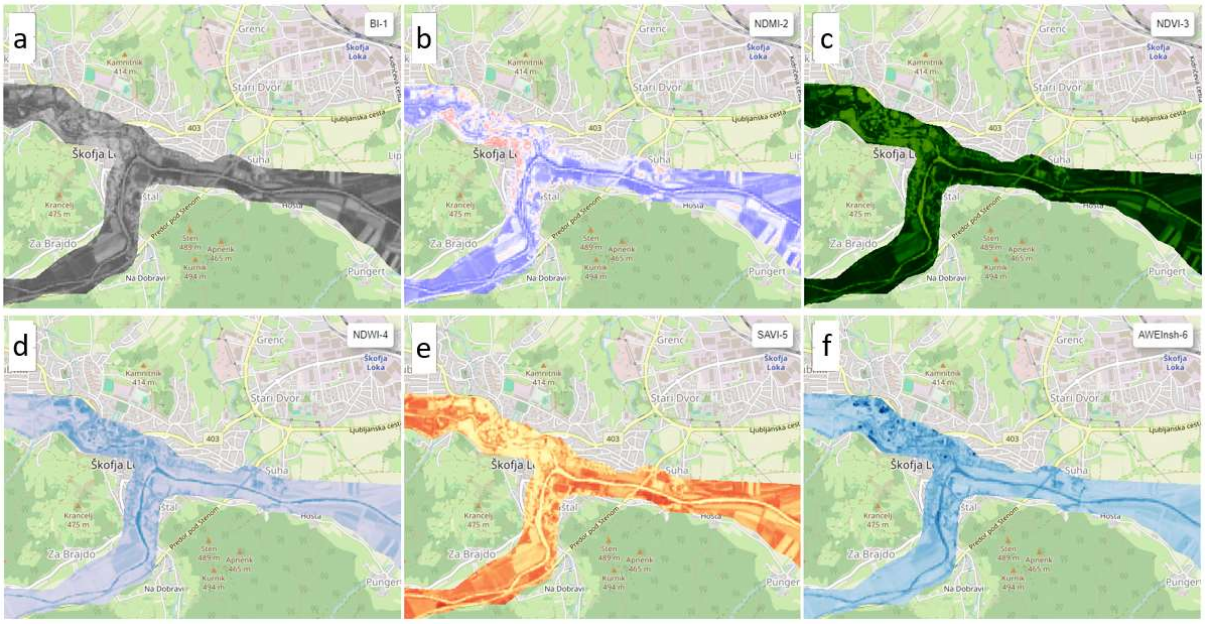


*Figure 18: Study area – demonstration region Škofja Loka: Pre-event S2 spectral indices a) BI b) NDMI c) NDVI d) NDWI e) SAVI and f)AWEInsh*

*Source: Contains modified Copernicus Sentinel data [2024] processed by Google Earth Engine*

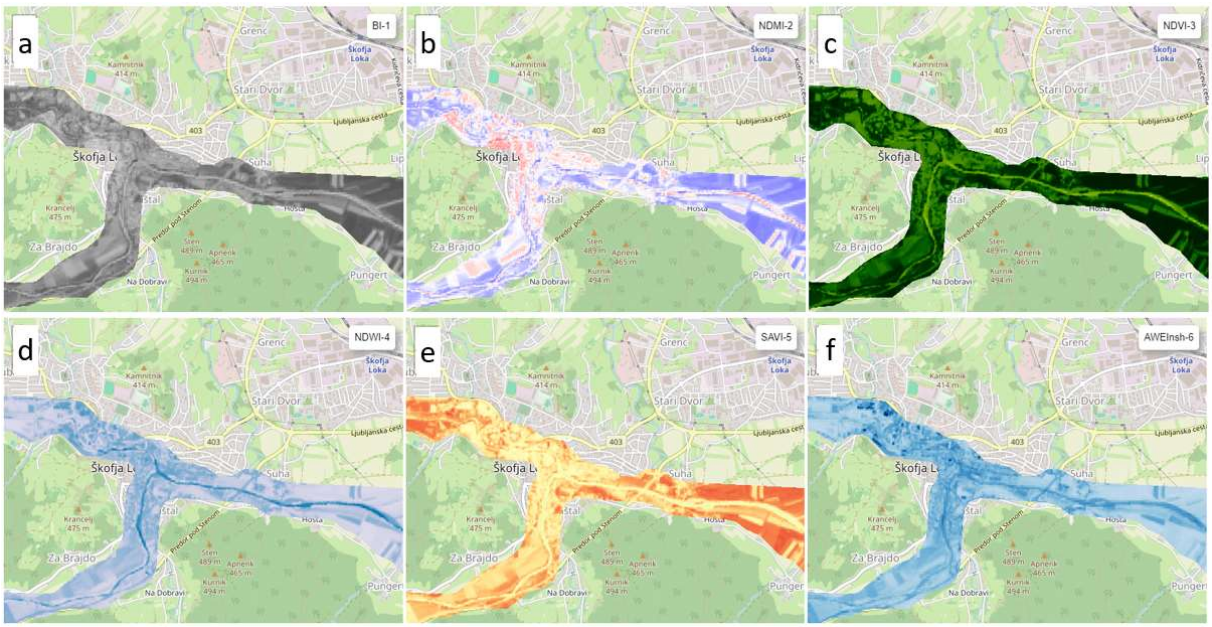

*Figure 19: Study area – demonstration region Škofja Loka: Post-event S2 spectral indices a) BI b) NDMI c) NDVI d) NDWI e) SAVI and f)AWEInsh*

*Source: Contains modified Copernicus Sentinel data [2024] processed by Google Earth Engine*

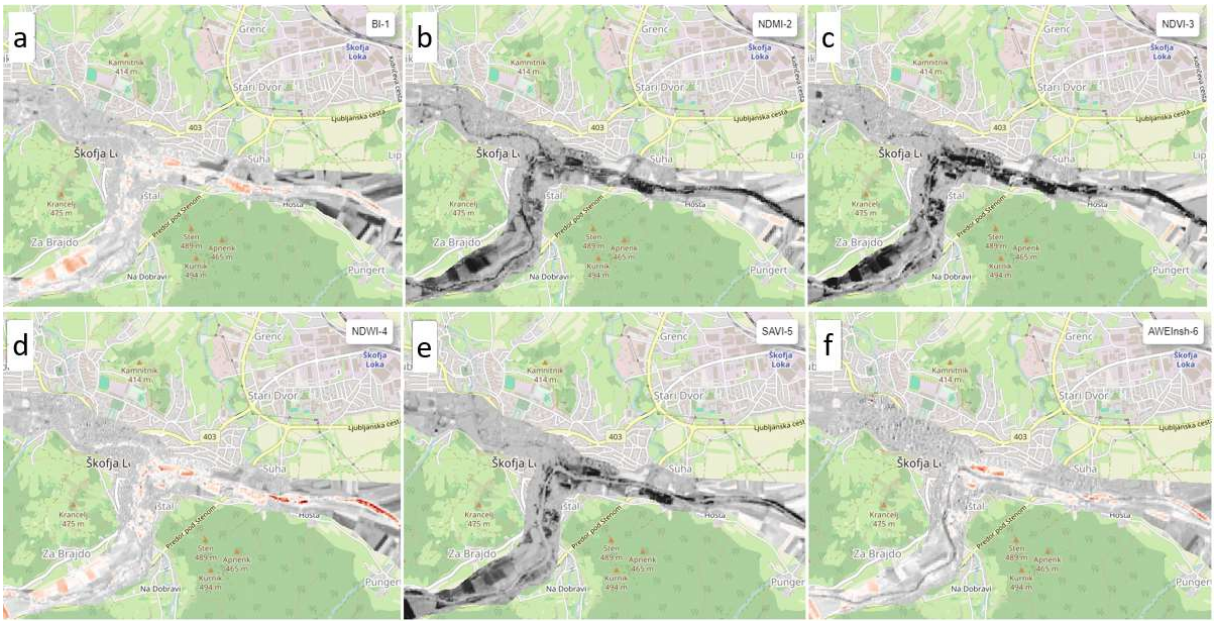


*Figure 20: Study area – demonstration region Škofja Loka: Post-pre event difference in S2 spectral indices a) BI b) NDMI c) NDVI d) NDWI e) SAVI and f)AWEInsh*

*Source: Contains modified Copernicus Sentinel data [2024] processed by Google Earth Engine*

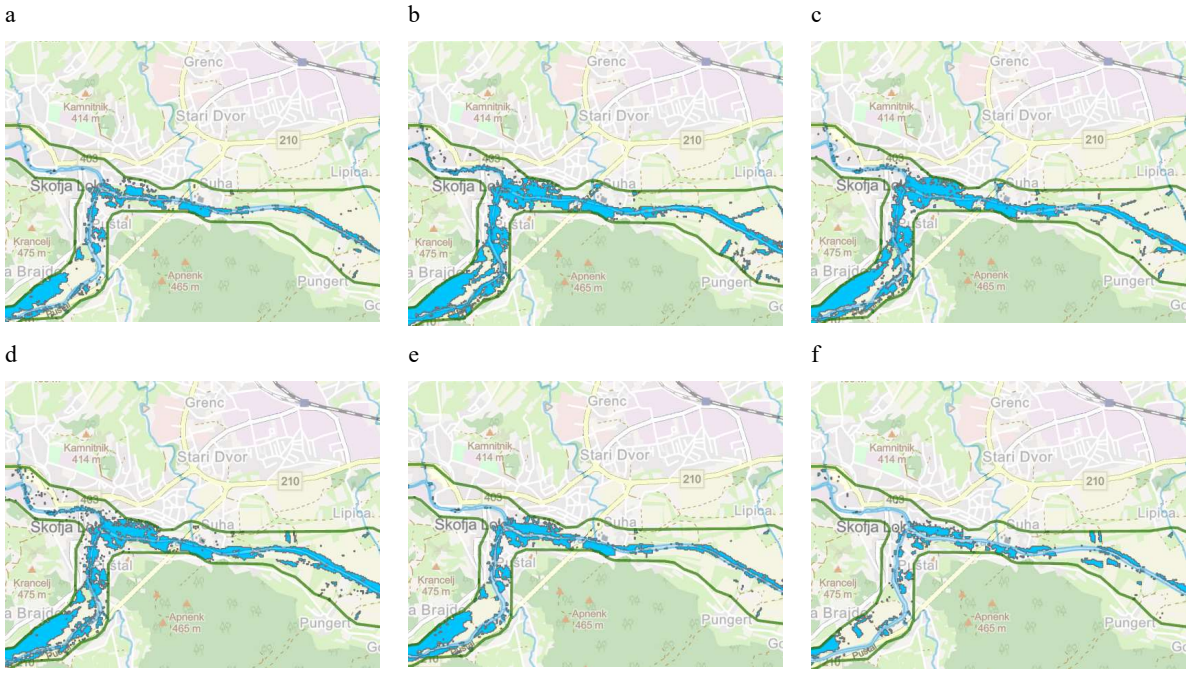


*Figure 21: Study area – demonstration region Škofja Loka: Flooded area as detected by S2 spectral indices and thersholding a) BI b) NDMI c) NDVI d) NDWI e) SAVI and f)AWEInsh*

*Source: Contains modified Copernicus Sentinel data [2024] processed by Google Earth Engine*

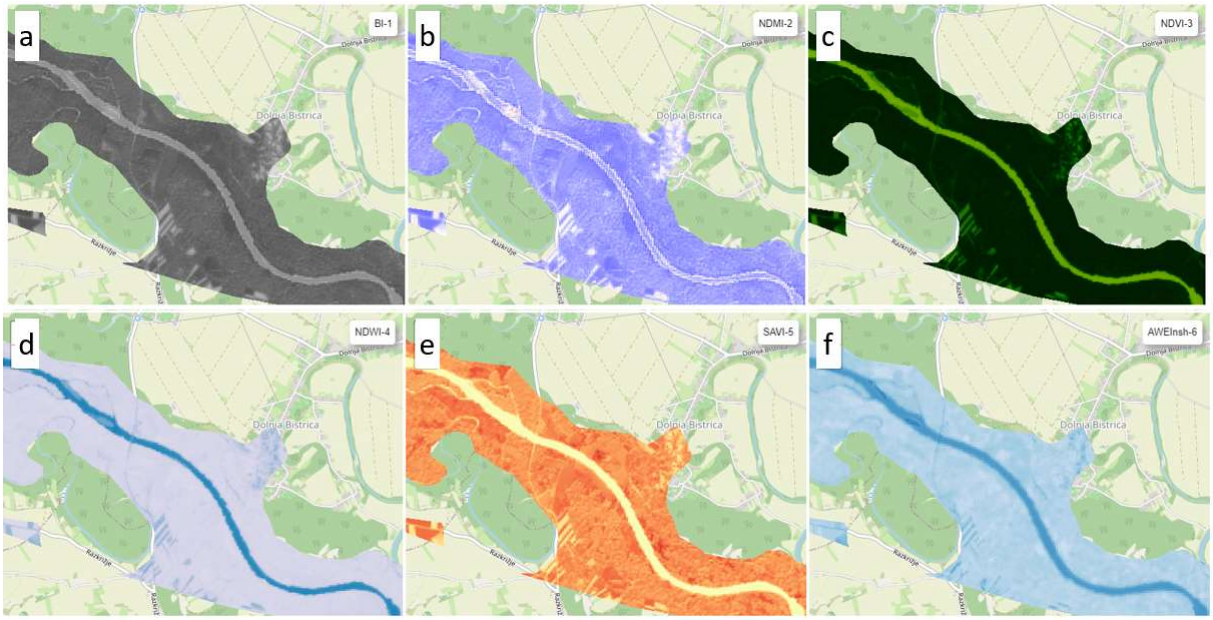


*Figure 22: Study area – demonstration region Mura - Bistrica: Pre-event S2 spectral indices a) BI b) NDMI c) NDVI d) NDWI e) SAVI and f) AWEInsh*

*Source: Contains modified Copernicus Sentinel data [2024] processed by Google Earth Engine*

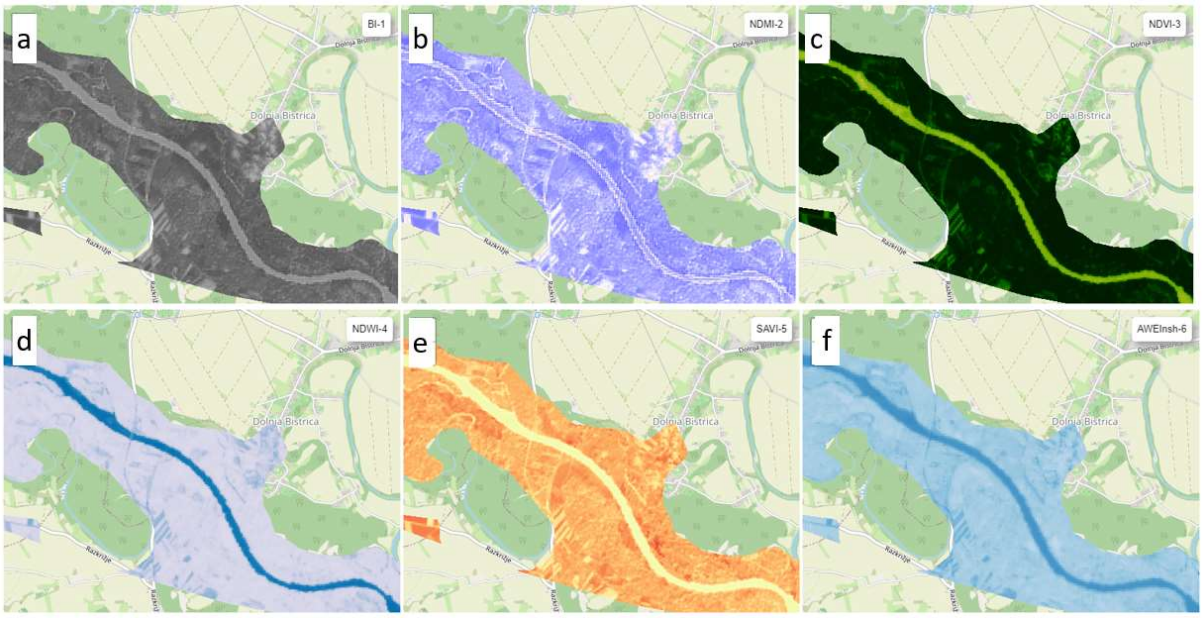


*Figure 23: Study area – demonstration region Mura - Dolenja Bistrica: Post-event S2 spectral indices a) BI b) NDMI c) NDVI d) NDWI e) SAVI and f)AWEInsh*

*Source: Contains modified Copernicus Sentinel data [2024] processed by Google Earth Engine*

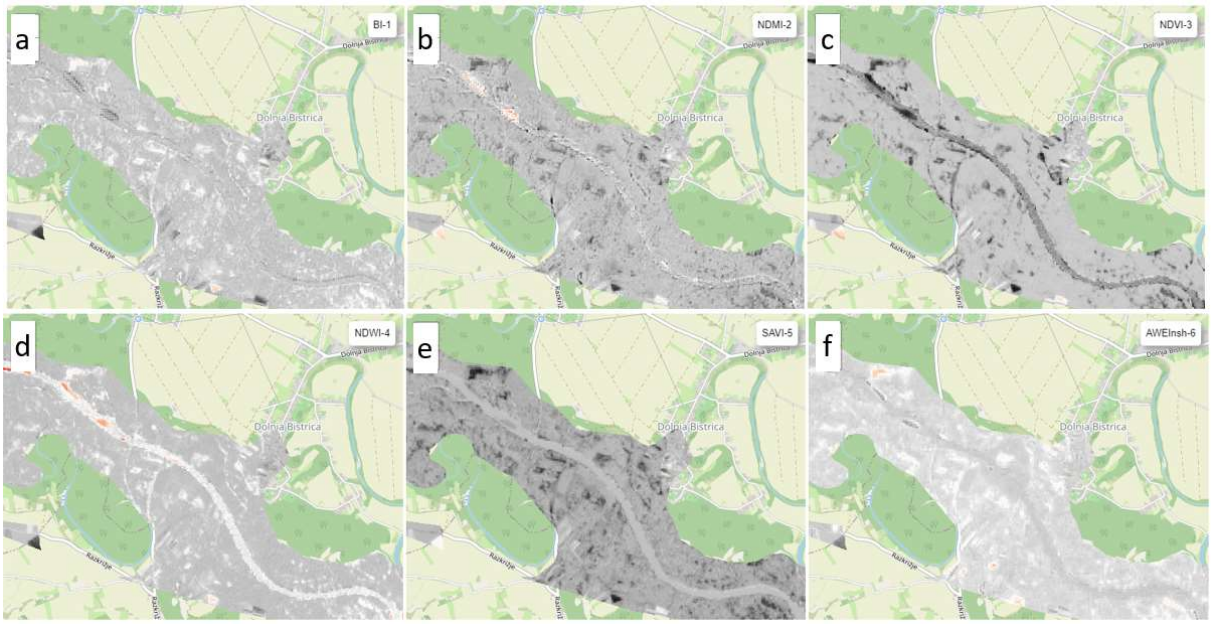


*Figure 24: Study area – demonstration region Mura - Dolenja Bistrica: Post-pre event difference in S2 spectral indices a) BI b) NDMI c) NDVI d) NDWI e) SAVI and f)AWEInsh*

*Source: Contains modified Copernicus Sentinel data [2024] processed by Google Earth Engine*

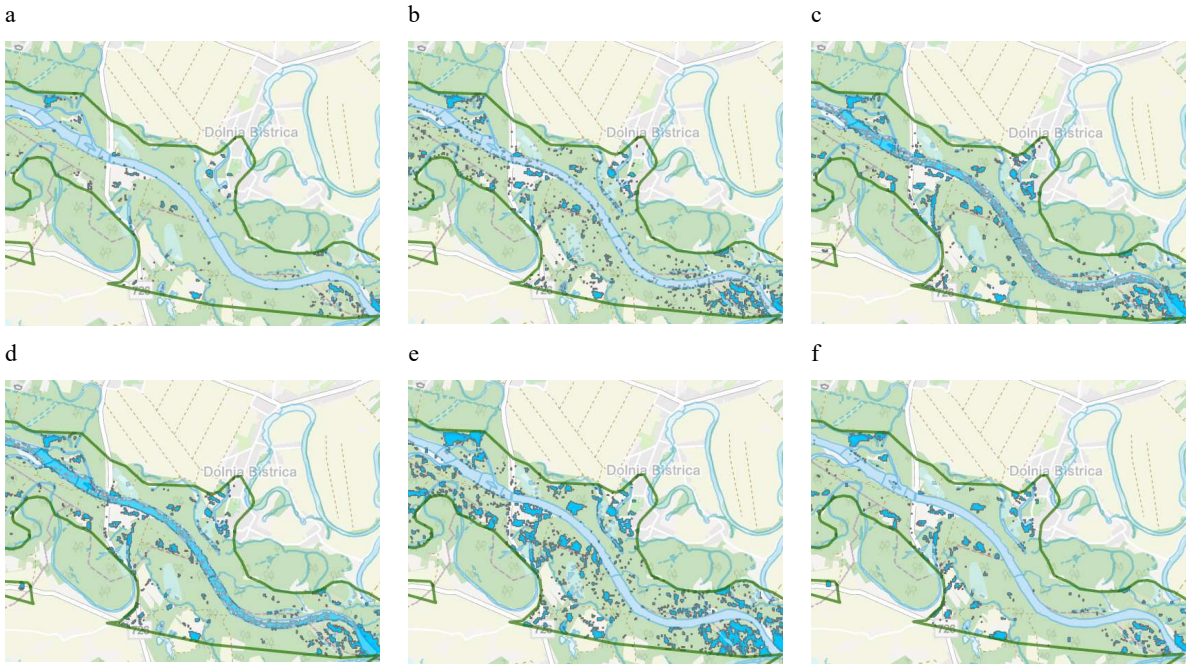


*Figure 25: Study area – demonstration region Mura – Dolenja Bistrica: Flooded area as detected by S2 spectral indices and thersholding a) BI b) NDMI c) NDVI d) NDWI e) SAVI and f) AWEInsh*

*Source: Contains modified Copernicus Sentinel data [2024] processed by Google Earth Engine*

*Table 14: Water area/ flooded area - results of single image water detection approach and change detection approach based on spectral indices from Sentinel-2*

| | **Single image approach** | | | **Change detection approach** | | |
|---|---|---|---|---|---|---|
| | Water surface area (ha) | | | Areas (ha) | | Flooded area (ha) |
| | Pre-event | Post-event | Water area difference | Post–pre difference detected (flooded) | Post-pre difference detected on permanent water areas | **Post-pre difference outside permanent water areas** |
| **NDWI** | 5.431 | 5.959 | 528 | 7.502 | 4.465 | **3.038** |
| **AWEInsh** | 4.720 | 5.960 | 1.240 | 4.738 | 3.254 | **1.484** |
| **NDVI** | 2.935 | 3.682 | 747 | 8.251 | 4.928 | **3.323** |
| **SAVI** | 4.338 | 5.165 | 827 | 5.189 | 4.778 | **411** |
| **NDMI** | 14.258 | 15.327 | 1.069 | 6.687 | 5.555 | **1.132** |
| **BI** | 20.037 | 19.038 | -999 | 2.915 | 2.649 | **266** |

Table 14 presents the results of water and flooded area detection using a single-image and change-detection approach with S2 mosaics and spectral indices. For each S2 mosaic, six spectral indices were calculated using different combinations of Sentinel-2 optical bands. These spectral indices were designed to enhance the detection of various elements. NDWI and AWEInsh utilize green, NIR and SWIR bands to enhance the detection of water surfaces in a single image. Both methods detected a very similar extent of around 5,960 ha of water areas in post-event images, captured 9 days after the main event, which are the first available post-event images, as prior scenes are nearly completely covered with clouds (Figure 5). Not surprisingly, this is only slightly more than the water areas detected in pre-event images taken a month earlier. It was not expected to detect vast open water areas in optical images, as the flood receded relatively fast, within a few hours in the sub-alpine (flash-flood) region and within a few days in the downstream riverine flood region. Both indices use green and NIR bands, with AWEInsh also including SWIR bands, which have a lower (20m) pixel resolution and are therefore expected to be less precise. The difference in resolution can also significantly influence change-detection analysis, where AWEInsh detects fewer changes in areas outside permanent water bodies, which could be attributed to the flood event, than NDVI – 1,484 ha and 3,038 ha. The only index that detects more flooded areas (3,323 ha) with the change detection approach is NDVI. NDVI detects only 2,935 ha of water areas in the pre-event image and 3,682 ha in the post-event image. SAVI, designed to reduce the effects of soil moisture in vegetation detection compared to NDVI, detects more water areas in single images, but much fewer changes outside water bodies in the post-pre-flood comparison. The NDMI - index designed to detect moisture indeed identifies significant moist areas (14,258 ha in pre- and 15,327 ha in post-event situations), which exceeded water areas, but are consistent with reports of extremely water-saturated soil in July as well as August (also post-floods) due to persistent precipitation (Agencija Republike Slovenije za okolje, 2023). NDMI detected increased areas of soil moisture outside

permanent water areas, but only to the extent of 1,132 ha, placing it among the least sensitive indices. The least sensitive and most confusing results are from BI. It is designed to detect sealed urban surfaces, and its' application reasoning was to test its applicability to detect increased gravel and other non-vegetation material deposits to previously vegetated areas. The index detected 20,037 ha of water areas, and even slightly fewer in the post-event situation. Changes detected were relatively small, mostly inside the water areas.

### 3.2.3. Ground Truth Points

*Table 15: Ground Truth points – number by land cover/ land use classification*

| | Agricultural | Forest and semi-natural land | Grassland | Urban | Water and wetlands | Total |
|---|---|---|---|---|---|---|
| **Study Area by category** | 12.534 ha (29%) | 9.973 ha (23%) | 7.578 ha (17%) | 7.421 ha (17%) | 6.301 (14%) | 43809 ha (100%) |
| **GT Points** | 41 | 31 | 24 | 25 | na | 121 |
| **GT Points - Flooded** | 16 | 22 | 12 | 13 | na | 63 |

*Table 16: Ground Truth points – number by flood type classification*

| | Flash flood | Riverine flood | Total |
|---|---|---|---|
| **Study Area by category** | 17.184 ha (39%) | 26.625 ha (61%) | 43.809 ha (100%) |
| **GT Points** | 58 | 63 | 121 |
| **GT Points - Flooded** | 31 | 32 | 63 |

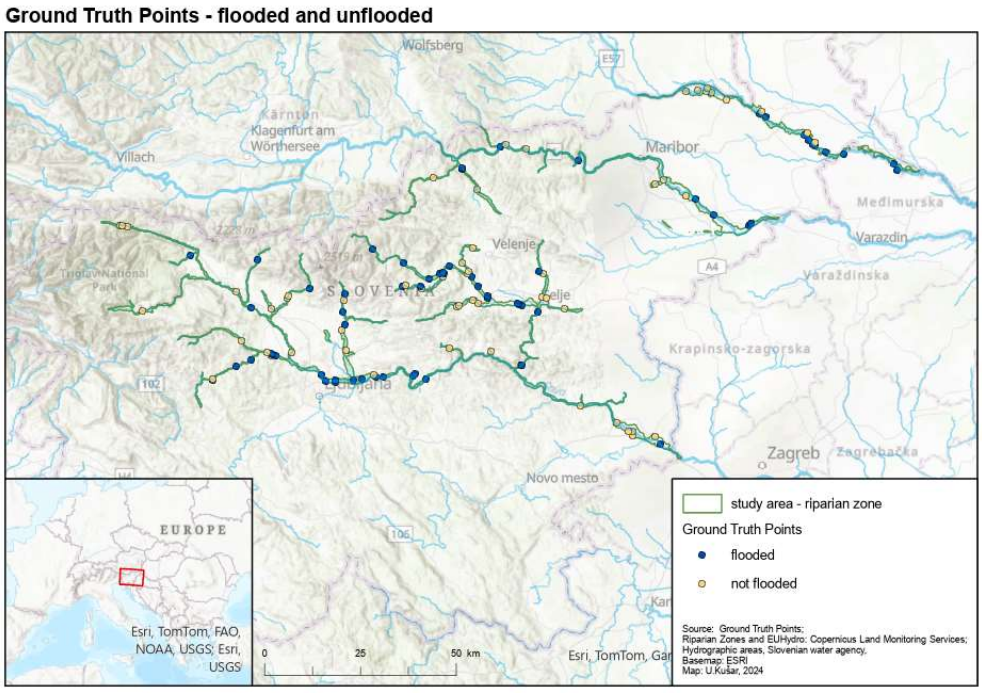


*Figure 26: Ground Truth Samples by class – flooded/ unflooded*

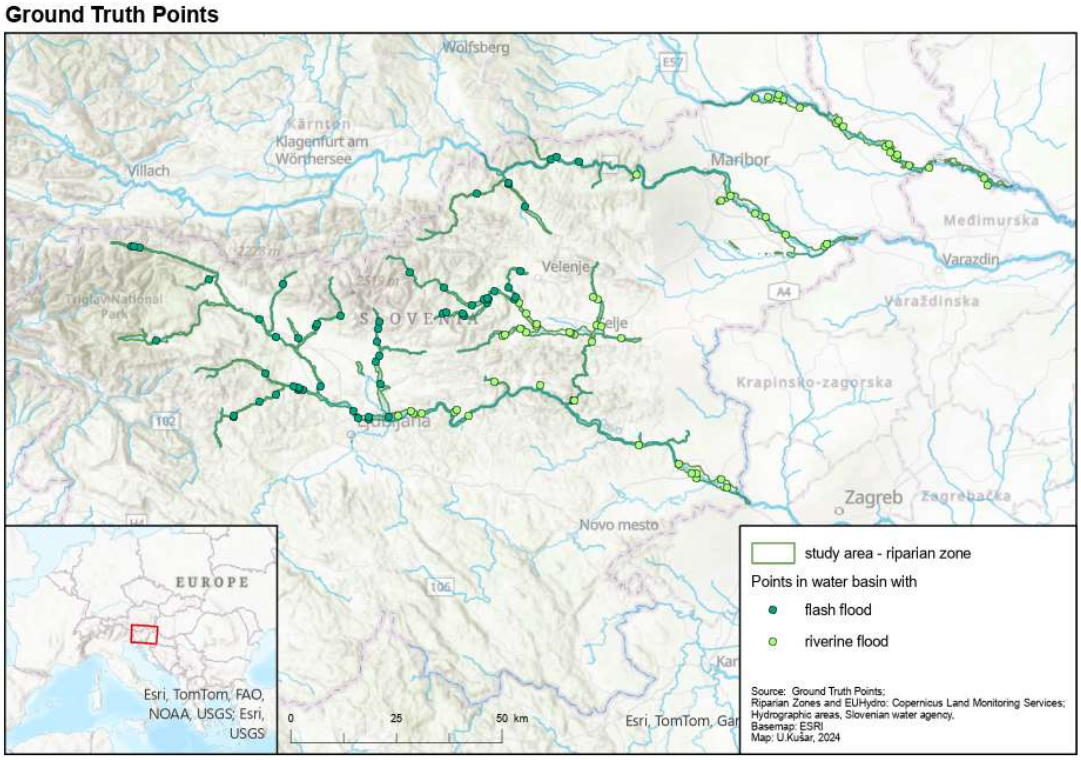


*Figure 27: Ground Truth Samples by class – flash flood/ riverine flood*

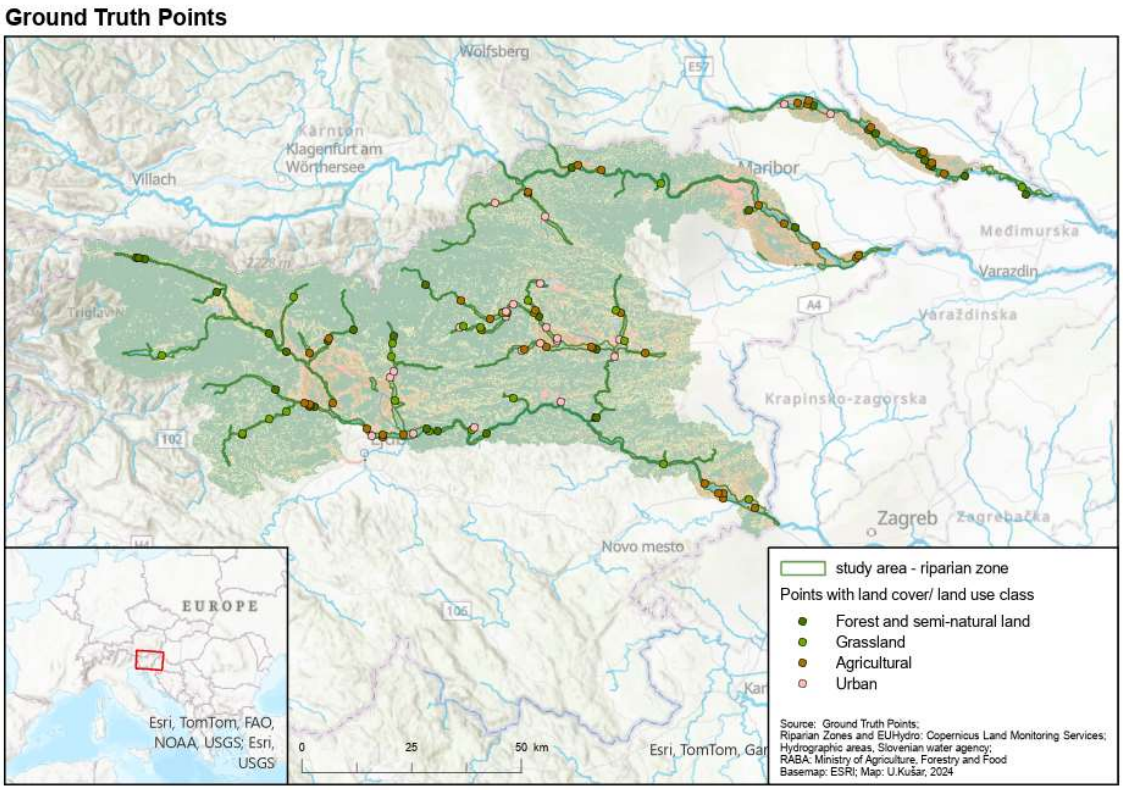


*Figure 28: Ground Truth Samples by class – land use class (forest, grassland, agriculture, urban)*

In order to enable accuracy assessment of selected SAR and spectral indices, a collection sample of points was created. Points were classified as flooded or unflooded with point-by-point manual assessment with available spatial data resources: post-event areal ortophotos, humanitarian organisations damage claims, Copernicus Rapid Mapping Products. 121 points were selected randomly from study area; 58 points were selected from flash-flood region and 63 from riverine flood region. Sample was stratified also according to land cover/ land use classes: agricultural, forested, grassland and urban (Figure 28). Points were classified in the resolution which corresponded the 10m pixel size, considering the majority of 10m circle around the point as a reference.

Classification resulted in 63 or 52% of the ground truth points detected as flooded (Figure 26). Flooded points were nearly equally distributed between flash flood and riverine flood regions, with relatively more flooded points in forest areas than their land cover shares of the riparian zone (Table 16).

Although there were several reliable resources available to assess the status of each points some uncertainty remained, particularly in the regions that were not covered by areal orthophotos in the Spodnja Sava and Spodnja Drava water basins. Consultations with local practitioners and expert assessment was employed where necessary.

#### 3.2.4. Accuracy assessment

Tables 17 to 20 present the accuracy assessment for the results of water detection and flooded area detection studies from previous steps.

From the analysis of single images, only S1 during-event was assessed as it was the only image available potentially capturing flooded areas themselves, not by approximation with their impacts. The accuracy assessment revealed poor correlation with ground truth assessment – the overall accuracy was 0.52 for the flash flood region and 0.60 for the riverine region with VH polarization, and similar, 0.55 and 0.58 for VV polarization. Particularly, the producer's accuracy was low (0.34 or lower).

*Table 17: Accuracy assessment – flash flood vs riverine flood*

| | Flash flood | Riverine Flood | Flash flood | Riverine Flood | Flash flood | Riverine Flood |
|---|---|---|---|---|---|---|
| | Producers' accuracy | | Users' accuracy | | Overall accuracy | |
| **S1 single image – during event** | | | | | | |
| **polarisation** | | | | | | |
| **VH** | **0,16** | **0,31** | **0,71** | **0,77** | **0,52** | **0,60** |
| **VV** | **0,23** | **0,34** | **0,78** | **0,69** | **0,55** | **0,58** |
| **S1 - change detection** | | | | | | |
| **polarisation** | | | | | | |
| **VH** | **0,03** | **0,16** | **0,20** | **0,71** | **0,41** | **0,53** |
| **VV** | **0,68** | **0,59** | **0,64** | **0,68** | **0,62** | **0,65** |
| | | | | | | |
| **S2 Spectral Index** | | | | | | |
| **NDWI** | 0,65 | 0,56 | **1,00** | **1,00** | 0,81 | 0,77 |
| **AWEInsh** | 0,26 | 0,47 | **1,00** | **1,00** | 0,60 | 0,73 |
| **NDVI** | **0,74** | **0,75** | 0,96 | **1,00** | **0,84** | **0,87** |
| **SAVI** | 0,39 | 0,66 | 0,92 | 0,95 | 0,66 | 0,81 |
| **NDMI** | 0,58 | 0,47 | 0,90 | 0,94 | 0,74 | 0,71 |
| **BI** | 0,39 | 0,22 | 0,92 | **1,00** | 0,66 | 0,60 |

*Table 18: Accuracy assessment – producers' accuracy – by land cover/land use class*

| | Forest | Grasssland | Agricultural | Urban | Overall |
|---|---|---|---|---|---|
| **S1 single image – during event** | | | | | |
| **polarisation** | | | | | |
| **VH** | **0,32** | **0,33** | **0,13** | **0,15** | **0,24** |
| **VV** | **0,36** | **0,42** | **0,19** | **0,15** | **0,29** |
| **S1 - change detection** | | | | | |
| **polarisation** | | | | | |
| **VH** | **0,00** | **0,17** | **0,19** | **0,08** | **0,10** |
| **VV** | 0,68 | **0,50** | **0,63** | **0,69** | **0,63** |
| | | | | | |
| **S2 Spectral Index – change detection** | | | | | |
| **NDWI** | **0,55** | **0,75** | **0,50** | **0,31** | **0,60** |
| **AWEInsh** | **0,18** | **0,58** | **0,63** | **0,15** | **0,37** |
| **NDVI** | 0,64 | 0,83 | 0,81 | 0,77 | 0,75 |
| **SAVI** | **0,55** | **0,75** | **0,50** | **0,31** | **0,52** |
| **NDMI** | **0,50** | 0,83 | **0,38** | **0,46** | **0,52** |
| **BI** | **0,27** | **0,58** | **0,19** | **0,23** | **0,30** |

*Table 19: Accuracy assessment – users' accuracy – by land cover/land use class*

| Index | Forest | Grasssland | Agricultural | Urban | Overall |
|---|---|---|---|---|---|
| **S1 single image – during event** | | | | | |
| **polarisation** | | | | | |
| **VH** | **1,00** | **1,00** | 0,50 | 0,40 | 0,75 |
| **VV** | **1,00** | **1,00** | 0,43 | 0,40 | 0,72 |
| **S1 - change detection** | | | | | |
| **polarisation** | | | | | |
| **VH** | 0,00 | **1,00** | 0,50 | 0,33 | 0,50 |
| **VV** | 0,83 | 0,67 | 0,59 | 0,53 | 0,66 |
| | | | | | |
| **S2 Spectral Index** | | | | | |
| **NDWI** | **1,00** | **1,00** | 0,80 | **1,00** | **1,00** |
| **AWEInsh** | **1,00** | **1,00** | **1,00** | **1,00** | **1,00** |
| **NDVI** | **1,00** | **1,00** | 0,93 | **1,00** | 0,98 |
| **SAVI** | **1,00** | **1,00** | 0,80 | **1,00** | 0,94 |
| **NDMI** | **1,00** | **1,00** | 0,67 | **1,00** | 0,92 |
| **BI** | **1,00** | **1,00** | 0,75 | **1,00** | 0,95 |

*Table 20: Accuracy assessment – overall accuracy – by land cover/land use class*

| Index | Forest | Grasssland | Agricultural | Urban | Overall |
|---|---|---|---|---|---|
| **S1 single image – during event** | | | | | |
| **polarisation** | | | | | |
| **VH** | **0,52** | **0,65** | **0,61** | 0,44 | **0,56** |
| **VV** | **0,55** | **0,79** | 0,59 | 0,44 | **0,57** |
| **S1 - change detection** | | | | | |
| **polarisation** | | | | | |
| **VH** | 0,26 | 0,57 | **0,61** | 0,44 | 0,48 |
| **VV** | **0,68** | **0,61** | **0,68** | **0,52** | **0,63** |
| | | | | | |
| **S2 Spectral Index** | | | | | |
| **NDWI** | **0,68** | **0,87** | **0,76** | **0,64** | **0,79** |
| **AWEInsh** | **0,42** | **0,78** | **0,85** | **0,56** | **0,67** |
| **NDVI** | 0,74 | 0,91 | 0,90 | 0,88 | 0,86 |
| **SAVI** | **0,68** | **0,87** | **0,76** | **0,64** | **0,73** |
| **NDMI** | **0,65** | 0,91 | **0,68** | **0,72** | **0,73** |
| **BI** | **0,48** | **0,78** | **0,66** | **0,60** | **0,63** |

According to the accuracy assessment, the quality of the results of single image analysis was comparable to the results of change detection analysis for VH polarization. Conversely, change detection with VV polarization presented relatively good results also in producer's accuracy (0.68 for the flash flood region), but only slightly better for overall accuracy (0.62 for flash flood and 0.65 for riverine flood water basins). Comparing AA results between the two classes – flash flood and riverine flood – riverine assessments performed consistently better than the flash flood region in both polarizations and in both approaches (single image and change detection), in some cases with significantly better results.

Comparing to S1 imagery, indexes derived from S2 mosaics performed better in most cases, but with significantly different results between them. The best result for detecting flooded areas in the riverine region was achieved with NDVI (0.87), and overall accuracy was just a bit lower for the flash flood region (0.84) with this index as well. BI performed worst, similarly to S1 products. All S2 indices had high AA scores with user's accuracy and worse scores with producer's accuracy, ranging from 0.22 to 0.75. In almost all scores, NDVI change detection approach performed best. Comparing riverine and flash flood region's results with S2 indices change detection approach presents mixed results – with some performing better in one or the other.

Some significant differences in the quality of detecting flooded areas with S1 and S2 imagery can be noticed also comparing land use classes of the affected region. Similarly, to previous accuracy assessment results, also analysis according to LCLU classes reveal that user's accuracy is mostly predominantly satisfactory, whereas producer's accuracy is suboptimal for a lot of instances. Again, generally, S2 products are better than S1, with S1 VV change detection and BI being positive and negative exceptions.

Producer's accuracy shows that the best results with S1 products are achieved for forest and urban areas, with VV polarization, which is consistent with literature reports of VV polarization usage for vertically oriented objects. Also, S2 products present quality consistent with the ones reported in the literature: best results are achieved on grassland, with exposed green vegetation, followed almost consistently with agricultural areas, with worst performances in urban land cover areas and slightly better in forests. User's accuracy is high, not revealing much diversity except worse performance in agricultural land class. Overall accuracy, therefore, reconfirms that the best results are expected on grassland and agricultural land, with scores above achieved 0.85 also in other categories, except for forests, where results are worse, but for some indices still above 0.75. Overall accuracy reaffirms the superiority of NDVI change detection method for all categories.

### 3.2.5. Map of flooded area

Accuracy assessment analysis demonstrated significant differences in the performance of different approaches, but also some similarities. Almost all indices presented high users' accuracy and many of them at the same time low scores for producers' accuracy. Low producer's accuracy suggests that the

algorithm tends to miss flooded pixels. Despite the low producer's accuracy, high user's accuracy indicates that when the algorithm does classify pixels as being flooded, it is often correct. It can be assumed that flooded areas are mostly underdetected by most of the algorithms individually. To test the possibility of achieving better results with combination of indices overlay and union of resulting flooded areas were executed and tested for accuracy. Composites included:

- S1U4: S1 water areas detected in images captured during the flood with VV and VH polarisation and S1 flooded areas detected with change detection analysis for VV and VH polarisation (S1 U4)
- S2U6: S2 flooded areas detected with change detection analysis for 6 spectral indices (NDVI, NDWI, SAVI, AWEInsh, NDMI and BI) (S2U6)
- S1S2: Union of S1U4 and S2U6 flooded areas
- S_VV_NDVI: Union of flooded areas with best performing results from S1 products (change detection with VV polarisation) and S2 (change detection with NDVI).

a


b


c


d

*Figure 29: Study area – demonstration region Sora - Škofja Loka: Flooded area as detected by composites of a) S1U4 b) S2U6 c) S1S2 d) S_VV_NDVI.*

*Source: Contains modified Copernicus Sentinel data [2024] processed by Google Earth Engine*

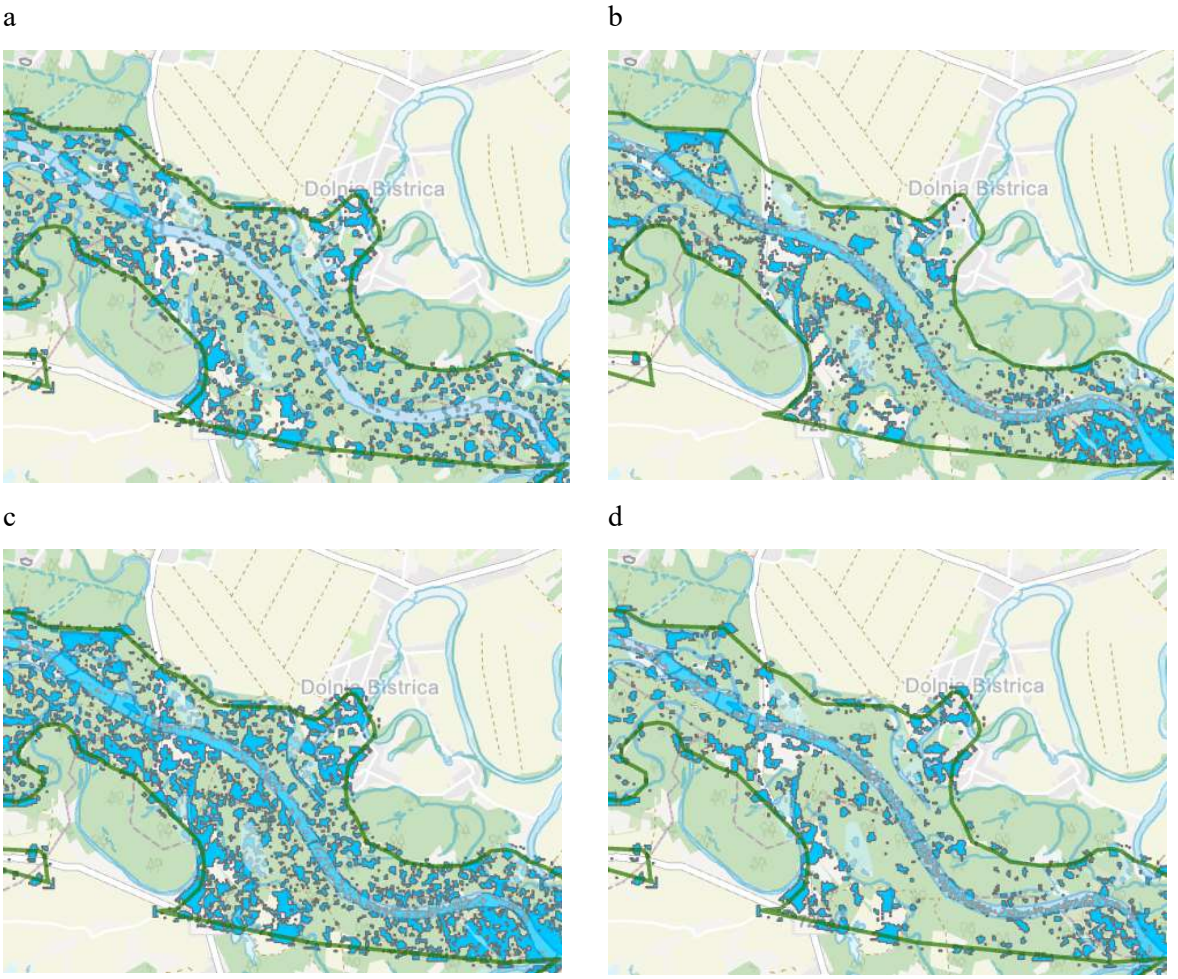


*Figure 30: Study area – demonstration region Mura – Dolenja Bistrica: Flooded area as detected by composites of a) S1U4 b) S2U6 c) S1S2 d) S_VV_NDVI.*

*Source: Contains modified Copernicus Sentinel data [2024] processed by Google Earth Engine*

Results are presented in tables 21-23 and maps of demonstration areas in figures 29 and 30. Overall accuracy and to even larger degree producers' accuracy improved significantly in all presented composites.

*Table 21: Composites' Accuracy assessment – producers' accuracy*

| | **Overall** | **Land Cover/ Land Use** | | | | **Type of Flood** | |
|---|---|---|---|---|---|---|---|
| **Index** | | **Forest** | **Grasssland** | **Agricultural** | **Urban** | **Flash Flood** | **Riverine Flood** |
| **S1U4** | **0,43** | **0,41** | **0,58** | **0,38** | **0,38** | **0,42** | **0,44** |
| **S2U6** | 0,90 | **0,86** | **0,92** | 0,94 | 0,92 | 0,90 | **0,91** |
| **S1S2** | 0,90 | 0,91 | 1,00 | **0,88** | **0,85** | **0,87** | 0,94 |
| **S_VV_NDVI** | 0,90 | **0,86** | 1,00 | 0,94 | **0,85** | 0,90 | **0,91** |

*Table 22: Composites' Accuracy assessment – users' accuracy*

| | **Overall** | **Land Cover/ Land Use** | | | | **Type of Flood** | |
|---|---|---|---|---|---|---|---|
| **Index** | | Forest | Grasssland | Agricultural | Urban | Flash | Riverine |
| **S1U4** | 0,68 | 0,82 | 0,88 | 0,60 | 0,45 | 0,65 | 0,70 |
| **S2U6** | **0,88** | **1,00** | **0,92** | **0,83** | 0,75 | **0,88** | **0,88** |
| **S1S2** | 0,78 | 0,91 | **0,92** | 0,67 | 0,65 | 0,75 | 0,81 |
| **S_VV_NDVI** | 0,77 | 0,86 | 0,86 | 0,71 | 0,65 | 0,74 | 0,81 |

*Table 23: Composites' Accuracy assessment – overall accuracy*

| | **Overall** | **Land Cover/ Land Use** | | | | **Type of Flood** | |
|---|---|---|---|---|---|---|---|
| **Index** | | Forest | Grasssland | Agricultural | Urban | Flash F | Riverine F |
| **S1U4** | 0,59 | 0,52 | 0,74 | 0,66 | 0,44 | 0,57 | 0,61 |
| **S2U6** | **0,88** | **0,90** | **0,91** | **0,90** | **0,80** | **0,88** | **0,89** |
| **S1S2** | 0,82 | 0,87 | 0,96 | 0,78 | 0,68 | 0,78 | 0,85 |
| **S_VV_NDVI** | 0,81 | 0,81 | 1,00 | 0,83 | 1,00 | 0,78 | 0,84 |

Best performing composite index was S1U6, which achieved satisfactory results of overall accuracy above 0,85 for flash flood and riverine flood, and almost all land cover classes, except for urban, where the score was 0,80. Therefor S2U6 index result was used for further application. To reduce noise and enhance spatial coherence spatial filtering of small isolated areas and merging adjacent areas into larger polygons were applied.

The result is a vector layer with polygons representing riparian zone areas that were flooded in the August 2023 flood event in Slovenia, with minimum mapping unit of 10x10m in ETRS89 / LAEA Europe (EPSG 3035) projection.

*Table 24: Water area/ flooded area – indices and composites*

| | **Flooded area** | **Flooded area detected on permanent water areas** | **Flooded area detected outside permanent water areas** |
|---|---|---|---|
| **S1U4** | 18.626 | 16.877 | 1.749 |
| **S2U6** | 13.205 | 8.957 | 4.248 |
| **S1S2** | 26.439 | 21.760 | 4.679 |
| **S_VV_NDVI** | 17.996 | 14.197 | 3.799 |

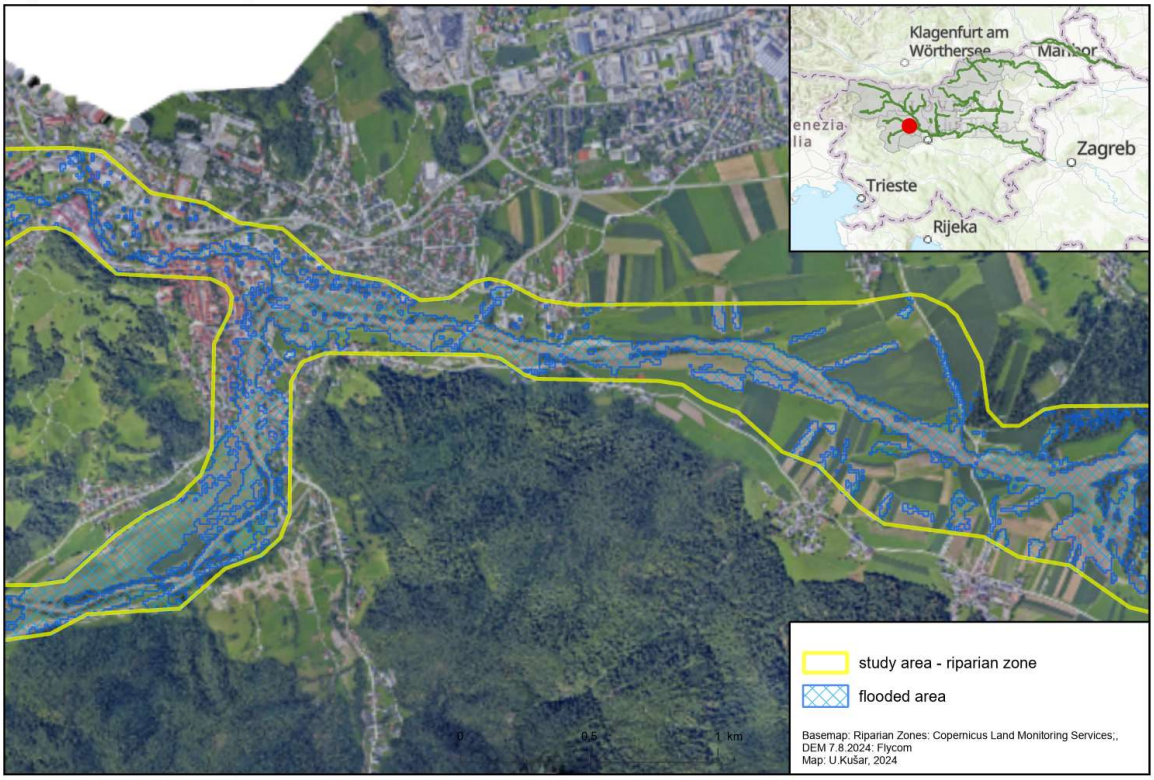


*Figure 31: Study area – demonstration region Sora - Škofja Loka: Flooded areas*

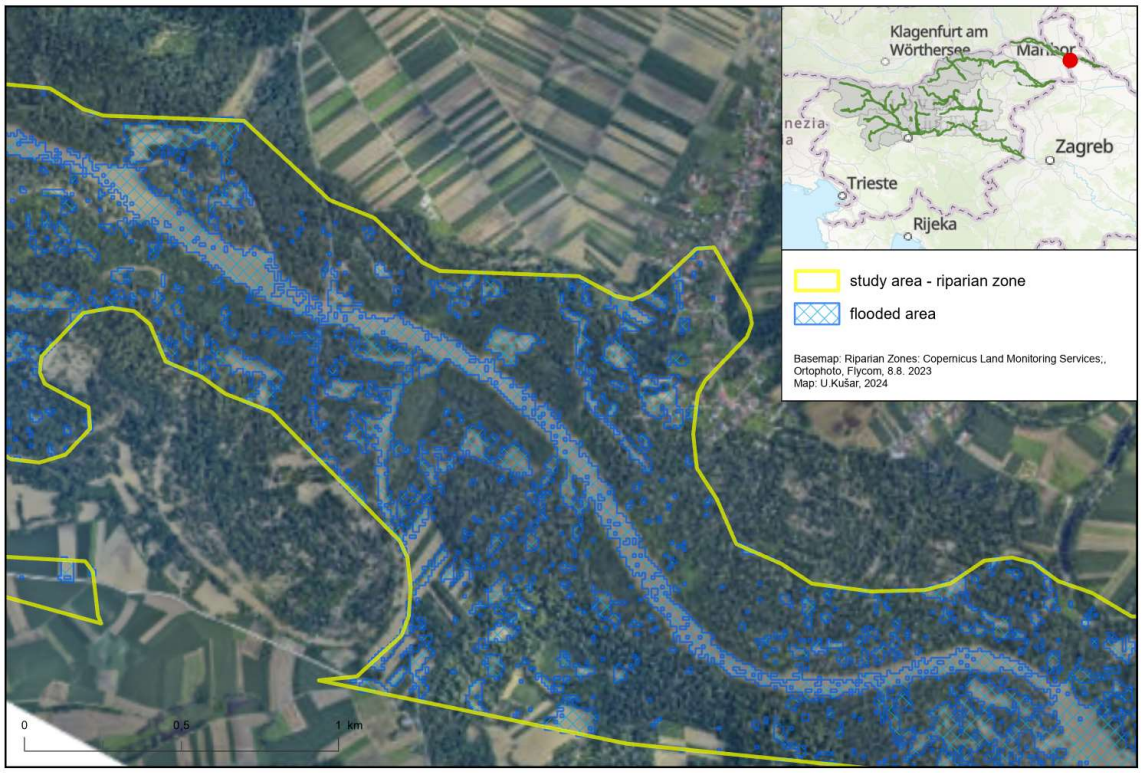


*Figure 32: Study area – demonstration region Mura – Dolenja Bistrica: Flooded areas*

## 3.3. Results – riparian land zone and floods

### 3.3.1. Flooded riparian zone and land cover/ land use

#### 3.3.1.1. Flooded area

Areas affected by floods during the August 2023 flood event extended to 8,396 hectares, constituting 23% of the total riparian zone land area. Riparian zones within water basins affected by flash floods encompassed 14,852 hectares, of which 3,475 hectares, or 23%, were affected. The riparian zone in regions affected by riverine floods is larger, covering 21,939 hectares, with a comparable share of flood-affected areas (4,921 hectares, or 22%). Analysis shows that the most severely affected water basin is the Zgornja Savinja, with 38% of its land flooded, followed by the Sora, Meža, and Kamniška Bistrica water basins, all with over 20% of flooded riparian zones. None of the water basins experiencing riverine floods saw more than 30% of flooded riparian zones, but the Spodnja Sava and Spodnja Drava basins came close with over 25% (Table 25).

*Table 25: Areas and flooded areas by water basins and type of flood*

| Flood Type | WBASIN | Riparian zone area (ha) | Riparian zone dry land (ha) | | |
|---|---|---|---|---|---|
| | | | | of which - flooded | % |
| **Flash flood** | | 17.180 | 14.852 | 3.475 | 23% |
| | **Kamniška Bistrica** | **2.381** | **2.285** | **556** | **24%** |
| | **Meža** | **1.626** | **1.555** | **379** | **24%** |
| | **Sora** | **1.892** | **1.742** | **520** | **30%** |
| | **Zgornja Drava** | **1.667** | **1.021** | **125** | **12%** |
| | **Zgornja Sava** | **6.917** | **5.798** | **966** | **17%** |
| | **Zgornja Savinja** | **2.698** | **2.450** | **930** | **38%** |
| **Riverine flood** | | 26.625 | 21.939 | 4.921 | 22% |
| | **Mura** | **7.234** | **5.529** | **1.074** | **19%** |
| | **Spodnja Drava** | **6.806** | **5.468** | **1.374** | **25%** |
| | **Spodnja Sava** | **7.327** | **5.994** | **1.611** | **27%** |
| | **Spodnja Savinja** | **5.259** | **4.948** | **862** | **17%** |
| **Total** | | 43.809 | 36.791 | 8.396 | 23% |

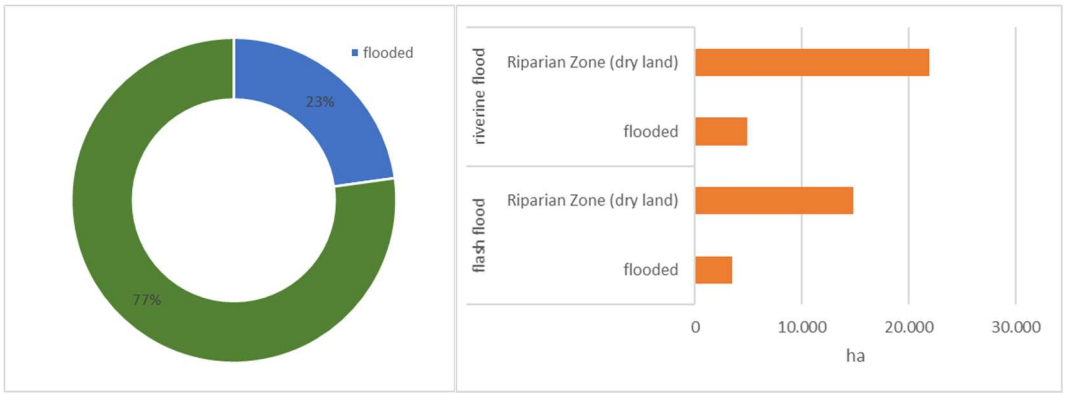


*Figure 33: Comparison of riparian zone (excl. permanent water areas) flooded a) share of total area b) flooded areas by flood type*

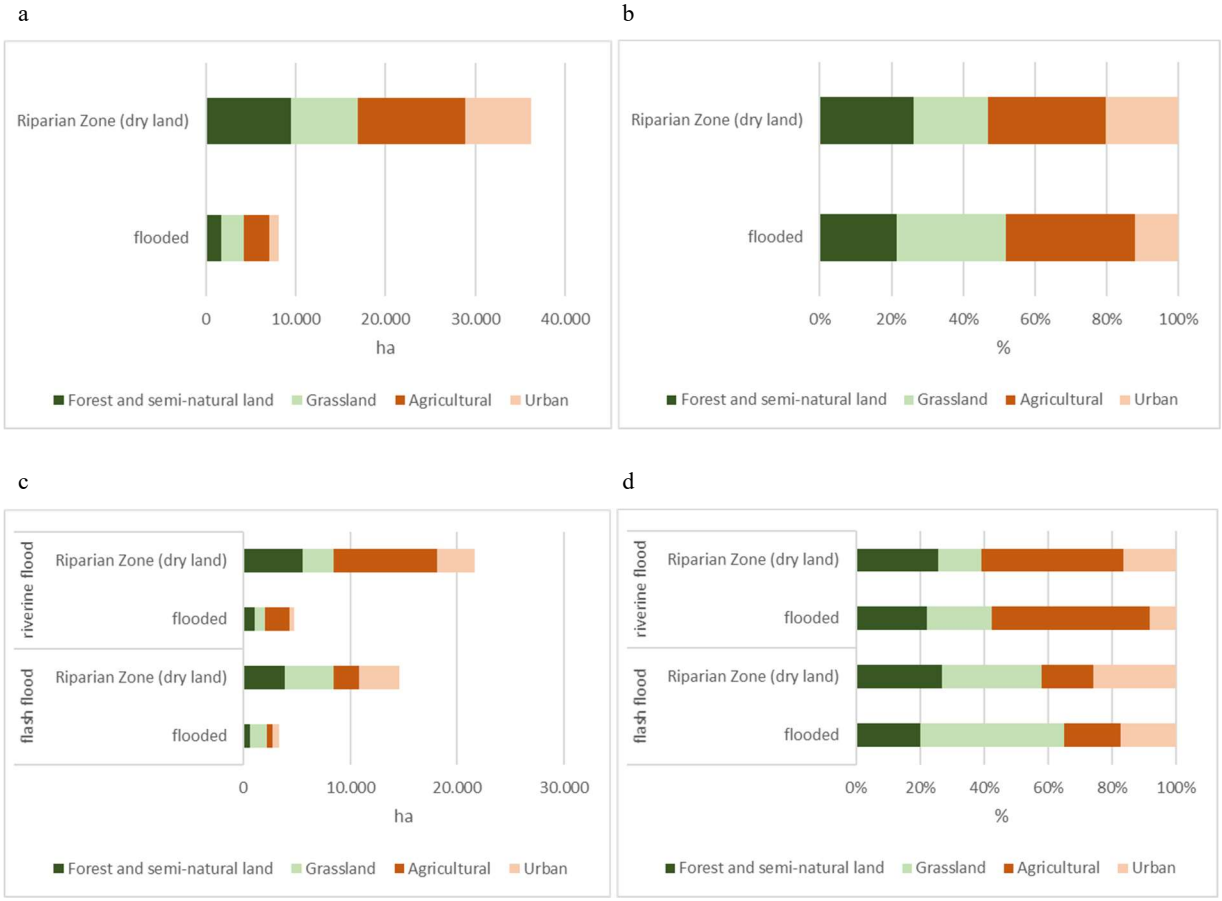


*Figure 34: Comparison of riparian zone (excl. permanent water areas) flooded by land cover/ land use a) in study area in hectares b) in study area as share of total area c) in study area by flood type in hectares d) in study area by flood type as share of total area*

Shares of land cover/land use (LC/LU) classes that were flooded indicate, as shown in Figure 34, that flood impacts correlate with the proportion of LC/LU classes in the total riparian zones across all observed spatial units (the total study area, study area divided by flood type, or study area divided into water basins). Generally, grassland and agricultural land are the classes most impacted, whereas forests and urban areas are less affected.

Riparian zones within the studied water basins vary in size and LC/LU patterns. Landscape metrics conducted (as shown in Table 26) describe the diversity of land use within the riparian zone of each water basin. High diversity serves as an indicator of various development tensions in the area. In Slovenian sub-alpine and sub-pannonian areas, higher diversity typically signifies greater biodiversity and ecosystem services, albeit at the expense of a lower share of forested and semi-natural areas due to competition for space.

Riparian zones in sub-alpine water basins such as Kamniška Bistrica, Sora, Meža, and Zgornja Savinja typically exhibit higher patch density, smaller patch size, and higher edge density compared to downstream water basins, which experienced riverine flood (see Table 26).

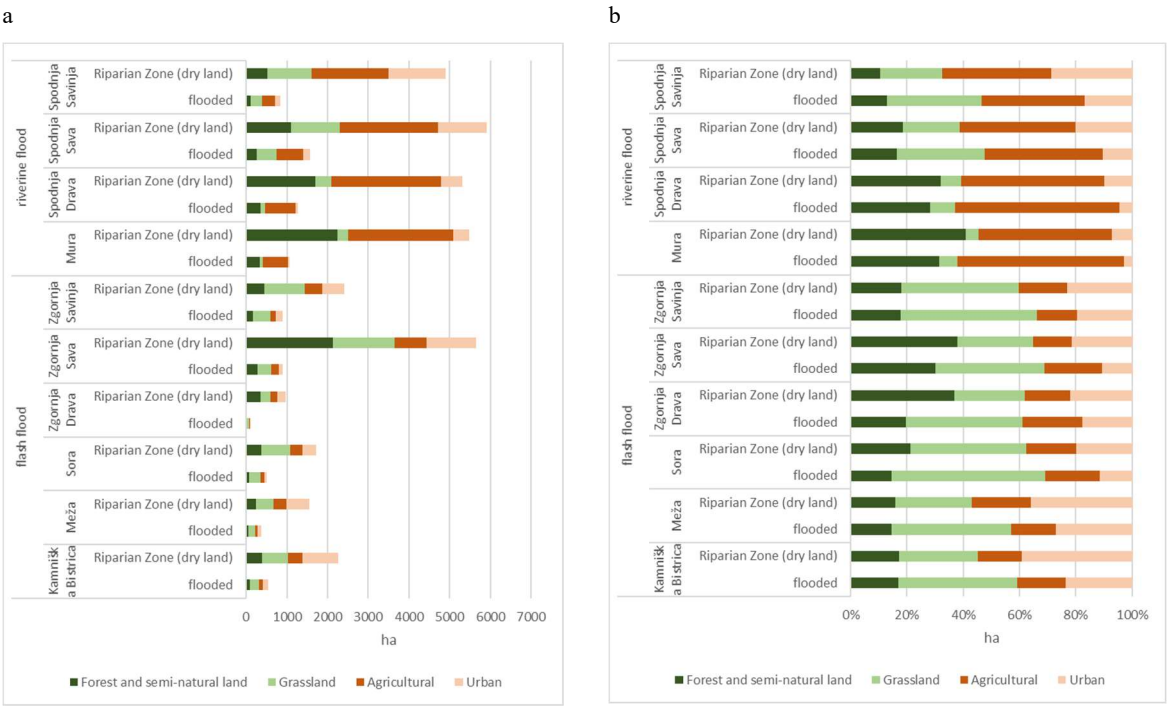


*Figure 35: Comparison of riparian zone (excl. permanent water areas) flooded by land cover/ land use by water basins a) in study area in hectares b) in study area as share of total area*

*Table 26: Landscape pattern metrics of study area, by water basins*

| Index | Patch Density (PD) | Patch Size (PS) | Edge Density (ED) |
|---|---|---|---|
| | no/ha | m2/no | km/ha |
| **Flash flood** | 1,59 | 6.283 | 0,72 |
| Kamniška Bistrica | **1,38** | **7.238** | **0,63** |
| Meža | **1,80** | **5.542** | **0,81** |
| Sora | **1,88** | **5.329** | **0,85** |
| Zgornja Drava | **1,73** | **5.785** | **0,77** |
| Zgornja Sava | **1,41** | **7.115** | **0,64** |
| Zgornja Savinja | **1,84** | **5.429** | **0,81** |
| **Riverine flood** | 1,06 | 9.416 | 0,55 |
| Mura | **0,76** | **13.092** | **0,41** |
| Spodnja Drava | **0,88** | **11.418** | **0,46** |
| Spodnja Sava | **1,13** | **8.870** | **0,61** |
| Spodnja Savinja | **1,55** | **6.450** | **0,71** |
| Total | 1,28 | 7.836 | 0,62 |

### 3.3.2. Flood risk assessments and flooded areas

*Table 27: Surface area of riparian zone, area of riparian zone, that was included in flood risk studies, area recognized as at flood risk (Q100) and Q100 flood risk areas where flood was detected by water basins*

| Water basin | Riparian zone | Flood risk area assessed | | Flood risk Q100 | Q100 flooded | |
|---|---|---|---|---|---|---|
| | ha | ha | % | ha | ha | % |
| **Flash flood - total** | 14.852 | 8.990 | 61% | 3.704 | 1.372 | 37% |
| **Kamniška Bistrica** | **2.285** | **1.987** | **87%** | **696** | **232** | **33%** |
| **Meža** | **1.555** | **1.071** | **69%** | **587** | **179** | **30%** |
| **Sora** | **1.742** | **1.224** | **70%** | **638** | **282** | **44%** |
| **Zgornja Drava** | **1.021** | **76** | **7%** | **41** | **4** | **10%** |
| **Zgornja Sava** | **5.798** | **2.711** | **47%** | **833** | **204** | **24%** |
| **Zgornja Savinja** | **2.450** | **1.921** | **78%** | **909** | **470** | **52%** |
| **Riverine flood -total** | 21.939 | 14.200 | 65% | 11.182 | 2.595 | 23% |
| **Mura** | **5.529** | **1.590** | **29%** | **2.417** | **284** | **12%** |
| **Spodnja Drava** | **5.468** | **3.645** | **67%** | **3.423** | **878** | **26%** |
| **Spodnja Sava** | **5.994** | **4.664** | **78%** | **3.571** | **1.006** | **28%** |
| **Spodnja Savinja** | **4.948** | **4.301** | **87%** | **1.771** | **427** | **24%** |
| **Total** | 36.791 | 23.190 | 63% | 14.886 | 3.967 | 27% |

Available flood risk assessments cover 63% of the riparian zone land area. Since flood risk assessment studies are typically commissioned for areas where land development activities are planned, it can be assumed that the studied areas are biased towards urban and agricultural land use. There is a significant difference in the share of areas with valid results for flood risks in water basins – Zgornja Drava and Mura have less than 30%, while Kamniška Bistrica and Savinja have 87% of the assessment-covered land area.

Most of the sub-alpine flash flood water basins were severely impacted by floods; in Zgornja Savinja, detected flooded areas covered most of the areas with allocated flood risk. A comparison of assessed areas, areas at risk, and areas with detected floods is presented in Figure 34.

To assess the relationship between flood effects and different land cover/land use areas, Figure 35 presents the relative share of LC/LU categories in the riparian zone, the riparian zone with validity of results, flood risk areas, and flooded flood risk areas. Consistent with previous findings, agricultural land is impacted proportionately more than flood risk assessments predicted. All other areas were less impacted, except for Zgornja Drava, where results cover only 7% of the riparian area.


*Figure 35: Surface area of riparian zone, area of riparian zone, that was included in flood risk studies, area recognized as at flood risk (Q100) and Q100 flood risk areas where flood was detected by water basins and land cover/ land use type a) in hectares b) as share of surface area*

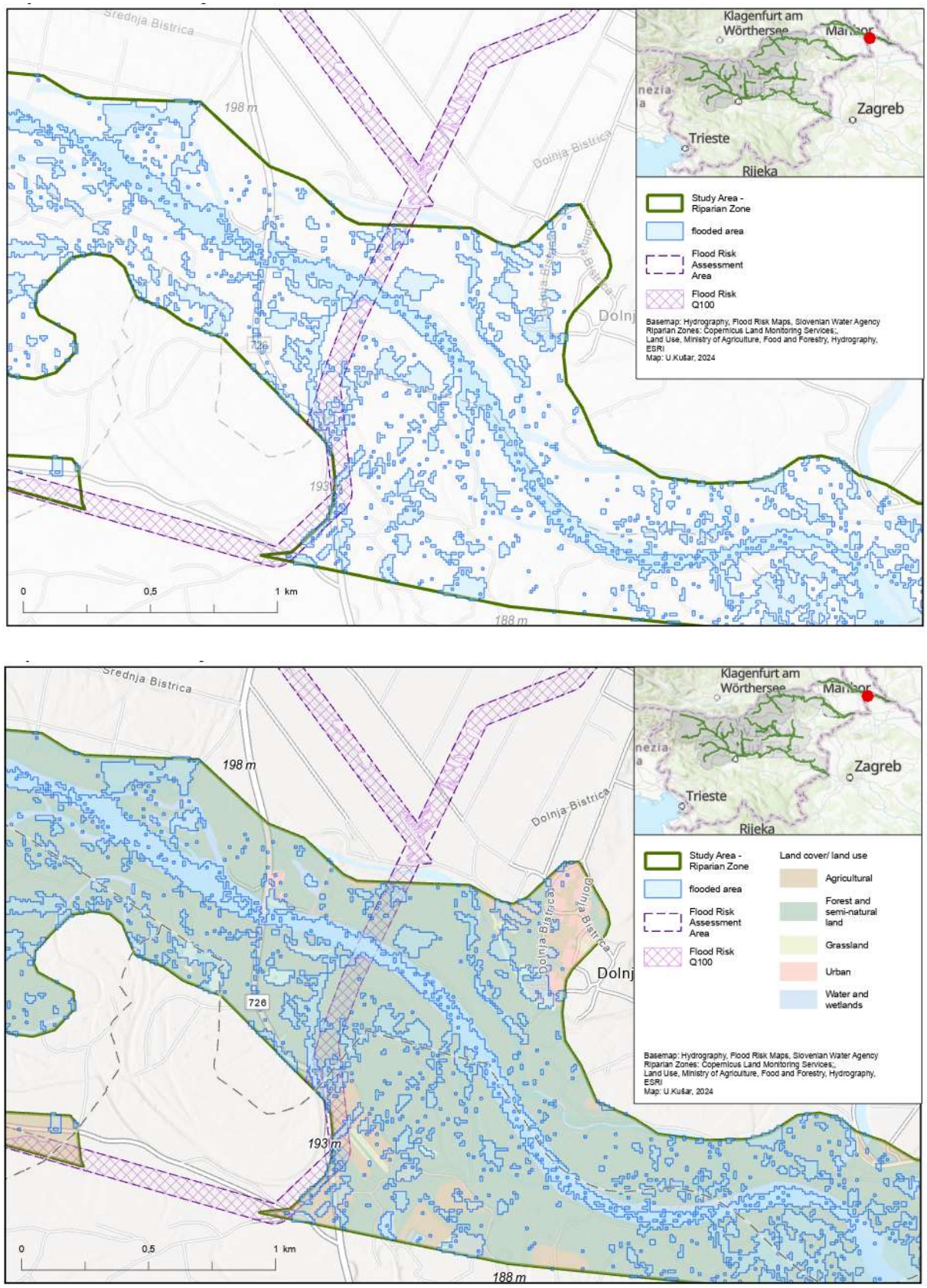


*Figure 36: Study area – demonstration region Mura – Dolenja Bistrica: Flooded area and comparison with previous flood risk assessments – areas included in flood risk assessment and areas with flood risk (Q100)*

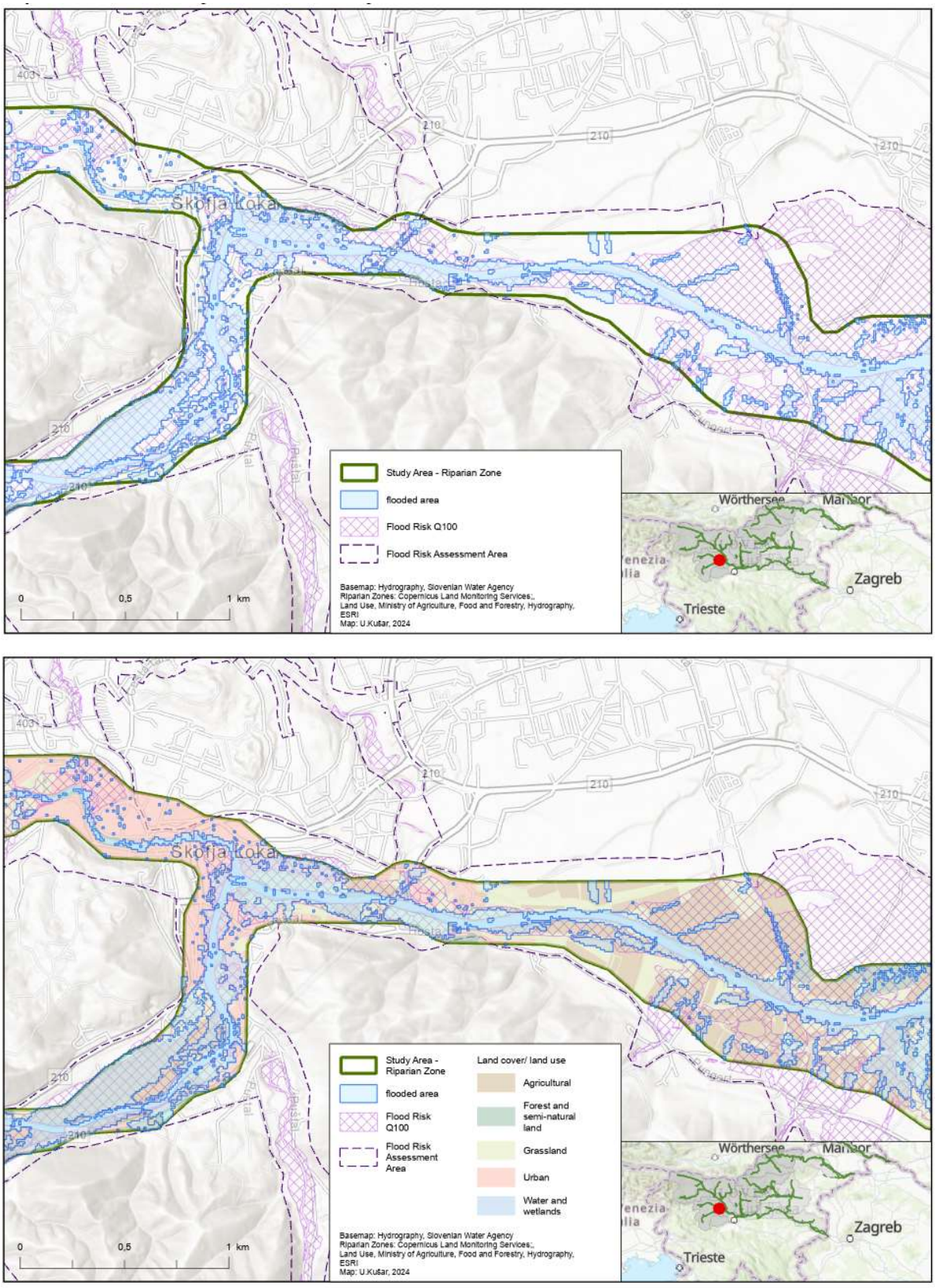


*Figure 37: Study area – demonstration region Sora - Škofja Loka: Flooded area and comparison with previous flood risk assessments – areas included in flood risk assessment and areas in with flood risk (Q100).*

### 3.3.3. Riparian vegetation buffer

Landscape metrics (Table 26) indicate smaller patches and greater diversity in upstream sub-alpine water basins and larger patches in downstream riparian zones. Smaller patch sizes of forested and semi-natural vegetation (Table 28) suggest more fragmented areas. Landscape fragmentation of forested land in riparian zones can disturb green buffer zones. Areal and connectedness metrics of the study area by water basins revealed that although similar in their share of land, patches of forest and semi-natural vegetation in Kamniška Bistrica, Meža, Sora, Zgornja Drava, and Zgornja Savinja riparian zones are smaller and less connected than in the riparian zones downstream, apart from Spodnja Savinja, where the share of forest buffer is smaller and more fragmented. The Mura forested buffer zone extends to almost 40% of the riparian zone area, while riparian zones with the least share of forest buffers are Spodnja Sava, Spodnja Savinja, Meža, and Kamniška Bistica.

#### 3.3.3.1. Forest buffers

a b

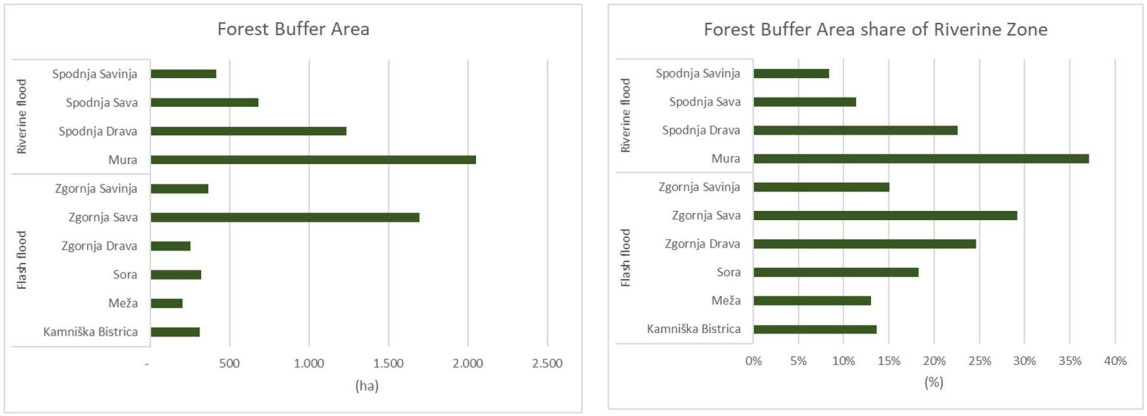


*Figure 38: Forest buffer area and share of forest buffer in riparian zone by water basins*

*Table 28: Landscape metrics – Areal metrics and Connectedness metrics of forest and semi-natural vegetation class by water basin*

| | **Basic Zonal Metrics** | | | | | **Connectedness Index (CI)** | | | |
|---|---|---|---|---|---|---|---|---|---|
| | Class Area (CA) | Number of patches per class (NPC) | Patch density (PD) | Zone area (ZA) | Percentage of zone (PZONE) | Number of Patches (CI-NP) | Connected area (CI-PA) | Patch density (PD) | Share of connected area (CI-PP) |
| | ha | no | no/ha | ha | % | no | ha | no/ha | % |
| **Flash flood** | **3.928** | **8.783** | **2,2** | **14.852** | **26%** | **2626** | **3151** | **0,8** | **21%** |
| Kamniška Bistrica | 389 | 944 | 2,4 | 2.285 | 17% | 271 | 324 | 0,8 | 14% |
| Meža | 244 | 812 | 3,3 | 1.555 | 16% | 317 | 203 | 1,6 | 13% |
| Sora | 366 | 998 | 2,7 | 1.742 | 21% | 363 | 321 | 1,1 | 18% |
| Zgornja Drava | 357 | 1.037 | 2,9 | 1.021 | 35% | 314 | 252 | 1,2 | 25% |
| Zgornja Sava | 2.134 | 3.803 | 1,8 | 5.798 | 37% | 913 | 1685 | 0,5 | 29% |
| Zgornja Savinja | 438 | 1.189 | 2,7 | 2.450 | 18% | 448 | 367 | 1,2 | 15% |
| **Riverine flood** | **5.552** | **7.652** | **1,4** | **21.939** | **25%** | **2524** | **4878** | **0,5** | **22%** |
| Mura | 2.238 | 1.245 | 0,6 | 5.529 | 40% | 169 | 2051 | 0,1 | 37% |
| Spodnja Drava | 1.702 | 1.924 | 1,1 | 5.468 | 31% | 237 | 1236 | 0,2 | 23% |
| Spodnja Sava | 1.095 | 2.590 | 2,4 | 5.994 | 18% | 548 | 677 | 0,8 | 11% |
| Spodnja Savinja | 517 | 1.893 | 3,7 | 4.948 | 10% | 612 | 415 | 1,5 | 8% |
| **Total** | **9.480** | **16.435** | **1,7** | **36.791** | **26%** | **4192** | **7530** | **0,6** | **20%** |

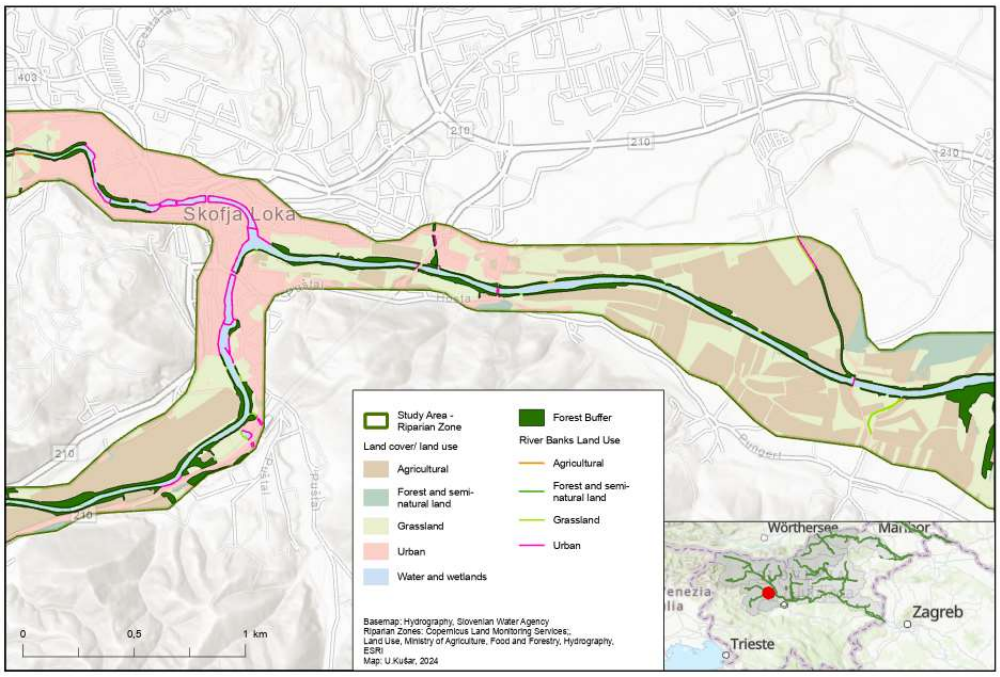


*Figure 39: Study area – demonstration region Sora - Škofja Loka: Patches of forest buffers and land cover/ land use of riverbanks*

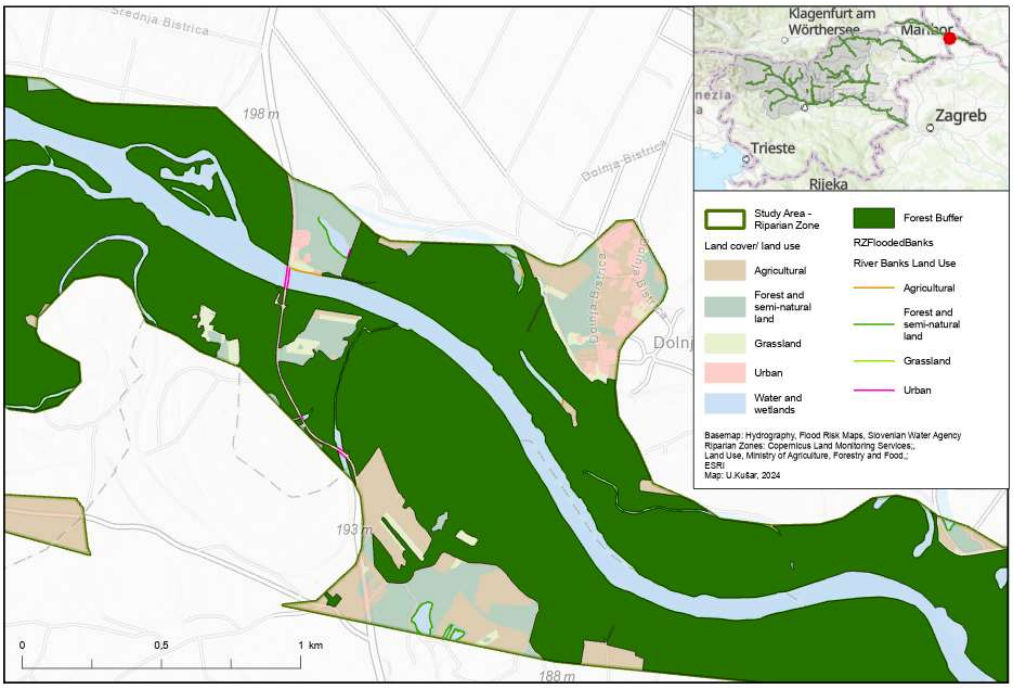


*Figure 40: Study area – demonstration region Mura- Dolenja Bistrica: Patches of forest buffers and land cover/ land use of riverbanks*

### 3.3.3.2. River banks land cover/ land use and flooded area

Riverbanks covered by forest and semi-natural vegetation account for more than half of the riverbanks in all study units, with Zgornja Sava and Mura having more than 80% of riverbanks in their riparian zones covered by forests. Spatial analysis with overlay presented the proportions of riverbanks where water overflowed the water channel (water land area) and overflowed, potentially eroded, riverbanks. The land use structure of flooded and unflooded riverbanks is similar.

a b

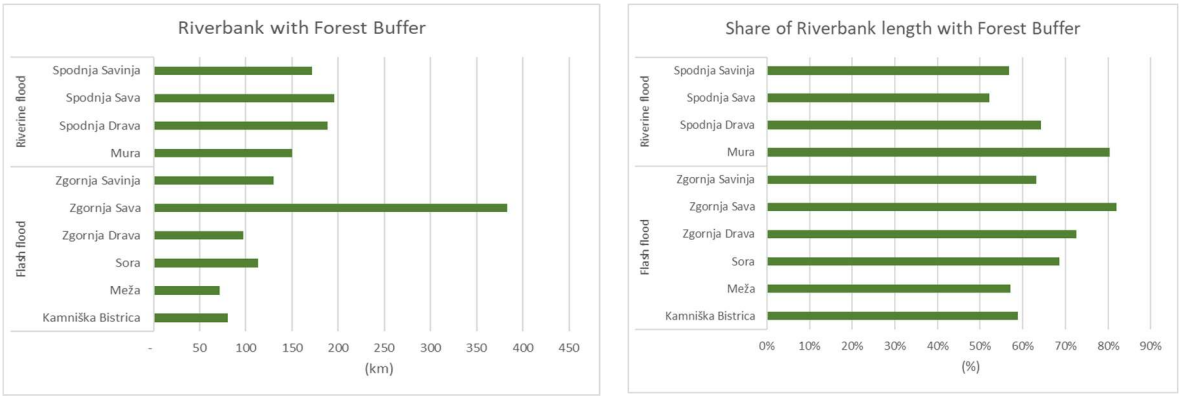


*Figure 41: Length of riverbanks with forest buffer and share of riverbanks with forest buffer in total riverbanks length by water basins*


*Figure 42: Flooded and unflooded river banks by LULC type of neighbouring land by water basins a) length in km b) share of total length*

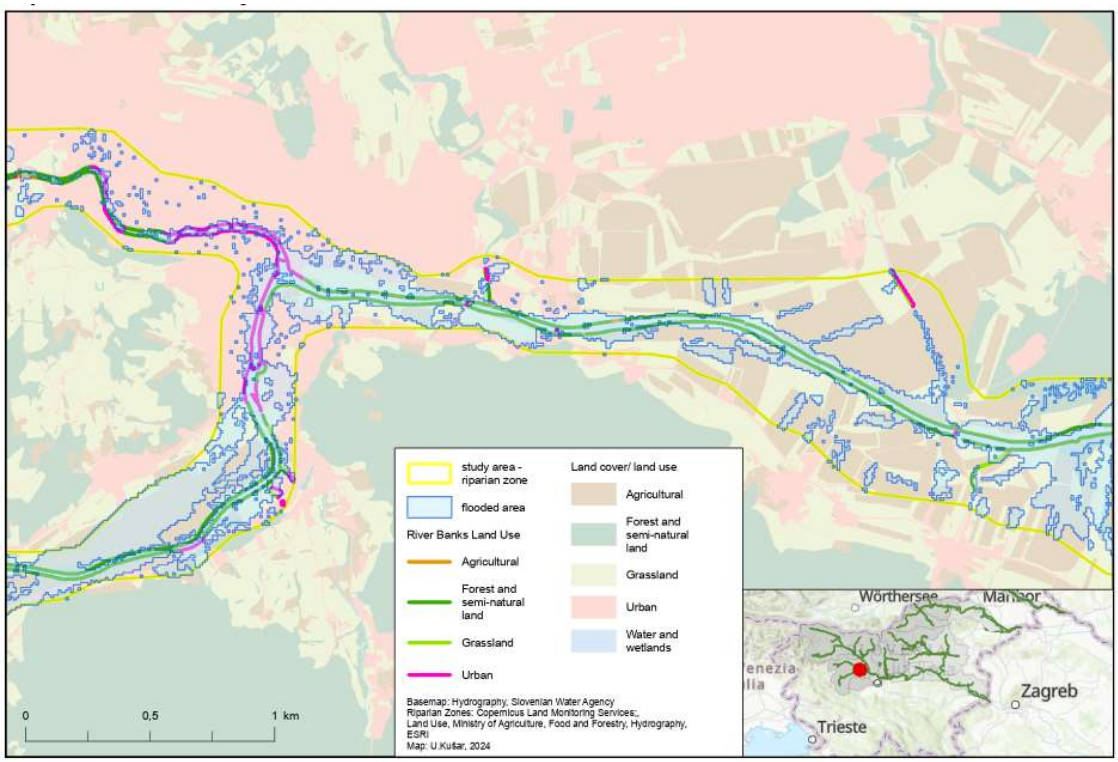


*Figure 43: Study area – demonstration region Sora - Škofja Loka: Flooded and unflooded river banks by LULC type of neighbouring patches*

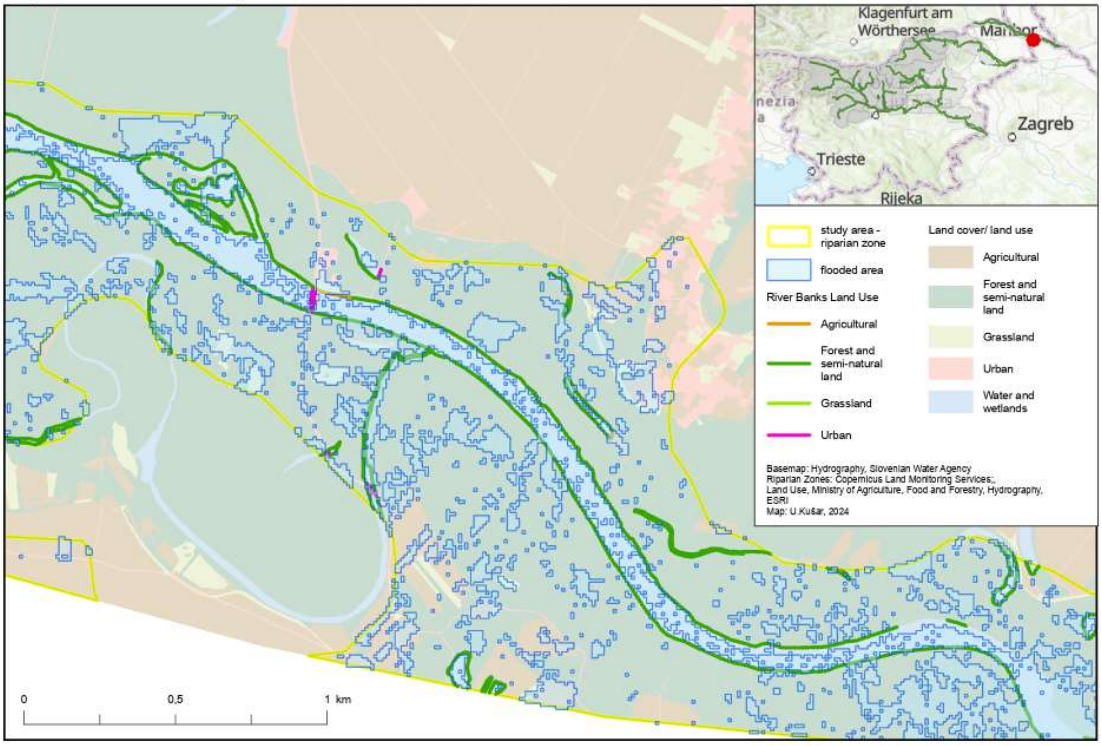


*Figure 44: Study area – demonstration region Mura – Dolenja Bistrica: Flooded and unflooded river banks by LULC type of neighbouring patches*

### 3.3.4. Urban area and buildings

Despite the vulnerability to flood-related disruptions, riparian zones are attractive areas for developing settlements and human infrastructure, particularly in mountainous regions where floodplains offer flat surfaces suitable for agricultural and urban land use. The results of the land cover/land use analysis presented in Figure 34 indicate that 20% of riparian zones are covered by urban land, while the analysis of riverbanks shows that 17% of riverbanks are part of settlements or other urban infrastructure (such as roads and industrial zones).

To evaluate the impact of floods in riparian zones on urban areas and buildings, with a focus on the presence of riparian forest buffers, spatial pattern analysis and spatial proximity analysis were employed. Contrast Metrics were utilized to characterize individual study units concerning the spatial position of urban areas next to water areas. A high level of this contrasting relationship is assumed to indicate a lack of riparian green buffers and less protection from them in the event of flood-related overflow and bank erosion events. Table 29 shows that the Contrast Class Edge (CEE) indicator expresses a relatively equal distribution of water/urban land patches in all units, varying between 7% and 10%, with exceptions of more exposed urban areas in Spodnja Sava (12%) and less exposed areas in Mura and Spodnja Savinja (3% and 4%, respectively).

*Table 29: Landscape metrics – Contrastness metrics by water basin*

| | | **Edge Length (EL):** | **Contrast Class Edge (CCE):** |
|---|---|---|---|
| | | Edge Length(EL) of a selected focus class (urban land) sharing a boundary with corresponding contrast classes (water | Contrast Class Edge (CCE)- percentage of edge length of the focus class (urban land) shared with contrast class (water) |
| | | km | % |
| **Flash flood** | | 216 | 8% |
| | Kamniška Bistrica | 32 | 8% |
| | Meža | 34 | 10% |
| | Sora | 31 | 9% |
| | Zgornja Drava | 19 | 7% |
| | Zgornja Sava | 63 | 7% |
| | Zgornja Savinja | 37 | 7% |
| **Riverine flood** | | 232 | 8% |
| | Mura | 14 | 3% |
| | Spodnja Drava | 48 | 8% |
| | Spodnja Sava | 131 | 12% |
| | Spodnja Savinja | 38 | 4% |
| | | 447 | 8% |

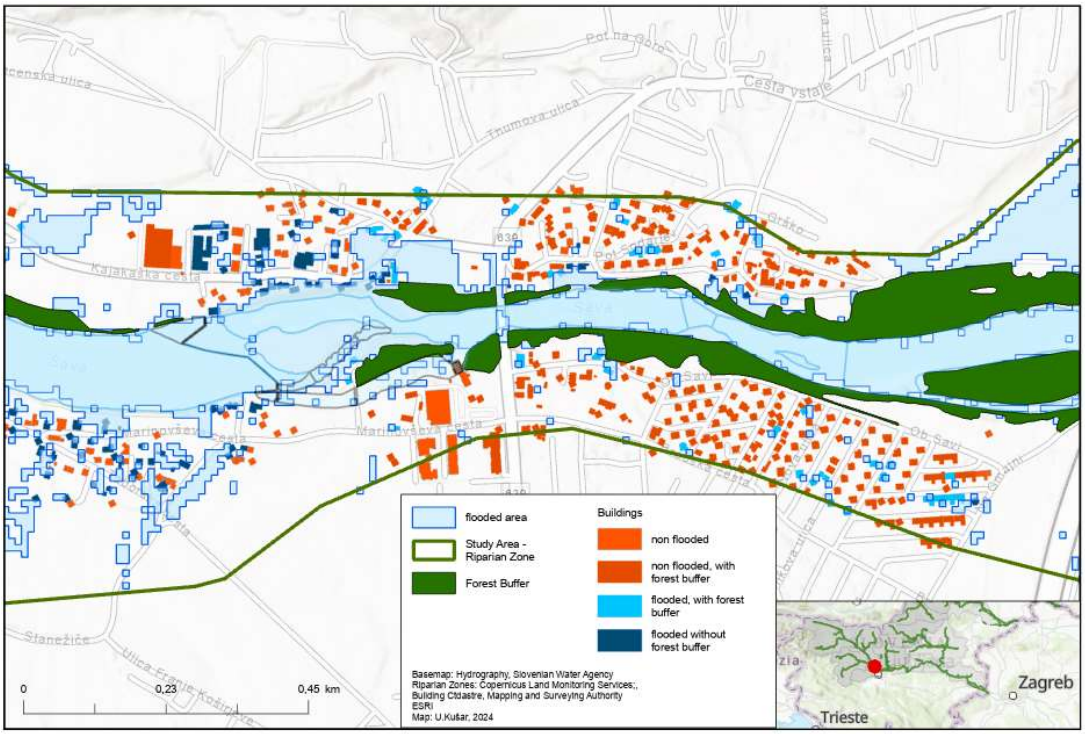


*Figure 45: Study area – demonstration area Sava – Brod: Flooded and unflooded buildings and forest buffer*

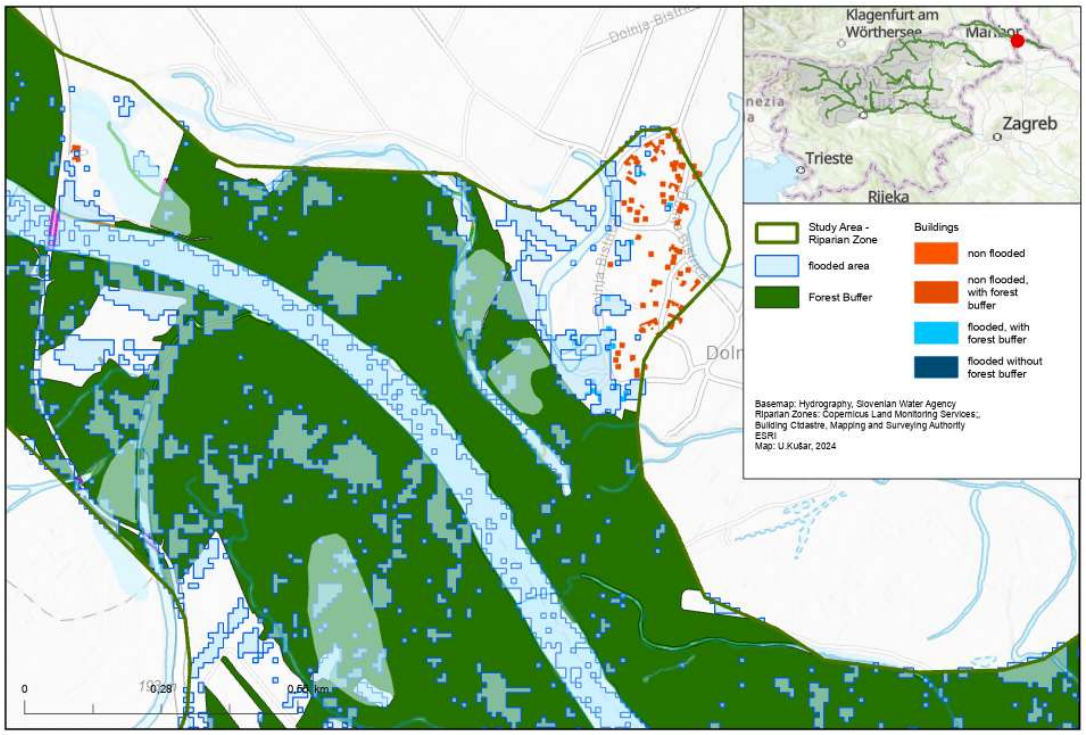


*Figure 46: Study area – demonstration area Mura – Dolenja Bistrica: Flooded and unflooded buildings and forest buffer*

From an anthropogenic perspective, flooded buildings are especially vulnerable to floods. Spatial analysis was conducted using overlay and proximity analysis to evaluate the impact of floods on buildings in relation to riparian forest buffers. Buildings from the BA layer were classified as flooded or unflooded with the overlay of the flooded area layer (FA). Table 30 presents the results: There are 61,031 buildings in the riparian zone study area, of which 15,797, or 26%, were flooded.

For each building, the shortest distance to the nearest riparian forest buffer polygon (RFB) and the distance to the nearest water area polygon (VZ) were calculated. Buildings for which the distance to the RFB was shorter than to the VZ were assumed to be protected by the forest buffer. Around 36% (39,107) of all buildings are closer to the forest buffer than to the river, and 69% of all flooded buildings were those not protected by the forest buffer. Generally, no strong relationship between the forest buffer and flooded buildings can be confirmed, particularly considering many other factors influencing the results.

On the other hand, distance to water is an expectedly important factor in determining whether a building was flooded or not in all water basins (Table 30). This relationship is observable in scatter plots in Figure 47, where each building is presented by a point in relation to the distance to water (x-axis) and forest (y-axis). Blue flooded points in all water basins cluster closer to water, and no significant "unflooded" cluster is observed below the x=y line, which would indicate that forest buffer-protected buildings are generally safer.

*Table 30: Buildings in riparian zone – number of buildings, number of buildings where water is closer than forest buffer (without forest buffer) and number and share of flooded buildings with number and share of flooded buildings without forest buffer, by water basins.*

| | **Buildings in riparian zone** | | | | | | |
|---|---|---|---|---|---|---|---|
| | | | | flooded | | | |
| | total | without forest buffer | | total | | without forest buffer | |
| | No | no | % | no | % | no | % |
| **Flash flood** | **35.866** | **23907** | **67%** | **10.979** | **31** | **7662** | **70%** |
| Kamniška Bistrica | 9.167 | 6642 | 72% | 2.969 | 32 | 2147 | 72% |
| Meža | 4.825 | 3856 | 80% | 1.869 | 39 | 1515 | 81% |
| Sora | 3.383 | 2671 | 79% | 1.051 | 31 | 786 | 75% |
| Zgornja Drava | 1.765 | 1222 | 69% | 304 | 17 | 216 | 71% |
| Zgornja Sava | 10.999 | 5395 | 49% | 1.833 | 17 | 910 | 50% |
| Zgornja Savinja | 5.727 | 4121 | 72% | 2.953 | 52 | 2088 | 71% |
| **Riverine flood** | **25.165** | **15200** | **60%** | **4.818** | **19** | **3217** | **67%** |
| Mura | 3.683 | 915 | 25% | 409 | 11 | 175 | 43% |
| Spodnja Drava | 3.821 | 2069 | 54% | 440 | 12 | 257 | 58% |
| Spodnja Sava | 6.964 | 4419 | 63% | 1.635 | 23 | 1196 | 73% |
| Spodnja Savinja | 10.697 | 7797 | 73% | 2.334 | 22 | 1589 | 68% |
| **Total** | **61.031** | **39107** | **64%** | **15.797** | **26** | **10879** | **69%** |

*Table 31: Buildings in riparian zone – distance form flooded and unflooded buildings to the nearest water area*

| | **Buildings in riparian zone - distance to water** | | |
|---|---|---|---|
| | m | | |
| **Water basin/ class** | **Unflooded** | **Flooded** | **Average** |
| **Flash flood** | **101** | **76** | **93** |
| Kamniška Bistrica | 148 | 118 | 138 |
| Meža | 105 | 63 | 89 |
| Sora | 60 | 49 | 57 |
| Zgornja Drava | 46 | 40 | 45 |
| Zgornja Sava | 87 | 67 | 83 |
| Zgornja Savinja | 99 | 61 | 79 |
| **Riverine flood** | **151** | **111** | **143** |
| Mura | 252 | 181 | 244 |
| Spodnja Drava | 161 | 119 | 156 |
| Spodnja Sava | 115 | 95 | 110 |
| Spodnja Savinja | 130 | 109 | 125 |
| **Total** | **123** | **87** | **114** |

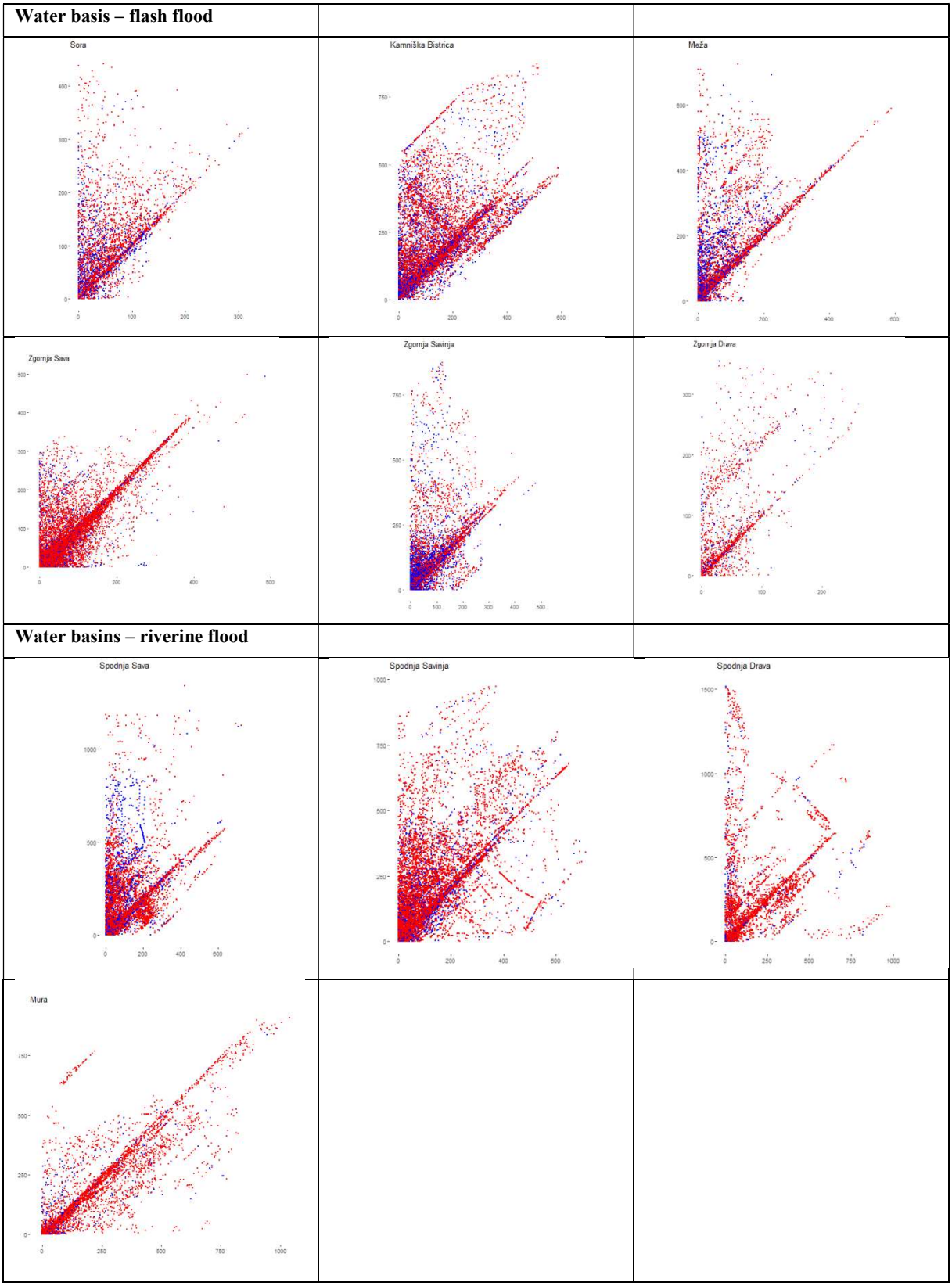


*Figure 47: Scatterplots – buildings in riparian zone flooded (blue) and unflooded (red) presented in relation to the nearest forest patch (y-axis) or water (x-axis), for each water basin*

# 4. DISCUSSION

## 4.1. Introduction

The study explores its subjects in two steps. First part is the delineation of flood affected areas in riparian zones using freely available remote sensing data. The second part presents possible utilisation of delineated flooded area to study the effects of floods on the riparian zone and its land cove/ land use.

## 4.2. Delineation of flood affected areas in riparian zones

Sentinel 1 SAR and Sentinel 2 optical data were processed with Google Earth Engine and geemap python package (Wu, 2020) with the aim to classify and delineate areas impacted by flood event in Slovenia in 2023.

Pre-event, during event and post-event mosaics were compiled from available scenes, filtered by date, orbit direction and quality parameters and clipped to study area (Figure 4, Figure 5). Area of interest – study area were riparian zones (as taken from Copernicus' product Potential Riparian Zones (EEA geospatial data catalogue, 2015)) in the water basins impacted by the flood event, as were reported by Slovenian Environmental Agency (Agencija Republike Slovenije za okolje, 2023). There is some uncertainty regarding the delineation of riparian zones, as the layer was not validated (EEA geospatial data catalogue, 2015) and suggestions for its improvement were encouraged by authors themselves (Weissteiner et al., 2016). Nevertheless, the layer presents important ecoregion, which needs more focus, no other comparable delineation was available, the production of the layer is documented (Weissteiner et al., 2016), and it was successfully used in other studies with similar scope (Piedelobo et al., 2019; Taramelli et al., 2019).

Areas referred in this study as water basins are hydrographical areas or watersheds of watercourses whose riparian zones were delineated (see chapter 2.3.1). To enable comparison between watercourses which were impacted by direct heavy precipitation and flash floods and those which experienced flood with slower, more gradual expansion and contraction of flooded area, watersheds were classified to two groups – Flash Flood water basins and Riverine Flood water basins. Certainly the borders of water basins do not coincide perfectly to precipitation pattern, so there is certain amount simplification and uncertainty regarding allocation of some river zone areas to one flood type or another, however literature suggest (Diakakis et al., 2020; Kobiyama and Goerl, 2007) that precise division of type of floods are difficult and more detailed study of the allocations was beyond the scope of this study.

Sentinel 1 – SAR products are promoted for their suitability to detect flooded areas because of their availability in dark and cloudy conditions. Images were available for situation of August 5 2024, when the flood event was still active in parts of the study area. Two approaches were tested – single image approach where water areas were detected using backscatter intensity and threshold, and change detection approach with pixel by pixel comparison of pre-event and post-event images. During-event

image suggest detection of extensive areas with (open) water, but only small part of the detected areas overlay permanent water bodies from control layer. Visual interpretation of maps with resulted binarisation layer (water/ non-water) reveals that surface roughness of rivers' surface was enhanced, possibly causing increased reflection of volume scatter, explaining lower water area detection on rivers and streams (Table 13). At the same time many smaller areas/ polygons of open water are detected on (previously dry) land, not connected to watercourses, suggesting possible importance of pluvial flooding.

Visual comparison of maps of demonstration areas of Sora – Škofja Loka in sub-alpine region and Mura – Dolenja Bistrica in sub-pannonian region reveal that permanent water areas are much better detected in S1 images in the case of wider rivers (Mura, Sora downstream) in both VV and VH polarisations. As most of the rivers and streams in the studied riparian zones are less than 10 m wide, this could explain why only smaller part of permanent water areas are detected in single S1 images.

Change detection approach confirmed that VV polarisation is suitable for detection of flooded vegetation (Tsyganskaya et al., 2018) due to its sensitivity to vertical objects (such as tree trunks). Flooded area was classified with two thresholds: the area that exhibits significant decreased backscatter, indicating increased water presence, and area with significantly increased backscatter, suggesting double bounce effect in flooded vegetation and possibly urban areas. As expected, only minor proportions of these changes were detected on permanent water areas.

Sentinel 2 uses optical instruments to detect reflection in different wavelengths. It is sensitive to atmospheric conditions, which is particularly relevant for detection of floods and other precipitation-related events, where cloud coverage can significantly reduce usability of available scenes. This proved to be the case during the event where images captured during the event were almost completely covered with clouds (Figure 5). Quality of data regarding the cloud coverage was an important issue also for the composition of pre-event and post-event mosaics, which needed to be cloudless in order to enable pixel based change detection approach. Suitable time-frames and pre-processing with existing parameters and layers (s2cloudless by created by Sentinel and included as service in GEE (Google Developers, n.d.)) were needed to create cloudless pre- and post- event image mosaics. For each S2 mosaic, six spectral indices were calculated using different combinations of Sentinel-2 optical imagery bands. Applied single image approach to detect water was, expectedly, not successful in detected flooded areas, but revealed that spectral indices designed to detect water areas (NDWI and AWEInsh) performed similarly. It was not expected to detect vast open water areas in optical images, as the flood receded relatively fast, within a few hours in the sub-alpine (flash-flood) region and within a few days in the downstream riverine flood region. Both indices use green and NIR bands, with AWEInsh also including SWIR bands, which have a lower (20m) pixel resolution and is therefore expected to be less precise, which was demonstrated in the results of change detection approach analysis. Pixel-by-pixel change detection analysis of pre-

and post-event mosaics of each of 6 applied spectral indices revealed detection of different changes caused by flood such as enhanced soil moisture, debris flows, mud deposits, landslides, and soil erosion as well as decreased health and vigour of green vegetation. Visual inspection of results and conducted accuracy assessments suggest that both, flash floods and riverine floods impacts in vegetated sub-alpine and sub-pannonian regions can be best observed by the impacts to vegetation, which is detected by changes in NDVI.

Floods effect vegetation by uprooting, debris, gravel and mud deposits and damaged structure, causing decline in its health and vigour (Gregory et al., 1991). The Normalized Difference Vegetation Index (NDVI) normalizes green leaf scattering in near-infrared (NIR) wavelengths with chlorophyll absorption in red wavelengths (Kriegler et al., 1969) and is designed to measure the health, density, and vigour of vegetation.

Single image approach and change detection approach used in this study were based on thresholding, setting the value of scattering or index value to classify image in two (or more) classes. This can be done by fixed, empirically based method, where visual interpretation of frequency histograms, prior knowledge of the data or trial and error techniques are used to set the threshold optimal for selected study (Lombana and Martínez-Graña, 2022) or by automatic histogram-based algorithms, such as the Otsu's method which automatically calculates an optimal threshold by maximizing the between-class variance in the image histogram. It demonstrates efficacy for bimodal histograms when the classes of interest are well-separated (Otsu, 1975). Both approaches were used in this study.

Thresholding based classification is straightforward and effective, and can be adapted to studied situation. At the same time this makes it very sensitive to local outliers and expert biases and therefore less suitable for generic, global approach or wider regions. The study area in this study is extensive and variable, not all local specificities could be considered, which and it proved to be difficult to set optimal thresholds.

To enable accuracy assessment of selected SAR and spectral indices, a stratified randomised sample of 121 points was created. Points were classified as flooded or unflooded with point-by-point manual assessment with available spatial data resources: post-event areal ortophotos, humanitarian organisations damage claims, Copernicus Rapid Mapping Products. Points were classified in the resolution which corresponded the 10m pixel size, considering the majority of 10m circle around the point as a reference. Although there were several reliable sources available to assess the status of each point, some uncertainty remained, particularly in the regions that were not covered by areal orthophotos in the Spodnja Sava and Spodnja Drava water basins.

Accuracy assessment analysis of results obtained from Sentine-1 and Sentinel-2 products demonstrated significant differences in the performance of different approaches, but also some similarities. Almost all indices presented high users' accuracy and many of them at the same time low scores for producers'

accuracy. Low producer's accuracy suggests that the algorithm tends to underperform in detecting targeted (flooded) areas. With combination of indices' results overlay and union combined results (composites) were obtained and tested for accuracy. Results revealed improved accuracy (tables 21-23), and achieved relatively high score (0,88) for indices obtained with change-detection in spectral imagery. Combined results show good and constant results in all classes – there is no significant difference between riverine and flash flood impacted areas. Land cover/ land use classes' accuracy assessment results show more disparity, with urban area flood detection performing less good in users' and overall accuracy and agricultural land class in user's accuracy score.

After post processing to reduce noise and enhance spatial coherence, the layer of flooded areas was finalized and maps of demonstration areas on Sora and Mura were prepared (Figure 31, Figure 32).

### 4.3. Impacts of floods in riparian zone

Riparian zones are transitional areas between land and water ecosystems, characterized by unique soil, hydrology, and biotic conditions. They extend from the low to high water marks of streams and include adjacent terrestrial areas like floodplains and terraces. (Naiman et al., 2010; Weissteiner et al., 2016). These zones are heavily influenced by stream water and are vulnerable to flooding, which can cause erosion of soil and uprooting of vegetation, deposition of sediments, affecting soil structure and nutrient content, displacing of the habitats of wildlife species dependent on riparian zones e.g. loss of nesting sites (Gregory et al., 1991). Changes in land use, such as urbanization and agricultural intensification, can alter riparian hydrology and increase flood risks. Encroachment into floodplain areas exacerbates these risks by reducing natural flood storage capacity and impairing ecosystem functions. Urbanization in riparian zones leads to habitat loss, water quality degradation, and intensified stormwater runoff, heightening flood risk in developed areas peaks (Jiménez-Jiménez et al., 2020; Miller et al., 2014). To minimize flood impacts and enhance ecosystem resilience, implementing flood-resilient land use practices in riparian zones is crucial.

The study aimed to exploit the layer of flooded areas identified in previous steps of the study, to examine spatial relationship between flooded areas and land cover/ land use of riparian zones. Its objective was to identify possible differences in effects to areas with various land cover/ land use (e.g. urban, forested/semi-natural, agricultural, grassland), taking into account also the different type of flood event (riverine flood, flash flood). Riparian zones of 10 different water basins (see chapter 2.3.1) were used as study subunits to examine their similarities and differences regarding land cover/ land use patterns and flood effects.

Several indicators and landscape metrics were used to characterize water basins regarding their landscape pattern characteristics, including existence of riparian forest buffer and forested riverbanks, and their exposure to flood risk and flood impacts.

Areas affected by floods during the August 2023 flood event extended to 8,396 hectares, constituting 23% of the total riparian zone land area. Although the extent of riparian zone in the sub-pannonian, riverine flood water basins is larger than in sub-alpine, flash flooded water basins, the share of flooded area is similar, 22% and 23%. Among most severely impacted subunits, measured as a share of flooded riverine zone, are Zgornja Savinja (38%) and Sora (30%), both sub-alpine waterbasins (Table 25).

Landscape pattern analysis showed that sub-alpine water basins typically have higher patch density, smaller patch size and higher edge density than downstream water basins, which experienced riverine flood (Table 26). Smaller patch sizes are usually linked with higher diversity (smaller agricultural plots, smaller urban settlements with smaller impact) and can indicate more limited space and higher demand for land suitable for anthropogenic use. This process usually limits forest and semi-natural vegetation areas to steeper slopes, using other areas with smaller inclines, for settlements and urban infrastructure, agriculture, and grassland. Process can be accompanied with rivers' and streams' regulations and embankment to mitigate floods and shifting channels as these areas exacerbates flood risks by reducing natural flood storage capacity and impairing ecosystem functions. Existing Flood Risk Assessments do not include all riparian zone areas and cannot be used as an adequate measure of actual flood risk (e.g. Figure 36 and 37). Comparison with detected flood risk areas and flooded area revealed that detected flood risk areas were indeed flooded in the event in sub-alpine water basins and less so in sub-pannonian basins. Differences in reported and assessed areas can be partially attributed to differences in the resolution - flood risk assessments are typically modelled and based on areal LIDAR derived DEM with sub-meter resolution.

One of the natural-based solutions to mitigate flood risks suggested by development strategies and spatial development literature are green or forested buffer zones. In the study riparian forest buffers were identified and their landscape metrics compared between water basins. Larger patch sizes of forested land indicate less fragmented and more intact riparian zone vegetation. Areal and Connectedness metrics revealed that although similar in its share of land, patches of forest and semi-natural vegetation of sub-alpine riparian zones are indeed smaller and less connected than in the riparian zones downstream, apart from Spodnja Savinja, where share of forest buffer is smaller and more fragmented. Outstanding is the riparian forested buffer of Mura, which extends to almost 40% of riparian zone area, while riparian zones with least share of forest buffers are also those whose urban areas take the largest share: Spodnja Sava, Spodnja Savinja, Meža and Kamniška Bistica. Same patterns appear when comparing the length and share of forested river banks (Figure 41). Spatial analysis with overlay presented the proportions of riverbanks where water overflowed the water channel (water land area) and overflowed, potentially eroded, riverbanks. Land use structure of flooded and unflooded riverbanks are similar (Figure 42), suggesting that, in general land cover/ land use of riverbanks did not play an important role in embarking flood water. On the other hand, LC/LU analysis of flooded areas (Figure 34) showed that forests are slightly less impacted by floods than grassland or agricultural land.

Shares of land cover/land use (LC/LU) classes that were flooded show (Figure 34) that flood impacts are correlated to the share of LC/LU classes in total riparian zones in all of the observed spatial units. Generally, grassland and agricultural land are classes which are more impacted, whereas forests and urban areas are less. To assess further the relationship between flood effects and different land cover/ land use areas Figure 35 presents relative share of LC/LU category in riparian zone, riparian zone with validity of results, flood risk areas and flooded flood risk areas. Consistent with previous findings, agricultural land is impacted more than flood risk assessments predicted and other areas, including urban, grassland and forested, less.

Riparian zones, despite their vulnerability to flood-related disturbances, are often chosen for human settlement and infrastructure development, especially in mountainous areas where floodplains offer flat land suitable for urban and agricultural purposes. LC/LU analysis reveals (Figure 34) that a significant portion of riparian zones is covered by urban areas, with a notable percentage of riverbanks integrated into settlements and other urban infrastructure. To assess flood impacts on urban areas and buildings within riparian zones, spatial pattern and proximity analyses were conducted, focusing on the presence of riparian forest buffers. Contrast Metrics were employed to characterize the spatial relationship between urban areas and water bodies, indicating varying degrees of exposure to flood risks across different study units (Table 29). Flooded buildings, particularly vulnerable to floods, were analysed in relation to their proximity to riparian forest buffers and water bodies. Results (Table 30, Figure 47) suggest that buildings closer to water are more likely to be flooded, and while forest buffers may offer some protection, their influence on flood outcomes appears less significant when considering other contributing factors.

### 4.4. Strength, weaknesses and future work

Timely response, coverage, consistency, multi-sensor integration and cost-effectiveness are the strengths of applied approach to delineate flooded areas using openly available satellite resources and cloud computing platform.

With this approach flood detection is possible within a few days from the event, allowing for emergency response and mitigation efforts. Large areas, including remote and inaccessible regions can be comprehensively covered consistently, using standardized flood detection methodology, ensuring uniformity in monitoring and analysis. Approach enable integration of SAR and optical sensors to enhance accuracy. Due to utilisation of open, freely available data and cloud-computing platform it is also very cost-effective and accessible to non-governmental and humanitarian organisations.

Weaknesses of the approach are based on limited spatial and temporal resolution of available products and data interpretation challenges, which are based on expertise and may be subjective, leading to potential inaccuracies or misinterpretations.

Riparian zone flood impact analysis is limited to simple landscape pattern metrics and overlay correlations observation and is not intended to be exhaustive cause and effect analysis. It presents possible utilisation of remote sensing products as a mean to expand the study areas of typical riparian zone study from limited, local to larger, more diverse region.

Future work can significantly improve reliability and usability of the results. With the development and application of advanced data processing techniques, such as machine learning algorithms and object-based image analysis existing data sources could be further exploited to reveal even more accurate results.

Adding data sources with better spatial and temporal resolution and different sensors would enable better precision and detection of smaller changes/ objects. Enhanced riparian zone delineation, employment of additional data, such as data form hydraulic/ hydrologic studies, DEM, structural/ infrastructure inventories, biodiversity monitoring data, additional flood risk assessments etc., would significantly improve understanding of flood impact to riparian zones.

## 5. CONCLUSION

The study used geospatial analysis and freely accessible remote sensing products to explore how floods impacted riparian zones in August 2023 flood event in Slovenia. Its focus was on different land cover/ land use areas in riparian zones and different flood types.

The study presents approach to successfully identify and map flood-affected areas in sub-alpine regions using open-source satellite remote sensing products from Copernicus earth observation programs Sentinel-1 and Sentinel-2. Several products were developed based on different polarisation of Sentinel-1 SAR and different band combinations (spectral indices) of Sentinel-2 products. Visual interpretation of the results and conducted accuracy assessments suggest that both, flash floods and riverine floods impacts in vegetated sub-alpine and sub-pannonian regions can be best observed by the impacts to vegetation. These can be detected by changes in vegetation sensitive spectral indices, such as NDVI. Floods effect vegetation by uprooting, debris, gravel and mud deposits and damaged structure, causing decline in its health and vigour (Gregory et al., 1991). The Normalized Difference Vegetation Index (NDVI) normalizes green leaf scattering in near-infrared (NIR) wavelengths with chlorophyll absorption in red wavelengths (Kriegler et al., 1969) and is designed to measure the health, density, and vigour of vegetation.

Single image approaches of both Sentinel-1 and Sentinel-2, which aim to detect increased water areas or moisture were only marginally successful, presumably because of the nature of flash floods, where water itself retreats rapidly and can only rarely be captured by particular remote sensing image. Optical sensors are additionally challenged by atmospheric disruptions in extreme precipitation events.

The riparian zones, acting as transition areas between land and water ecosystems, exhibit unique soil, hydrology, and biotic conditions, encompassing riverbanks and adjacent terrestrial areas like floodplains and terraces. Vulnerable to flooding, these zones suffer erosion, sediment deposition, and habitat displacement, exacerbated by changes in land use such as urbanization and agricultural intensification. Urbanization, especially in mountainous regions, where floodplains are attractive for development, increases flood risk through habitat loss, water quality degradation, and intensified stormwater runoff. The study aimed to explore flood effects in riparian zones by analyzing the spatial relationship between flooded areas and land cover/land use, employing landscape pattern analysis and assessing forest buffers' role in flood mitigation.

Key findings reveal that flood impacts disproportionately affect agricultural and grassland areas over urban and forested regions, although this effect is not significant. Riparian forest buffers, though potentially offering some protection, exhibit less significant influence on flood outcomes compared to other factors, such as distance to water.

The study investigated the differences in flood effects to riparian zones between sub-alpine/flash flood impacted and sub-pannonian/riverine flood impacted water basins. Findings revealed that while the extent of riparian zones was larger in sub-pannonian basins compared to sub-alpine basins, the share of flooded area was similar, around 22% to 23%. However, some sub-alpine basins experienced more severe impacts, with Zgornja Savinja and Sora being the most severely affected, constituting 38% and 30% of the flooded riparian zone, respectively. Landscape pattern analysis indicated that sub-alpine basins typically exhibited higher patch density, smaller patch size, and higher edge density compared to downstream water basins experiencing riverine flood. Smaller patch sizes in sub-alpine basins were linked to higher diversity and anthropogenic land use, such as settlements, urban infrastructure, agriculture, and grassland, possibly leading to increased flood risks. Riparian forest buffers were identified as a potential natural-based solution to mitigate flood risks, with larger and more connected patches of forested land observed in downstream basins. However, despite the presence of forest buffers, flood impacts were still significant, particularly on grassland and agricultural land. Overall, sub-alpine basins, despite covering smaller areas of riparian zones, experienced more severe flood impacts compared to sub-pannonian basins, highlighting the need for tailored flood management strategies in different riparian zone environments.

Despite their susceptibility to flood-related disturbances, riparian zones remain attractive for human settlement and infrastructure development, emphasizing the need for flood-resilient land use practices to mitigate adverse impacts and enhance ecosystem resilience.

## LIST OF REFERENCES

Adamczyk, J., Tiede, D., 2017. ZonalMetrics - a Python toolbox for zonal landscape structure analysis. Comput. Geosci. 99, 91–99. https://doi.org/10.1016/j.cageo.2016.11.005

Adeel, Z., Alarcón, A.M., Bakkensen, L., Franco, E., Garfin, G.M., McPherson, R.A., Méndez, K., Roudaut, M.B., Saffari, H., Wen, X., 2020. Developing a comprehensive methodology for evaluating economic impacts of floods in Canada, Mexico and the United States. Int. J. Disaster Risk Reduct. 50, 101861. https://doi.org/10.1016/j.ijdrr.2020.101861

Agencija Republike Slovenije za okolje, 2023. Izjemne poplave v Sloveniji med 4. in 8. avgustom 2023 (Poročilo o poplavah). Agencija RS za okolje, Ljubljana.

Agoha, C., Armstrong, A., Onwubuariri, C., Mgbeojedo, T., Obiageri, N., Begianpuye, A., Epuerie, E., 2024. Review of Spatial Analysis as a Geographic Information Management Tool. Am. J. Eng. Technol. Manag. 9, 8–20. https://doi.org/10.11648/j.ajetm.20240901.12

Anderson, J.R., 1976. A Land Use and Land Cover Classification System for Use with Remote Sensor Data. U.S. Government Printing Office.

Apan, A.A., Raine, S.R., Paterson, M.S., 2002. Mapping and analysis of changes in the riparian landscape structure of the Lockyer Valley catchment, Queensland, Australia. Landsc. Urban Plan. 59, 43–57. https://doi.org/10.1016/S0169-2046(01)00246-8

Atefi, M.R., Miura, H., 2022. Detection of flash flood inundated areas using relative difference in NDVI from sentinel-2 images: a case study of the August 2020 event in Charikar, Afghanistan. Remote Sens. 14, 3647.

Atreya, A., Ferreira, S., 2015. Seeing is Believing? Evidence from Property Prices in Inundated Areas. Risk Anal. 35, 828–848. https://doi.org/10.1111/risa.12307

Bakkensen, L., Blair, L., 2020. Flood damage assessments: theory and evidence from the United States, in: Oxford Research Encyclopedia of Politics.

Bangira, T., Iannini, L., Menenti, M., van Niekerk, A., Vekerdy, Z., 2021. Flood Extent Mapping in the Caprivi Floodplain Using Sentinel-1 Time Series. IEEE J. Sel. Top. Appl. Earth Obs. Remote Sens. 14, 5667–5683. https://doi.org/10.1109/JSTARS.2021.3083517

Batič, M., 2018. Sentinel Hub Cloud Detector — s2cloudless. Sentin. Hub Blog. URL https://medium.com/sentinel-hub/sentinel-hub-cloud-detector-s2cloudless-a67d263d3025 (accessed 4.14.24).

Bell, F.C., Om Kar, S., 1969. Characteristic response times in design flood estimation. J. Hydrol. 8, 173–196. https://doi.org/10.1016/0022-1694(69)90120-6

Brivio, P.A., Colombo, R., Maggi, M., Tomasoni, R., 2002. Integration of remote sensing data and GIS for accurate mapping of flooded areas. Int. J. Remote Sens. 23, 429–441. https://doi.org/10.1080/01431160010014729

Brodu, N., 2017. Super-Resolving Multiresolution Images With Band-Independent Geometry of Multispectral Pixels. IEEE Trans. Geosci. Remote Sens. 55, 4610–4617. https://doi.org/10.1109/TGRS.2017.2694881

Burdon, F.J., Ramberg, E., Sargac, J., Forio, M.A.E., de Saeyer, N., Mutinova, P.T., Moe, T.F., Pavelescu, M.O., Dinu, V., Cazacu, C., Witing, F., Kupilas, B., Grandin, U., Volk, M., Rîşnoveanu, G., Goethals, P., Friberg, N., Johnson, R.K., McKie, B.G., 2020. Assessing the Benefits of Forested Riparian Zones: A Qualitative Index of Riparian Integrity Is Positively Associated with Ecological Status in European Streams. Water 12, 1178. https://doi.org/10.3390/w12041178

Capon, S.J., Chambers, L.E., Mac Nally, R., Naiman, R.J., Davies, P., Marshall, N., Pittock, J., Reid, M., Capon, T., Douglas, M., Catford, J., Baldwin, D.S., Stewardson, M., Roberts, J., Parsons, M., Williams, S.E., 2013. Riparian Ecosystems in the 21st Century: Hotspots for Climate Change Adaptation? Ecosystems 16, 359–381. https://doi.org/10.1007/s10021-013-9656-1

Ceccato, P., Flasse, S., Tarantola, S., Jacquemoud, S., Grégoire, J.-M., 2001. Detecting vegetation leaf water content using reflectance in the optical domain. Remote Sens. Environ. 77, 22–33. https://doi.org/10.1016/S0034-4257(01)00191-2

Cerbelaud, A., Blanchet, G., Roupioz, L., Breil, P., Briottet, X., 2023. Mapping Pluvial Flood-Induced Damages with Multi-Sensor Optical Remote Sensing: A Transferable Approach. Remote Sens. 15, 2361. https://doi.org/10.3390/rs15092361

Cerbelaud, A., Roupioz, L., Blanchet, G., Breil, P., Briottet, X., 2021. A repeatable change detection approach to map extreme storm-related damages caused by intense surface runoff based on optical and SAR remote sensing: Evidence from three case studies in the South of France. ISPRS J. Photogramm. Remote Sens. 182, 153–175. https://doi.org/10.1016/j.isprsjprs.2021.10.013

Cerdà, A., Novara, A., Dlapa, P., López-Vicente, M., Úbeda, X., Popović, Z., Mekonnen, M., Terol, E., Janizadeh, S., Mbarki, S., Saldanha-Vogelmann, E., Hazrati, S., Sannigrahi, S., Parhizkar, M., Giménez-Morera, A., 2021. Rainfall and water yield in Macizo del Caroig, Eastern Iberian Peninsula. Event runoff at plot scale during a rare flash flood at the Barranco de Benacancil. Cuad. Investig. Geográfica 47, 95–119. https://doi.org/10.18172/cig.4833

Chughtai, A.H., Abbasi, H., Karas, I.R., 2021. A review on change detection method and accuracy assessment for land use land cover. Remote Sens. Appl. Soc. Environ. 22, 100482. https://doi.org/10.1016/j.rsase.2021.100482

Congalton, R.G., 1991. A review of assessing the accuracy of classifications of remotely sensed data. Remote Sens. Environ. 37, 35–46. https://doi.org/10.1016/0034-4257(91)90048-B

Congalton, R.G., Green, K., 2019. Assessing the Accuracy of Remotely Sensed Data: Principles and Practices, Third Edition, 3rd ed. CRC Press, Boca Raton. https://doi.org/10.1201/9780429052729

Da Silva, C.N., Palheta Da Silva, J.M., Nogueira Castro, C.J., 2015. Methodological Guidelines for the Use of Geoprocessing Tools: Spatial Analysis Operations—Kernel, Buffer and the Remote Sensing Image Classification. Agric. Sci. 06, 707–716. https://doi.org/10.4236/as.2015.67068

Diakakis, M., Deligiannakis, G., Antoniadis, Z., Melaki, M., Katsetsiadou, N.K., Andreadakis, E., Spyrou, N.I., Gogou, M., 2020. Proposal of a flash flood impact severity scale for the classification and mapping of flash flood impacts. J. Hydrol. 590, 125452. https://doi.org/10.1016/j.jhydrol.2020.125452

Direkcija RS za vode, 2024. Vodni kataster [WWW Document]. Minist. Za Okolje Prost. URL http://www.evode.gov.si/index.php?id=84 (accessed 5.6.24).

Douville, H., Raghavan, K., Renwick, J., Allan, R.P., Arias, P.A., Barlow, M., Cerezo-Mota, R., Cherchi, A., Gan, T.Y., Gergis, J., Jiang, D., Khan, A., Mba, W.P., Rosenfeld, D., Tierney, J., Zolina, O., 2021. Water cycle changes, in: Masson-Delmotte, V.P., Zhai, P., Pirani, A., Connors, S.L., Péan, C., Berger, S., Caud, N., Chen, Y., Goldfarb, L., Gomis, M.I., Huang, M., Leitzell, K., Lonno, E., Matthews, J.B.R., Maycock, T.K., Waterfield, T., Yelekçi, O., Yu, R., Zhou, B. (Eds.), . Cambridge University Press, Cambridge, UK, pp. 1055–1210.

EEA geospatial data catalogue, 2015. Riparian Zones Delineation (vector), Aug. 2015 [WWW Document]. EEA Geospatial Data Cat. URL https://sdi.eea.europa.eu/catalogue/srv/api/records/e61d0641-ef07-4224-a6ed-6d2d42a4ef23 (accessed 4.14.24).

EOS Data Analytics, 2022. NDMI: Vegetation Index Equation And Values Interpretation [WWW Document]. URL https://eos.com/make-an-analysis/ndmi/ (accessed 4.11.24).

European Flood Awareness System (EFAS), 2023. Flooding in Slovenia - August 2023 | Copernicus EMS - European Flood Awareness System [WWW Document]. URL https://www.efas.eu/en/news/flooding-slovenia-august-2023 (accessed 10.20.23).

Feyen, L., Ciscar Martinez, J.C., Gosling, S., Ibarreta Ruiz, D., Soria Ramirez, A., Dosio, A., Naumann, G., Russo, S., Formetta, G., Forzieri, G., Girardello, M., Spinoni, J., Mentaschi, L., Bisselink, B., Bernhard, J., Gelati, E., Adamovic, M., Guenther, S., de Roo, A., Cammalleri, C., Dottori, F., Bianchi, A., Alfieri, L., Vousdoukas, M., Mongelli, I., Hinkel, J., Ward, P. j, Gomes Da Costa, H., de Rigo, D., Liberta', G., Durrant, T., San-Miguel-Ayanz, J., Barredo Cano, J.I., Mauri, A., Caudullo, G., Ceccherini, G., Beck, P., Cescatti, A., Hristov, J., Toreti, A., Perez Dominguez, I., Dentener, F., Fellmann, T., Elleby, C., Ceglar, A., Fumagalli, D., Niemeyer, S., Cerrani, I., Panarello, L., Bratu, M., Després, J., Szewczyk, W., Matei, N., Mulholland, E., Olariaga-Guardiola, M., 2020. Climate change impacts and adaptation in Europe. JRC PESETA IV final report (JRC Research Reports No. JRC119178). Joint Research Centre (Seville site).

Feyisa, G.L., Meilby, H., Fensholt, R., Proud, S.R., 2014. Automated Water Extraction Index: A new technique for surface water mapping using Landsat imagery. Remote Sens. Environ. 140, 23–35. https://doi.org/10.1016/j.rse.2013.08.029

Fiedler, T., Pitman, A.J., Mackenzie, K., Wood, N., Jakob, C., Perkins-Kirkpatrick, S.E., 2021. Business risk and the emergence of climate analytics. Nat. Clim. Change 11, 87–94. https://doi.org/10.1038/s41558-020-00984-6

Foody, G.M., 2008. Harshness in image classification accuracy assessment. Int. J. Remote Sens. 29, 3137–3158. https://doi.org/10.1080/01431160701442120

Fribourg-Blanc, B., Matheiss, V., Iacovides, A., Kossida, M., Karavokiros, G., Amorsi, N., Siauve, S., Desmot, E., Strosser, P., n.d. Pilot Project—Atmospheric Precipitation—Protection and Efficient Use of Fresh Water: Integration of Natural Water Retention Measures in River Basin Management: Final Report; Publications Office of the European Union: Luxembourg, 2015. Google Sch. 2015.

Gao, B., 1996. NDWI—A normalized difference water index for remote sensing of vegetation liquid water from space. Remote Sens. Environ. 58, 257–266. https://doi.org/10.1016/S0034-4257(96)00067-3

Gardiner, J., 1994. Environmental impact of floods, in: Rossi, G., Harmancioğlu, N., Yevjevich, V. (Eds.), Coping with Floods, NATO ASI Series. Springer Netherlands, Dordrecht, pp. 529–548. https://doi.org/10.1007/978-94-011-1098-3_31

Gautam, K., Van Der Hoek, E., 2003. Literature study on environmental impact of floods. Neth. Delft Clust.

Google Developers, 2024. Sentinel-1 Algorithms | Google Earth Engine [WWW Document]. Google Dev. URL https://developers.google.com/earth-engine/guides/sentinel1 (accessed 4.13.24).

Google Developers, 2023. Harmonized Sentinel-2 MSI: MultiSpectral Instrument, Level-2A | Earth Engine Data Catalog | Google for Developers [WWW Document]. URL https://developers.google.com/earth-engine/datasets/catalog/COPERNICUS_S2_SR_HARMONIZED (accessed 4.13.24).

Google Developers, n.d. Sentinel-2 Cloud Masking with s2cloudless | Google Earth Engine [WWW Document]. Google Dev. URL https://developers.google.com/earth-engine/tutorials/community/sentinel-2-s2cloudless (accessed 4.14.24).

Gorelick, N., Hancher, M., Dixon, M., Ilyushchenko, S., Thau, D., Moore, R., 2017. Google Earth Engine: Planetary-scale geospatial analysis for everyone. Remote Sens. Environ., Big Remotely Sensed Data: tools, applications and experiences 202, 18–27. https://doi.org/10.1016/j.rse.2017.06.031

Graziano, M.P., Deguire, A.K., Surasinghe, T.D., 2022. Riparian Buffers as a Critical Landscape Feature: Insights for Riverscape Conservation and Policy Renovations. Diversity 14, 172. https://doi.org/10.3390/d14030172

Gregory, S.V., Swanson, F.J., McKee, W.A., Cummins, K.W., 1991. An Ecosystem Perspective of Riparian Zones. BioScience 41, 540–551. https://doi.org/10.2307/1311607

Hansana, P., Guo, X., Zhang, S., Kang, X., Li, S., 2023. Flood Analysis Using Multi-Scale Remote Sensing Observations in Laos. Remote Sens. 15, 3166. https://doi.org/10.3390/rs15123166

Hirabayashi, Y., Mahendran, R., Koirala, S., Konoshima, L., Yamazaki, D., Watanabe, S., Kim, H., Kanae, S., 2013. Global flood risk under climate change. Nat. Clim. Change 3, 816–821. https://doi.org/10.1038/nclimate1911

Hohensinner, S., Hauer, C., Muhar, S., 2018. River Morphology, Channelization, and Habitat Restoration, in: Schmutz, S., Sendzimir, J. (Eds.), Riverine Ecosystem Management: Science for Governing Towards a Sustainable Future. Springer International Publishing, Cham, pp. 41–65. https://doi.org/10.1007/978-3-319-73250-3_3

Huang, F., Chen, L., Yin, K., Huang, J., Gui, L., 2018. Object-oriented change detection and damage assessment using high-resolution remote sensing images, Tangjiao Landslide, Three Gorges Reservoir, China. Environ. Earth Sci. 77, 183. https://doi.org/10.1007/s12665-018-7334-5

Huang, S., Tang, L., Hupy, J.P., Wang, Y., Shao, G., 2021. A commentary review on the use of normalized difference vegetation index (NDVI) in the era of popular remote sensing. J. For. Res. 32, 1–6. https://doi.org/10.1007/s11676-020-01155-1

Huang, W., DeVries, B., Huang, C., Lang, M.W., Jones, J.W., Creed, I.F., Carroll, M.L., 2018. Automated Extraction of Surface Water Extent from Sentinel-1 Data. Remote Sens. 10, 797. https://doi.org/10.3390/rs10050797

Huete, A.R., 1988. A soil-adjusted vegetation index (SAVI). Remote Sens. Environ. 25, 295–309. https://doi.org/10.1016/0034-4257(88)90106-X

INSPIRE SI, 2023a. Slovenski INSPIRE metapodatkovni sistem - INSPIRE (SI) - Vodna zemljišča [WWW Document]. Vodna Zemljišča. URL https://eprostor.gov.si/imps/srv/eng/catalog.search#/metadata/5668b04d-27f1-4b57-ac8f-465841e9d0f8 (accessed 4.13.24).

INSPIRE SI, 2023b. Slovenski INSPIRE metapodatkovni sistem - INSPIRE (SI) - RABA [WWW Document]. Evidenca Dejanske Rabe Kmetijskih Gozdnih Zemljišč. URL https://eprostor.gov.si/imps/srv/eng/catalog.search#/metadata/67cea1ee-8f9d-463d-b5de-87518ec50b33 (accessed 4.13.24).

INSPIRE SI, 2023c. Integralna karta poplavne nevarnosti (IKPN) [WWW Document]. Slov. INSPIRE Metapodatkovni Sist. URL https://eprostor.gov.si/imps/srv/api/records/406932c9-87d0-4854-8fe9-c3d083768970 (accessed 4.14.24).

Jaybhay, J., Shastri, R., 2015. A Study of Speckle Noise Reduction Filters. Signal Image Process. Int. J. 6, 71–80. https://doi.org/10.5121/sipij.2015.6306

Jiménez-Jiménez, S.I., Ojeda-Bustamante, W., Ontiveros-Capurata, R.E., Marcial-Pablo, M. de J., 2020. Rapid urban flood damage assessment using high resolution remote sensing data and an object-based approach. Geomat. Nat. Hazards Risk 11, 906–927. https://doi.org/10.1080/19475705.2020.1760360

JNCC Sentinel-2 indices Analysis Ready Data (ARD) [WWW Document], n.d. URL https://catalogue.ceda.ac.uk/uuid/b42f524bc9cd4dd6850b2399b616f5c4 (accessed 4.11.24).

Kobiyama, M., Goerl, R.F., 2007. Quantitative method to distinguish flood and flash flood as disasters. SUISUI Hydrol. Res. Lett. 1, 11–14. https://doi.org/10.3178/suisui.1.11

Kriegler, F.J., Malila, W.A., Nalepka, R.F., Richardson, W., 1969. Preprocessing Transformations and Their Effects on Multispectral Recognition. Presented at the Remote Sensing of Environment, VI.

Kuntla, S.K., 2021. An era of Sentinels in flood management: Potential of Sentinel-1, -2, and -3 satellites for effective flood management. Open Geosci. 13, 1616–1642. https://doi.org/10.1515/geo-2020-0325

Kušar, U., Vrenko, D.Z., 2017. Vzposatvljanje vodega katastra kot temeljnje evidence upravljanja z vodami. 28 MIŠIČEV VODARSKI DAN 2017 2017.

Landuyt, L., Verhoest, N.E.C., Van Coillie, F.M.B., 2020. Flood Mapping in Vegetated Areas Using an Unsupervised Clustering Approach on Sentinel-1 and -2 Imagery. Remote Sens. 12, 3611. https://doi.org/10.3390/rs12213611

Laudan, J., Rözer, V., Sieg, T., Vogel, K., Thieken, A.H., 2017. Damage assessment in Braunsbach 2016: data collection and analysis for an improved understanding of damaging processes during flash floods. Nat. Hazards Earth Syst. Sci. 17, 2163–2179. https://doi.org/10.5194/nhess-17-2163-2017

Laudan, J., Zöller, G., Thieken, A.H., 2020. Flash floods versus river floods – a comparison of psychological impacts and implications for precautionary behaviour. Nat. Hazards Earth Syst. Sci. 20, 999–1023. https://doi.org/10.5194/nhess-20-999-2020

Liu, W., Chen, W., Peng, C., 2014. Assessing the effectiveness of green infrastructures on urban flooding reduction: A community scale study. Ecol. Model. 291, 6–14. https://doi.org/10.1016/j.ecolmodel.2014.07.012

Lombana, L., Martínez-Graña, A., 2022. A Flood Mapping Method for Land Use Management in Small-Size Water Bodies: Validation of Spectral Indexes and a Machine Learning Technique. Agronomy 12, 1280. https://doi.org/10.3390/agronomy12061280

Lozano de Sosa, L., Glanville, H., Marshall, M., Abood, S., Williams, A.P., Jones, D., 2017. Delineating and mapping riparian areas for ecosystem service assessment. Ecohydrology 11, e1928. https://doi.org/10.1002/eco.1928

Ma, L., Bo, J., Li, X., Fang, F., Cheng, W., 2019. Identifying key landscape pattern indices influencing the ecological security of inland river basin: The middle and lower reaches of Shule River Basin as an example. Sci. Total Environ. 674, 424–438. https://doi.org/10.1016/j.scitotenv.2019.04.107

Main-Knorn, M., Pflug, B., Louis, J., Debaecker, V., Müller-Wilm, U., Gascon, F., 2017. Sen2Cor for Sentinel-2, in: Image and Signal Processing for Remote Sensing XXIII. Presented at the Image and Signal Processing for Remote Sensing XXIII, SPIE, pp. 37–48. https://doi.org/10.1117/12.2278218

Marzi, D., Gamba, P., 2021. Inland Water Body Mapping Using Multitemporal Sentinel-1 SAR Data. IEEE J. Sel. Top. Appl. Earth Obs. Remote Sens. 14, 11789–11799. https://doi.org/10.1109/JSTARS.2021.3127748

McFeeters, S.K., 1996. The use of the Normalized Difference Water Index (NDWI) in the delineation of open water features. Int. J. Remote Sens. 17, 1425–1432. https://doi.org/10.1080/01431169608948714

Merz, B., Kreibich, H., Schwarze, R., Thieken, A., 2010. Review article "Assessment of economic flood damage." Nat. Hazards Earth Syst. Sci. 10, 1697–1724. https://doi.org/10.5194/nhess-10-1697-2010

Meyer, F., 2019. Spaceborne Synthetic Aperture Radar: Principles, data access, and basic processing techniques. Synth. Aperture Radar SAR Handb. Compr. Methodol. For. Monit. Biomass Estim. 21–64.

Miller, J.D., Kim, H., Kjeldsen, T.R., Packman, J., Grebby, S., Dearden, R., 2014. Assessing the impact of urbanization on storm runoff in a peri-urban catchment using historical change in impervious cover. J. Hydrol. 515, 59–70. https://doi.org/10.1016/j.jhydrol.2014.04.011

Montero, D., 2021. eemont: A Python package that extends Google Earth Engine. J. Open Source Softw. 6, 3168. https://doi.org/10.21105/joss.03168

Montero, D., Aybar, C., Mahecha, M.D., Martinuzzi, F., Söchting, M., Wieneke, S., 2023. A standardized catalogue of spectral indices to advance the use of remote sensing in Earth system research. Sci. Data 10, 197. https://doi.org/10.1038/s41597-023-02096-0

Mooney, H., Larigauderie, A., Cesario, M., Elmquist, T., Hoegh-Guldberg, O., Lavorel, S., Mace, G.M., Palmer, M., Scholes, R., Yahara, T., 2009. Biodiversity, climate change, and ecosystem services. Curr. Opin. Environ. Sustain. 1, 46–54. https://doi.org/10.1016/j.cosust.2009.07.006

Mudashiru, R.B., Sabtu, N., Abustan, I., Balogun, W., 2021. Flood hazard mapping methods: A review. J. Hydrol. 603, 126846. https://doi.org/10.1016/j.jhydrol.2021.126846

Munich RE, 2000. World of Natural Hazards (CD ROM). Münch. Münch. Rückversicher.-Ges.

Naiman, R., Bilby, R.E., 2001. River Ecology and Management: Lessons from the Pacific Coastal Ecoregion. Springer Science & Business Media.

Naiman, R.J., Decamps, H., McClain, M.E., 2010. Riparia: Ecology, Conservation, and Management of Streamside Communities. Elsevier.

Olokeogun, O.S., Ayanlade, A., Popoola, O.O., 2020. Assessment of riparian zone dynamics and its flood-related implications in Eleyele area of Ibadan, Nigeria. Environ. Syst. Res. 9, 6. https://doi.org/10.1186/s40068-020-00167-4

O'Neill, R., Krummel, J., Gardner, R., Sugihara, G., Jackson, B., Deangelis, D., Milne, B., Turner, M., Zygmunt, B., Christensen, S., Dale, V., Graham, R., 1988. Indices ?of Landscape Pattern. Landsc. Ecol. 1, 153–162. https://doi.org/10.1007/BF00162741

Otsu, N., 1975. A Tlreshold Selection Method from Gray-Level Histograms. Automatica 11, 23–27.

Piedelobo, L., Taramelli, A., Schiavon, E., Valentini, E., Molina, J.-L., Nguyen Xuan, A., González-Aguilera, D., 2019. Assessment of Green Infrastructure in Riparian Zones Using Copernicus Programme. Remote Sens. 11, 2967. https://doi.org/10.3390/rs11242967

Pörtner, H.O., Roberts, D.C., Adams, H., Adler, C., Aldunce, P., 2022. Climate change 2022: Impacts, adaptation and vulnerability. https://doi.org/10.1017/9781009325844

Rahman, Md.S., Di, L., Yu, E., Lin, L., Yu, Z., 2021. Remote Sensing Based Rapid Assessment of Flood Crop Damage Using Novel Disaster Vegetation Damage Index (DVDI). Int. J. Disaster Risk Sci. 12, 90–110. https://doi.org/10.1007/s13753-020-00305-7

Rango, A., Salomonson, V.V., 1974. Regional flood mapping from space. Water Resour. Res. 10, 473–484. https://doi.org/10.1029/WR010i003p00473

Refice, A., Capolongo, D., Pasquariello, G., D'Addabbo, A., Bovenga, F., Nutricato, R., Lovergine, F.P., Pietranera, L., 2014. SAR and InSAR for Flood Monitoring: Examples With COSMO-SkyMed Data. IEEE J. Sel. Top. Appl. Earth Obs. Remote Sens. 7, 2711–2722. https://doi.org/10.1109/JSTARS.2014.2305165

Rikimaru, A., Roy, P., Miyatake, S., others, 2002. Tropical forest cover density mapping. Trop. Ecol. 43, 39–47.

Rodríguez-González, P.M., Abraham, E., Aguiar, F., Andreoli, A., Baležentienė, L., Berisha, N., Bernez, I., Bruen, M., Bruno, D., Camporeale, C., Čarni, A., Chilikova-Lubomirova, M., Corenblit, D., Ćušterevska, R., Doody, T., England, J., Evette, A., Francis, R., Garófano-Gómez, V., González del Tánago, M., Gultekin, Y.S., Guyard, F., Hellsten, S., Hinkov, G., Jakubínský, J., Janssen, P., Jansson, R., Kail, J., Keles, E., Kelly-Quinn, M., Kidová, A., Kiss, T., Kulvik, M., La Porta, N., Laslier, M., Latella, M., Lorenz, S., Mandžukovski, D., Manolaki, P., Martinez-Fernández, V., Merritt, D., Michez, A., Milovanović, J., Okruszko, T., Papastergiadou, E., Penning, E., Pielech, R., Politti, E., Portela, A., Riis, T., Škvorc, Ž., Slezák, M., Stammel, B., Stella, J., Stesevic, D., Stupar, V., Tammeorg, O., Tammeorg, P., Fosholt, T.M., Urbanič, G., Villar, M., Vogiatzakis, I., Vrchovsky, P., Yousefpour, R., Zinke, P., Zlatanov, T., Dufour, S., 2022. Bringing the margin to the focus: 10 challenges for riparian vegetation science and management. WIREs Water 9, e1604. https://doi.org/10.1002/wat2.1604

Salazar, S., Francés, F., Komma, J., Blume, T., Francke, T., Bronstert, A., Blöschl, G., 2012. A comparative analysis of the effectiveness of flood management measures based on the concept of "retaining water in the landscape" in different European hydro-climatic regions. Nat. Hazards Earth Syst. Sci. 12, 3287–3306. https://doi.org/10.5194/nhess-12-3287-2012

Sanchez, A.H., Picoli, M.C.A., Camara, G., Andrade, P.R., Chaves, M.E.D., Lechler, S., Soares, A.R., Marujo, R.F.B., Simões, R.E.O., Ferreira, K.R., Queiroz, G.R., 2020. Comparison of Cloud Cover Detection Algorithms on Sentinel–2 Images of the Amazon Tropical Forest. Remote Sens. 12, 1284. https://doi.org/10.3390/rs12081284

Schmidt-Thomé, P., Kallio, H., Jarva, J., Tarvainen, T., 2005. The spatial effects and management of natural and technological hazards in Europe. Final Rep. Eur. Spat. Plan. Obs. Netw. ESPON Proj. 1, 1–197.

Sentinel Online, 2023. User Guides - Sentinel-1 SAR - Interferometric Wide Swath - Sentinel Online [WWW Document]. Sentin. Online. URL https://copernicus.eu/user-guides/sentinel-1-sar/acquisition-modes/interferometric-wide-swath (accessed 4.14.24).

Sentiwiki, 2024. S1 Mission [WWW Document]. URL https://sentiwiki.copernicus.eu/web/s1-mission (accessed 4.13.24).

Sentiwiki, 2023. Sentinel-2 [WWW Document]. URL https://sentiwiki.copernicus.eu/web/sentinel-2 (accessed 4.13.24).

Sinergise, S.-H. by, n.d. NDWI Normalized Difference Water Index, PlanetScope [WWW Document]. Sentin. Hub Cust. Scr. URL https://custom-scripts.sentinel-hub.com/custom-scripts/planet_scope/ndwi/ (accessed 4.11.24a).

Sinergise, S.-H. by, n.d. Barren Soil Script [WWW Document]. Sentin. Hub Cust. Scr. URL https://custom-scripts.sentinel-hub.com/custom-scripts/sentinel-2/barren_soil/ (accessed 4.11.24b).

Small, D., 2011. Flattening Gamma: Radiometric Terrain Correction for SAR Imagery. IEEE Trans. Geosci. Remote Sens. 49, 3081–3093. https://doi.org/10.1109/TGRS.2011.2120616

Smith, N., 2006. There's no such thing as a natural disaster. Underst. Katrina Perspect. Soc. Sci. 11.

Staembatch, n.d. SAVI from First Principles [WWW Document]. URL https://www.streambatch.io/knowledge/savi-from-first-principles (accessed 4.11.24).

Stehman, S.V., Wickham, J.D., 2011. Pixels, blocks of pixels, and polygons: Choosing a spatial unit for thematic accuracy assessment. Remote Sens. Environ. 115, 3044–3055. https://doi.org/10.1016/j.rse.2011.06.007

Stembatch, n.d. NDVI from First Principles [WWW Document]. URL https://www.streambatch.io/knowledge/ndvi-from-first-principles (accessed 4.11.24).

Strashok, O., Ziemiańska, M., Strashok, V., 2022. Evaluation and Correlation of Sentinel-2 NDVI and NDMI in Kyiv (2017–2021). J. Ecol. Eng. Vol. 23. https://doi.org/10.12911/22998993/151884

Taramelli, A., Lissoni, M., Piedelobo, L., Schiavon, E., Valentini, E., Nguyen Xuan, A., González-Aguilera, D., 2019. Monitoring Green Infrastructure for Natural Water Retention Using Copernicus Global Land Products. Remote Sens. 11, 1583. https://doi.org/10.3390/rs11131583

Tarpanelli, A., Mondini, A.C., Camici, S., 2022. Effectiveness of Sentinel-1 and Sentinel-2 for Flood Detection Assessment in Europe (preprint). Hydrological Hazards. https://doi.org/10.5194/nhess-2022-63

Tavus, B., Kocaman, S., Gokceoglu, C., 2022. Flood damage assessment with Sentinel-1 and Sentinel-2 data after Sardoba dam break with GLCM features and Random Forest method. Sci. Total Environ. 816, 151585. https://doi.org/10.1016/j.scitotenv.2021.151585

Thépaut, J.-N., Dee, D., Engelen, R., Pinty, B., 2018. The Copernicus Programme and its Climate Change Service, in: IGARSS 2018 - 2018 IEEE International Geoscience and Remote Sensing Symposium. Presented at the IGARSS 2018 - 2018 IEEE International Geoscience and Remote Sensing Symposium, pp. 1591–1593. https://doi.org/10.1109/IGARSS.2018.8518067

Tockner, K., Stanford, J.A., 2002. Riverine flood plains: present state and future trends. Environ. Conserv. 29, 308–330. https://doi.org/10.1017/S037689290200022X

Tóth, T., 2019. Application of Natural Water Retention Measures in Flood Management. Műszaki Katonai Közlöny 29, 139–152. https://doi.org/10.32562/mkk.2019.1.11

Tsyganskaya, V., Martinis, S., Marzahn, P., Ludwig, R., 2018. SAR-based detection of flooded vegetation – a review of characteristics and approaches. Int. J. Remote Sens. 39, 2255–2293. https://doi.org/10.1080/01431161.2017.1420938

Tucker, C.J., 1979. Red and photographic infrared linear combinations for monitoring vegetation. Remote Sens. Environ. 8, 127–150. https://doi.org/10.1016/0034-4257(79)90013-0

TV, B., K N, N., 2019. A Comparative Study of Spectral Indices for Surface Water Delineation Using Landsat 8 Images.

Tzeng, Y.-C., Fan, K.-T., Chen, K.-S., 2009. An Adaptive Thresholding Multiple Classifiers System for Remote Sensing Image Classification. Photogramm. Eng. Remote Sens. 75, 679–687. https://doi.org/10.14358/PERS.75.6.679

UN-SPIDER, 2023. Step-by-Step: Recommended Practice: Flood Mapping and Damage Assessment Using Sentinel-1 SAR Data in Google Earth Engine | UN-SPIDER Knowledge Portal [WWW Document]. URL https://www.un-spider.org/advisory-support/recommended-practices/recommended-practice-google-earth-engine-flood-mapping/step-by-step (accessed 4.14.24).

van Oorschot, M., Kleinhans, M., Buijse, A.D., Geerling, G., Middelkoop, H., 2018. Combined effects of climate change and dam construction on riverine ecosystems. Ecol. Eng. 120. https://doi.org/10.1016/j.ecoleng.2018.05.037

Vollrath, A., Mullissa, A., Reiche, J., 2020. Angular-Based Radiometric Slope Correction for Sentinel-1 on Google Earth Engine. Remote Sens. 12, 1867. https://doi.org/10.3390/rs12111867

Weissteiner, C.J., Ickerott, M., Ott, H., Probeck, M., Ramminger, G., Clerici, N., Dufourmont, H., De Sousa, A.M.R., 2016. Europe's Green Arteries—A Continental Dataset of Riparian Zones. Remote Sens. 8, 925. https://doi.org/10.3390/rs8110925

Wu, Q., 2020. geemap: A Python package for interactive mapping with Google Earth Engine. J. Open Source Softw. 5, 2305. https://doi.org/10.21105/joss.02305

Ye, S., Pontius, R.G., Rakshit, R., 2018. A review of accuracy assessment for object-based image analysis: From per-pixel to per-polygon approaches. ISPRS J. Photogramm. Remote Sens. 141, 137–147. https://doi.org/10.1016/j.isprsjprs.2018.04.002

Zaimes, G.N., Iakovoglou, V., 2020. Assessing Riparian Areas of Greece—An Overview. Sustainability 13, 309. https://doi.org/10.3390/su13010309

Zaimes, G.N., Tufekcioglu, M., Schultz, R.C., 2019. Riparian Land-Use Impacts on Stream Bank and Gully Erosion in Agricultural Watersheds: What We Have Learned. Water 11, 1343. https://doi.org/10.3390/w11071343

Zhang, Y., Gong, J., Sun, K., Yin, J., Chen, X., 2018. Estimation of Soil Moisture Index Using Multi-Temporal Sentinel-1 Images over Poyang Lake Ungauged Zone. Remote Sens. 10, 12. https://doi.org/10.3390/rs10010012